/N-26

P.156

The Influence of Chromium on Structure and Mechanical Properties of B2 Nickel Aluminide Alloys

James Dean Cotton
University of Florida
Gainesville, Florida

March 1992

NASA

National Aeronautics and
Space Administration

TABLE OF CONTENTS

THE INFLUENCE OF CHROMIUM ON STRUCTURE AND MECHANICAL PROPERTIES OF B2 NICKEL ALUMINIDE ALLOYS

James Dean Cotton
University of Florida
Gainesville, Florida 32601

ABSTRACT

Major obstacles to the use of NiAl-base alloys and composites are low ductility and toughness. These shortcomings result, in part at least, from a lack of sufficient slip systems to accommodate plastic deformation of polycrystalline material (the von Mises Criterion). It has been reported that minor additions of chromium to polycrystalline NiAl cause the predominant slip system to shift from the usual $<001>\{110\}$ to $<111>\{112\}$. If this is true, then a major step toward increasing ductility in this compound may be realized. The purpose of the present study was to verify this phenomenon, characterize it with respect to chromium level and nickel-to-aluminum ratio, and correlate any change in slip system with microstructure and mechanical properties. Compression and tensile specimens were prepared from alloys containing 0 to 5 at.% chromium and 45 to 55 at. % aluminum. Following about one percent strain, TEM foils were produced and the slip systems determined using the $\mathbf{g \cdot b} = 0$ invisibility criterion. Contrary to the previous results, chromium was found to have no effect on the preferred slip system in of any of the alloys

studied. Possible reasons for the inconsistency of the current results with previous work are considered. Composition-structure-property relationships are discerned for the alloys, and good correlations are demonstrated in terms of conventional strengthening models for metallic systems.

CHAPTER 1
INTRODUCTION

Background

A class of materials termed "intermetallics" has been the subject of an increasing amount of study for the past decade. There are several reasons for this interest, most of which revolve around a need for stable high-temperature ("high" with respect to most metals) materials. The intermetallics are considered to occupy a position somewhere between metals and ceramics, due to a significant covalent contribution to the overall bonding of the compound which lends thermal stability. This often causes an intermetallic to have a melting point above one, or both, of its pure constituent elements. In addition, intermetallics often exhibit, relative to most pure metals, higher room temperature strength, higher moduli and lower thermal expansion coefficients. Thermal and electrical conductivities can exceed competing metallic alloys, due to the increased rigidity of the structure. However, the same covalent component which creates such attractive properties will, by nature, also reduce the ability of the material to undergo plastic deformation by dislocation motion. Thus, the ductility and toughness of intermetallic compounds are usually low compared with metals. This latter deficiency has been a major obstacle in the development of intermetallics and is the reason for the current study.

One very important application for intermetallics is high-temperature components of advanced turbine engines, such as blades and vanes [1, 2]. For such applications, B2 nickel aluminide (NiAl) is a material of choice and the next logical step in materials evolution beyond current superalloys. Nickel aluminide has a high melting point (300K above superalloys), a low density (75 percent that of superalloys or Ni_3Al), a high thermal

1

conductivity (as much as eight times that of superalloys), a wide solubility range, good processability, and is inexpensive [3].

In spite of these advantages, NiAl is brittle and rarely attains a tensile ductility in excess of 2 percent at room temperature [4, 5, 6, 7, 8]. Room-temperature plastic deformation in NiAl occurs predominantly by dislocation glide on the <100>{011} systems [9, 10, 11], of which only three are independent [12]. According to the von Mises Criterion [13], a minimum of five independent deformation mechanisms are required for arbitrary deformation of any three-dimensional body. This requirement restricts plastic flow in polycrystalline NiAl, as each grain must undergo arbitrary deformation to maintain shape compatibility with the adjacent grains, and is at least one reason why it is not ductile. However, if other slip systems could be activated, such as those which operate in body-centered-cubic metals (<111>{0$\bar{1}$1}), then sufficient slip systems would be available and a major obstacle to ductility and toughness will have been removed.

One avenue to activating other slip systems that has been suggested is through ternary alloying [14, 15, 16]. In fact, Law and Blackburn [15] reported in 1985 that the addition of five atom percent chromium to NiAl caused the primary Burgers vector to change from <100> to <111>. However, no increase in tensile ductility was observed. This result is intriguing and several questions are obvious. If the Burgers vector was truly altered and sufficient slip systems were available, then what other factor is restricting plastic flow? Are there other compositions in this ternary system which may demonstrate similar behavior? The primary question, fundamental to any scientific study is, "Are the results reproducible?" As of the time of this writing, there have been no other studies which confirm the effect of chromium on plastic flow in polycrystalline NiAl. Thus, the objective of the current study is to examine, in a systematic fashion, the effect of chromium on slip and mechanical properties in NiAl.

Approach

Since Law and Blackburn [15] initially studied cast alloys, and the room temperature solubility of chromium in NiAl is less than two atom percent [17, 18], the chromium content of the alloys in the current study was varied from zero to five atom percent (0, 1, 2, 5). To examine the effects of stoichiometry, the aluminum content was also varied, from 45 to 55 percent. A set of 15 alloys within this composition range was cast and homogenized, including one exactly at the composition reported to exhibit <111> slip [15]. To study processing effects and improve specimen integrity, five of the compositions (binary stoichiometric NiAl and four aluminum-lean ternaries) were also produced in extruded form. Both the cast and the extruded alloys were utilized for an overall survey of Burgers vectors in this system. In addition, the relationships between composition, processing, dislocation type and mechanical properties were examined. The greater microstructural integrity of the extrusions allowed the determination of tensile properties as well as brittle-to-ductile-transition-temperatures.

CHAPTER 2
REVIEW OF THE LITERATURE

This review covers topics germane to understanding the chemical and structural factors controlling plastic deformation in NiAl under ambient conditions. The primary topics are phase equilibria, mechanical behavior, deformation and fracture, and alloying effects. The latter topic deals with the effect of ternary additions on slip behavior and mechanical properties and is mainly confined to single phase alloys of the B2 structure.

Nickel-Aluminum Phase Equilibria

The binary nickel-aluminum phase diagram is shown in Figure 2-1. Five intermetallic phases are present in this system. Of the five, the compound NiAl exhibits the highest melting point, 1911K. Nickel aluminide also displays an unusually wide range of solubility, an indication of high stability, spanning more than 20 atomic percent (all compositions will be given in atomic percent) at 1400°C. Deviations from stoichiometry are accommodated by the substitution of nickel atoms onto aluminum sites in nickel-rich compositions (antisite defects) and by the formation of vacancies on the nickel sites in aluminum-rich compositions [19]. The inability of aluminum atoms to occupy the nickel sites is usually explained by the larger atomic size of aluminum atoms. Vacancies are formed because the overall alloy composition can only be maintained by the elimination of a proportionate number of nickel atoms. These antisite and vacancy point defects have been shown to locally order such that no defect has a similar defect as a first neighbor [20] which leads to clusters of Ni_2Al and Ni_2Al_3, respectively [21].

4

Structure of NiAl

Beta NiAl crystallizes in the CsCl (B2) structure, in which one atom type resides at the center position of a cubic unit cell and the other at the corners, thus comprising an ordered body-centered cubic (BCC) lattice [23]. The structure is shown in Figure 2-2.
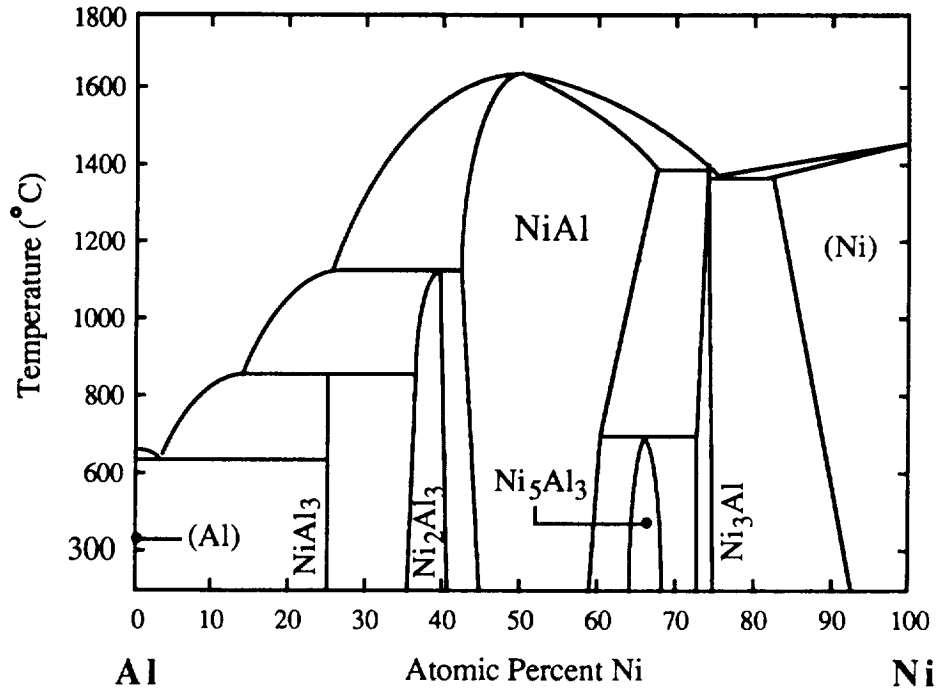

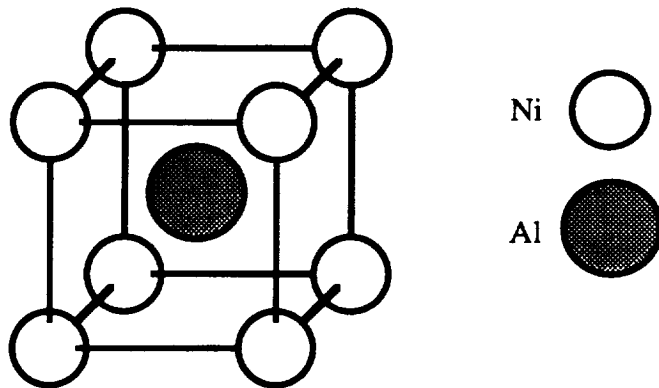Figure 2-1. Binary Phase Diagram for Nickel-Aluminum System [22]

Figure 2-2. NiAl B2 Structure

This compound is a congruently melting Hume-Rothery phase with an electron-to-atom ratio of 1.5, similar to CuZn, and is strongly ordered [24]. In addition, there is evidence that short-range order exists in the melt [25]. This strong tendency to order is indicative of a high ordering energy and a preference for bonding between aluminum and nickel atoms. X-ray and electron structure factor measurements [26, 27, 28, 29] provide evidence of a high degree of bond directionality, indicating electron concentration in <111> directions between first-neighbor aluminum-nickel pairs and a mixture of both metallic and covalent bonding. This large attraction between aluminum and nickel atoms accounts for many of the unusual properties of NiAl.

Mechanical Properties of NiAl

Polycrystalline

Strength and Ductility. Room-temperature mechanical properties of NiAl in tension and compression are summarized in Tables 2-1 and 2-2, respectively.

The earliest report on the mechanical properties of NiAl is that of Wachtell [30], which gives a room-temperature modulus-of-rupture for powder-processed material of 735 MPa, with nil ductility. This value is high compared to more recent reports and is likely a result of impurities introduced by powder processing. Later work by Maxwell and Grala [6, 31, 32] reported a much lower fracture strength for cast material, about 100 MPa, and zero ductility also. The first report of ambient temperature ductility in NiAl was by Rozner and Wasilewski [33], who measured about 4 percent elongation and a yield strength of 179 MPa in cast and extruded material. Quite recent studies have essentially confirmed the ambient ductility as being about 1-2 percent, while the yield strength varies, depending on the actual study, from 115 to 235 MPa, with a mean value of 167 MPa [4, 7, 33, 34, 35, 36, 37]. The differences in strength may result from variations in interstitial content, such as carbon (a common impurity in nickel) [35] or stoichiometry. The grain

size has been shown experimentally to have little effect on either the yield or fracture strengths of stoichiometric NiAl at ambient temperatures [36, 37], although fracture mechanical models predict otherwise [34, 38, 39, 40, 41]. The possible effect of grain size on mechanical properties is discussed in further depth below.

Table 2-1. Room-Temperature Tensile Properties of Polycrystalline NiAl

Reference	Year	TYS (MPa)	UTS (MPa)	Max. Strain (%)	Grain Size (μm)	Al (At.%)	Processing Method
[30]	1952	---	738	0	~40	~50	PM, HP
[32]	1957	---	103	0	~200	~50	cast
[33]	1966	179	207	4	no data	50.5	cast, extr.
[4]	1989	235	324	2.5	10-16	50.3	cast, extr.
[49]	1989	---	283	0	33	50.6	PM, extr.
[35]	1990	154	228	2	30	~50	cast, extr.
[36]	1990	115	220	2.3	13	~50	cast, extr.
[34]	1991	220	400	0-1	5	~50	PM, extr.
[68]	1991	---	350	0	10	50.6	PM, extr.

Table 2-2. Room-Temperature Compressive Properties of Polycrystalline NiAl

Reference	Year	CYS (MPa)	Max. Strain (%)	Grain Size (μm)	Al (At.%)	Processing Method
[7]	1968	137	17	50	49.6	cast, extr.
[37]	1991	130	---	10-400	~50	cast, extr.

Note the correlation in Table 2-1 between ductility and processing by extrusion. This correlation has been proposed to be due to a <111> fiber texture brought about by the extrusion process and the retention of a mobile dislocation substructure [4]. As with many metals, grains reorient during extrusion such that softer directions are aligned with the extrusion axis; a portion of this texture is retained following recrystallization. When test specimens are machined from the extrusions, the stress axis coincides with the extrusion axis and thus the soft orientation. This will tend to allow a lower yield stress and, for a given fracture stress, slightly higher ductility. In addition, higher ductility is apparent for

cast and extruded material compared with consolidated powder, which may be a result of contamination acquired during powder processing. Any contaminant phases may operate as critical flaws in the consolidated product.

Hardness. The room-temperature hardness of stoichiometric and near-stoichiometric NiAl is in the range 250 - 320 kgmm^{-2} (Vickers hardness), depending upon the exact composition and impurity content [6, 23, 42, 43, 44, 45, 46, 47].

Effect of Temperature. A substantial amount of data exists for the mechanical properties of NiAl as a function of temperature [6, 7, 23, 32, 33, 34, 48, 49], the most extensive of which are that of Rozner and Wasilewski (tension) and Pascoe and Newey (compression) [7, 33].

Stoichiometric NiAl displays a smooth decrease in yield strength with increasing test temperature and shows no indication of the strength anomaly sometimes observed in B2 compounds [50], Figure 2-3. The figure is adapted from Vedula and Khadikar [51] and represents the combined data of several investigators [4, 33, 34, 49], which agree quite well. The yield strength of polycrystalline NiAl is low, about 170 MPa (25 ksi) at room temperature, which makes it comparable to moderately strong aluminum alloys.

Similar to BCC metals, NiAl exhibits a transition from brittle to ductile behavior with increasing temperature, as illustrated in Figure 2-4 for several different studies. A Brittle-to-Ductile-Transition-Temperature (BDTT) may be determined for polycrystalline, stoichiometric NiAl to be about 600K (0.3 T_m), since the results indicating higher BDTTs may be due to nonstoichiometric material or impurity effects, both of which raise the tensile strength further above the fracture stress. It is quite interesting to note that the BDTT is lower for more recent studies, probably an effect of cleanliness (interstitial elements) or better compositional control. Other extrinsic effects which may limit apparent ductility (raise the BDTT) include defects in powder-processed material, surface roughness and misaligned tensile specimens. In addition, increasing the strain rate (typically at 10^{-4}/s) has the effect of raising the BDTT about 50K for each order of magnitude [34, 52].
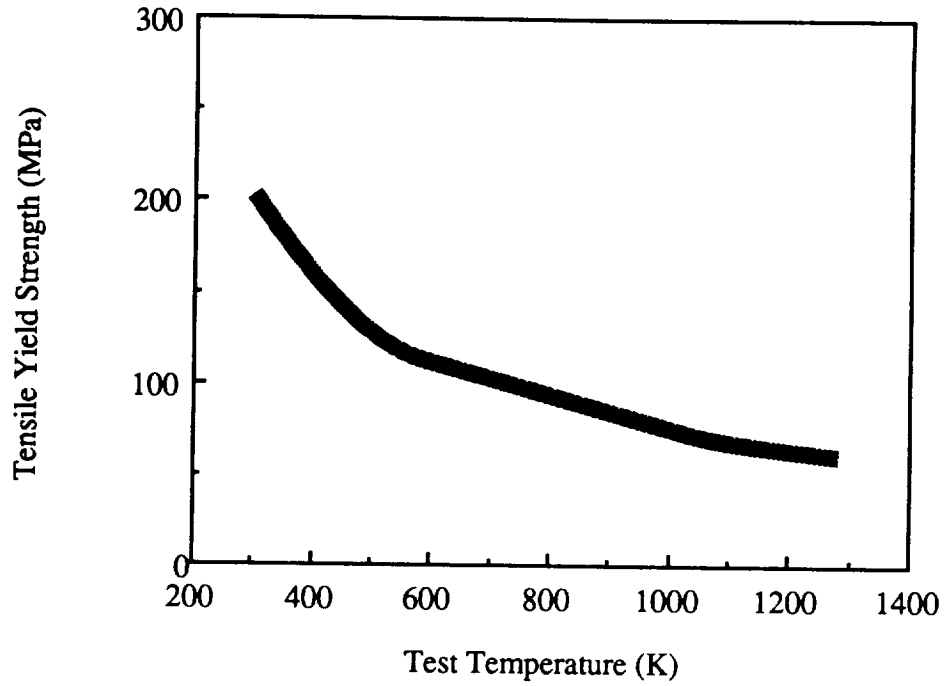
Figure 2-3. Tensile Yield Strength of Polycrystalline NiAl as a Function of Temperature. Adapted from Vedula and Khadikar [51]
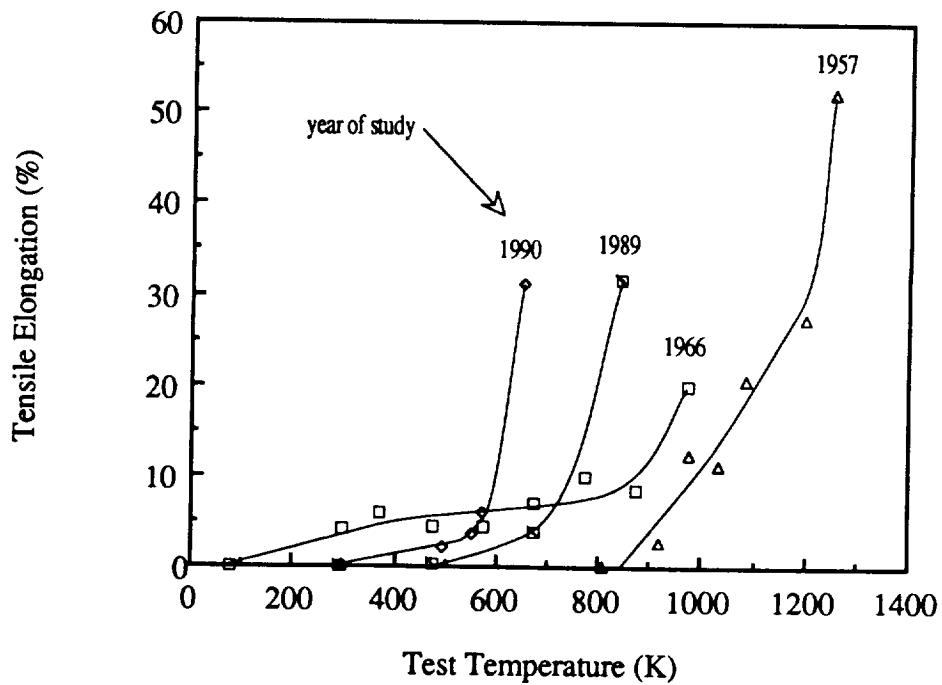

Figure 2-4. Ductility (Tension) of Polycrystalline NiAl as a Function of Temperature [32,33,34,49].

The collective ultimate tensile and fracture strength data of several investigators are plotted below in Figures 2-5 and 2-6. The behavior in compression is roughly regular, with approximately a 100 MPa increase in fracture strength for each 100K decrease in temperature. In contrast, the tensile fracture strengths show considerable variability and disagreement between studies below 1000K. This is probably due to differences in the defect size and population, as fracture strength is inversely related to maximum defect size. Although comparison between tensile and compressive fracture strengths is not strictly valid, it can be immediately seen from these plots that the large discrepancy is more pronounced at temperatures below 875K. This is likely due to the intervention of fracture in tension, which occurs at a lower stress than plastic deformation when at lower temperatures. In compression, although cracks form, they propagate in a stable fashion, and deformation can continue to greater strains without complete failure [34].
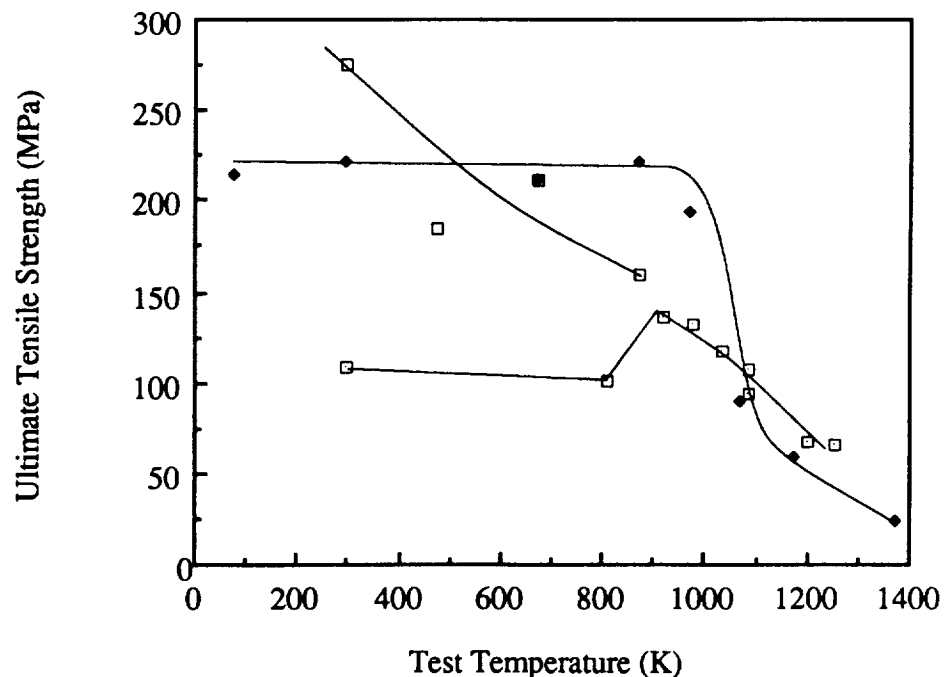

Figure 2-5. Ultimate Tensile Strength of Polycrystalline NiAl as a Function of Temperature [6, 32, 34, 49]
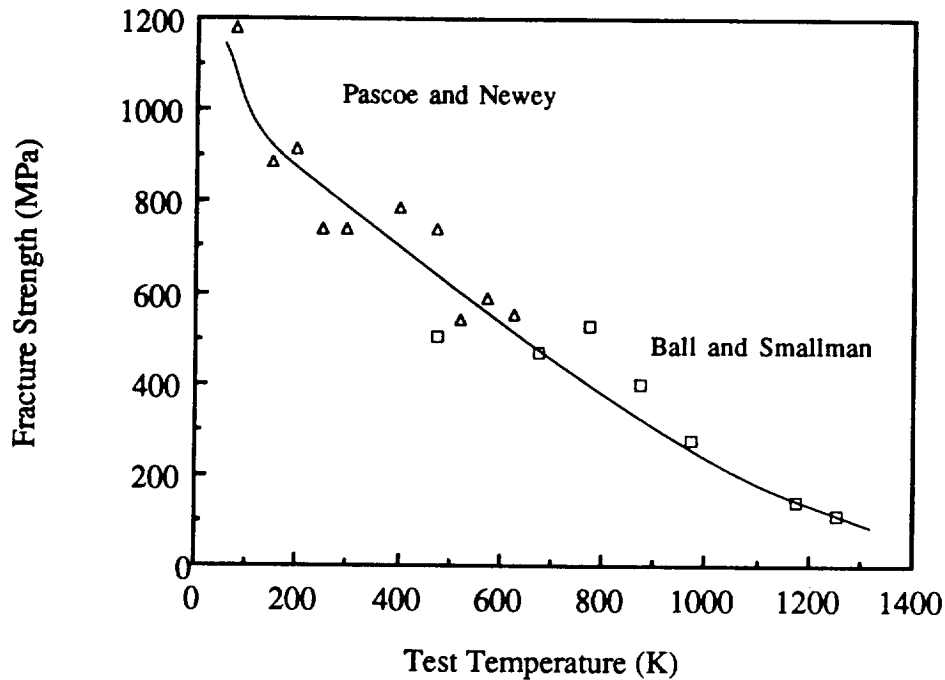
Figure 2-6. Fracture Strength in Compression of Polycrystalline NiAl as a Function of Temperature [7, 48]

Effect of Stoichiometry. The stoichiometry of the NiAl compound has been shown to have a marked effect on the mechanical properties. Exact stoichiometry, i.e. Ni/Al = 1, is associated with a maximum in ductility and a minimum in strength and hardness. Westbrook [23] first indicated this effect by microhardness testing of arc-melted buttons, Figure 2-7, and associated this behavior with the defect structures proposed by Bradley and Taylor [19]. Nickel-rich compositions are hardened relative to stoichiometric compositions by the presence of nickel atoms on aluminum sublattice sites (antisite defects) while aluminum-rich compositions are hardened to a greater extent by the occurrence of vacancies on the nickel sublattice. This behavior also extends to yield strength, which shows a minimum at the stoichiometric composition, Figure 2-8 [51].
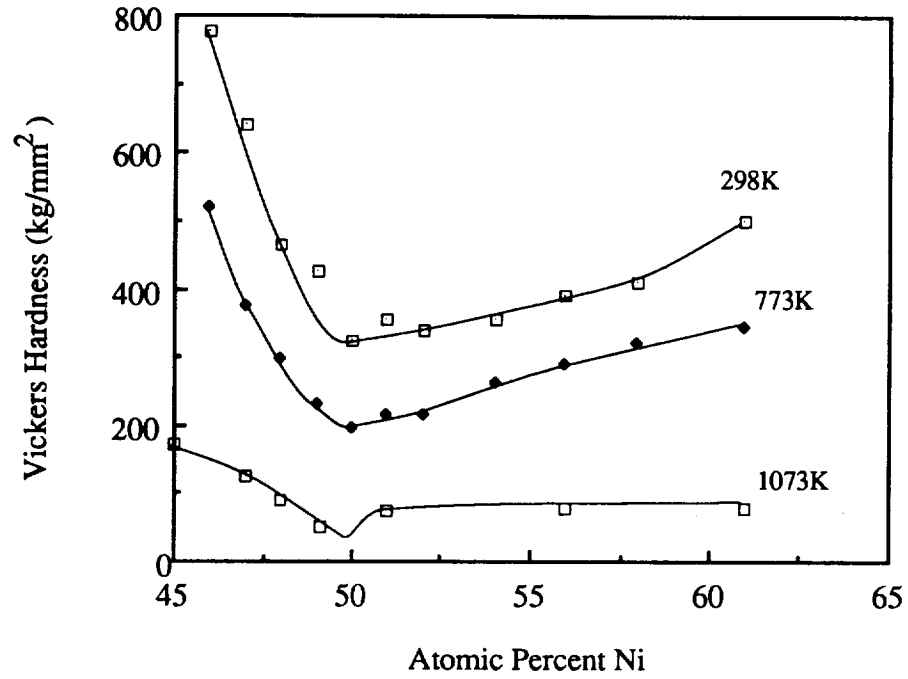
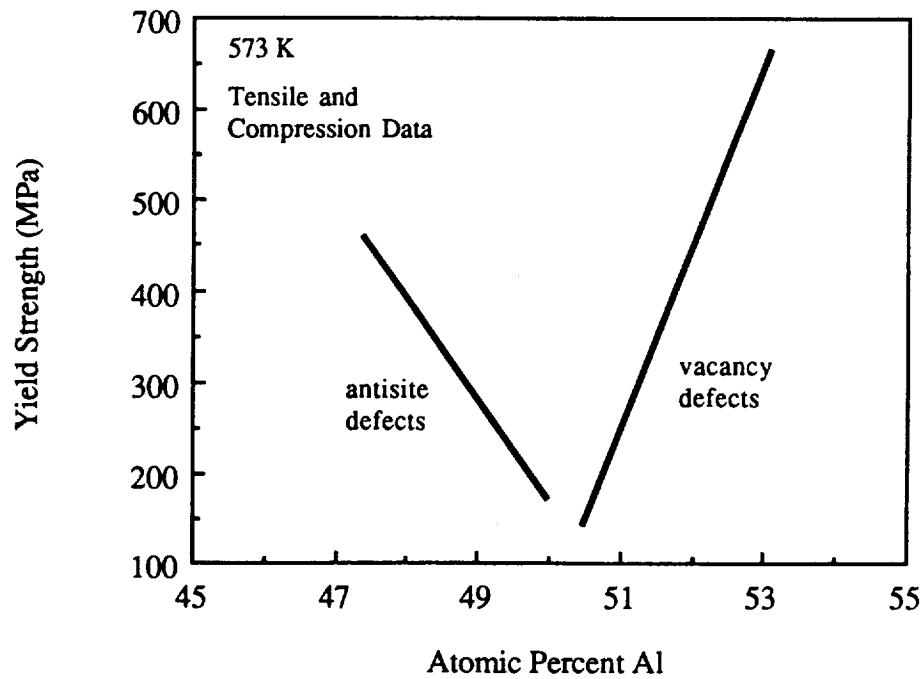Figure 2-7. Hardness of NiAl as a Function of Stoichiometry and Temperature [23]

Figure 2-8. Effect of Stoichiometry on Yield Strength of Polycrystalline NiAl [51]

There have been studies which appear to indicate that mechanical property maxima and minima occur for slightly aluminum-rich compositions [33, 51]. However, the difficulty in the exact determination of aluminum content (usually $\pm$ 1.0 atom percent) and the occurrence of physical property inflections at the exact stoichiometric composition [53, 54] indicate otherwise.

Effect of Grain Size. Based on early work by Cottrell [55], Schulson [39] suggested there may be a critical grain size, d_c, below which semi-brittle materials may exhibit tensile elongation. He derived the following expression:

$$d_c = \left[\frac{YK_{Ic} - k_y}{\sigma_o}\right]^2$$

where K_{Ic} is the plane strain fracture toughness, Y is a geometrical parameter (order of 1), and K_y and σ_o are the empirical Hall-Petch parameters. In this model, large grains are considered to develop larger stress concentrations at grain boundaries than small grains, due to the greater pileup of dislocations at the boundary. Assuming that the stresses to propagate slip across a boundary and to nucleate a microcrack are similar, larger grains should propagate cracks at a lower applied stress. Experimental verification of this concept was later reported by the same author [40, 41] for cast and extruded Ni-49Al. This alloy was extruded at a low temperature to retain a fine recrystallized grain structure, and subsequent annealing treatments were imposed to attain a range of grain diameters, from 5 to 140 μm. Tensile tests at temperatures ranging from 293 to 873K indicated the existence of a critical grain size, which was about 20 μm at 673K, Figure 2-9. However, the room-temperature ductility remained at about 2 percent, even at the finest grain size of 5 μm. This would seem to indicate the critical grain size for Ni-49Al at room temperature is somewhat less than 5 μm. This is supported by the work of Noebe et al. [34] who, using a

critical J-integral model developed by Chan [38], indicated that the critical grain size for NiAl was about 1 μm, and that only 5 percent elongation can be expected for a grain size of 0.1 μm. Further work by Nagpal and Baker [36] with cast and extruded Ni-50Al found no dependence of yield strength on grain size at 300K and, although finer grain sizes did produce greater elongation, only 2.3 percent was achieved for the finest size studied (13 μm). Quite recent results by Baker et al. [37] for Ni-45, -48 and -50Al again found little dependence of yield strength on grain size for Ni-50Al, but an increasing dependence with deviation from stoichiometry. Since these tests were conducted in compression, no ductility was reported.

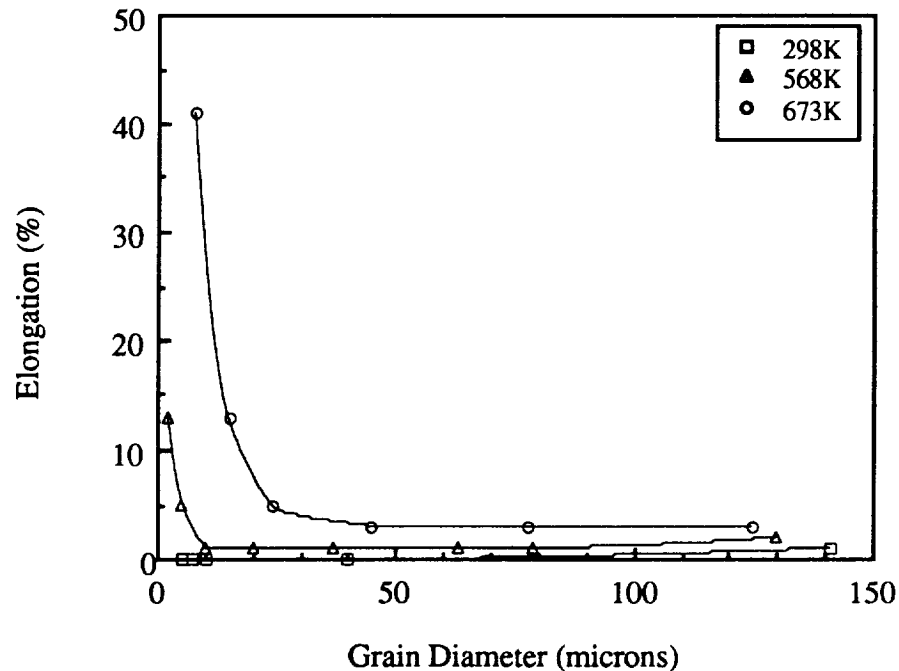Figure 2-9. Effect of Grain Size on Ductility of Ni-49Al [40]

There are current efforts to produce NiAl with a grain size less than 5 microns, utilizing special processing such as mechanical alloying plus extrusion to achieve a 1 μm grain size, and inert gas condensation to develop a 10 nm ("nanocrystalline") grain size [43, 56]. No tensile properties have been reported as yet for these materials.

Single Crystals

Yield Strength. The 0.2 percent offset yield strength for single crystal NiAl in several orientations is shown in Table 2-3 with data from several studies [7, 48, 57, 58, 59, 60]. A marked anisotropy in the yield strength is apparent, in spite of the differences between studies, and the typical strength of [100] (hard) oriented crystals is six times that of [111] (soft) oriented crystals. Such a large orientation dependence is a direct result of the preferred slip systems which are, in turn, a result of the directional bonding of NiAl. Despite the known elastic anisotropy of B2 compounds [61], there is little relationship between the elastic and plastic properties in this respect. For example, both NiAl and CuZn are B2 compounds and have Zener anisotropy factors of 3.28 and 4.95, respectively. However, because of the relatively larger metallic component of the bonding in CuZn, its yield strength ratio $\sigma_{[100]}/\sigma_{[111]} \sim 0.5$, versus 6 for NiAl [61]. Thus, the character of the bonding has a large effect in determining the properties of B2 compounds [62, 63, 64].

Table 2-3. Yield Strengths (MPa) of Single Crystal NiAl in Several Orientations at 300K

Reference	[001]	[011]	[111]	[001]/[111]	[001]/[011]
[56]	1050	297	145	7.2	3.5
[57]	981	294	147	6.7	3.3
[7]	1246	245	---	---	5.1
[18]	1385	195	---	---	7.1
[59]	---	217	264	5.25	---
[48]	497	120	---	---	4.1

Table 2-4. Ductility and Strain to Fracture Data for Single Crystal NiAl

Crystal Orientation	Tensile Ductility (%) (300 K)	Compressive Strain to Fracture (300 K)	BDTT (K)
[001]	0	0.03 to > 0.15	575-675
[011]	0.5 to 2.5	0.10 to > 0.50	475
[111]	0.5 to 2.5	0.12 to 0.17	475
[123]	0.7	0.06 to 0.36	450

Ductility. Contrary to the behavior of many metals, single crystals of NiAl display very limited ductility in tension at room temperature, although considerable strain to fracture is possible in compression. Measurable tensile ductility has not been observed in the "hard" [001] orientation. Some results of several single crystal studies [52, 59, 60, 65] are summarized in Table 2-4. Interestingly, superplastic-like behavior has been observed in [110] oriented crystals at 700K and $10^{-4}s^{-1}$ strain rate in which 200 percent elongation was achieved and "knife edge" fractures occurred [52].

These data bring to light a major concern, that the Peierls stress is very near to the fracture stress at low temperatures where thermal activation contributes only minimally to dislocation motion. Thus, the only way to increase the intrinsic toughness may be to decrease bond covalency and the degree of ordering, preferably without detracting significantly from the melting point or density.

Deformation and Fracture

The previous section was intended to give the reader an introduction to the mechanical behavior of NiAl at room temperature. The large anisotropy of the mechanical properties is a direct result of the operative slip systems and their relative difficulty of activation. This section on deformation and fracture will attempt to explain some of the controlling factors which determine the operative slip systems and their implications with respect to strength, ductility and fracture.

Plastic Deformation and Slip Systems

Plastic deformation, in the strict sense for crystalline materials, takes place by the motion of dislocations along particular directions and planes. For NiAl at ambient conditions there have been several studies, using both transmission electron microscopy (TEM) and surface slip trace analysis (SSTA), which have determined the operative slip

system to be <001>{110} for most cases [8, 9, 10, 57, 59, 60, 66, 67, 68, 69]. These are shown in Table 2-5. There are two special cases where the slip system differs. [100] oriented crystals, which have (ideally) no resolved shear stress on any <001>{110} system, may slip on <111>{110}, <111>{112}, or <110>{1$\bar{1}$0} [10, 59, 67, 68]. [110] oriented crystals appear to slip on {100} planes, which have a higher Schmid factor than {110} in this orientation [57, 60, 66, 68]. Only one detailed study of room-temperature deformed polycrystalline material (extruded powder) was noted, that of Bowman et al. [69]. Since extruded NiAl is known to develop a <111> fiber texture during extrusion [8, 42, 51], it might be expected that slip on the {100} plane would be quite rare, since in [111] single crystals slip occurs on the {110} plane.

Table 2-5. Observed Slip Systems in NiAl Deformed at 300K

Reference	Slip System	Method	Crystal Orientation
[56]	<001>{110}	SSTA	[111]
[7]	<001>{110}	SSTA	[111]
[67]	<001>{110}	TEM	[111]
[59]	<001>{110}	TEM	[111]
[48]	<001>{110}	TEM	[110]
[56]	<001>{100}	SSTA	[110]
[7]	<001>{100}	SSTA	[110]
[67]	<001>{100}	TEM	[110]
[59]	<001>{100}	TEM	[110]
[67]	<011>{0$\bar{1}$1}	TEM	[100]
[10]	<111>{???}	TEM	[100]
[66]	<111>{110}	TEM	[100]
[8]	<001>{???}	TEM	polycrystalline
[68]	<001>{110}	TEM	polycrystalline

The operation of <001> slip is not common to all B2 compounds; in a number of others, such as FeAl or CuZn, <111> slip is preferred [61]. The question of what factors are important in determining the slip system in B2 compounds was initially examined by Rachinger and Cottrell [64] who noted that highly ordered compounds of primarily ionic bonding displayed <001> slip while those with largely metallic bonding displayed <111>

slip. According to [64], perfect [111] or [011] dislocations, if present, should dissociate into unit dislocations according to

$$a[111] ---> a[011] + a[100]$$
$$a[011] ---> a[010] + a[001]$$

According to Frank's rule (the elastic energy of a dislocation is proportional to the square of the Burgers vector, $E_{el} \alpha \mu b^2$), there is no reduction in elastic energy in the above reactions. Therefore, any imposed stress with a component containing a unit dislocation will cause that component to move independently and dissociate the original dislocation. For <111> slip to occur, dissociation according to

$$a[111] ---> a/2[111] + a/2[111]$$
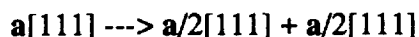
must take place. This reaction is accompanied by a reduction in elastic energy. The resulting antiphase boundary (APB) which must form between the two partial dislocations prevents <100> or <110> slip as long as the separation is significant, say the length of the Burgers vector. This model allows an estimate of a critical APB energy, above which <100> slip occurs, and below which <111> slip occurs, by the formula

$$\gamma_c = \alpha \mu b$$

where, μ is the shear modulus, $\alpha \mu$ is the theoretical shear strength ($\alpha \simeq 1/30$), and b is the Burgers vector. With typical values, γ_c is about 250 ergs/cm^2. By the nearest neighbor approximation, this equates to an ordering energy of about -0.06 eV, which may be considered the critical ordering energy separating the two slip behaviors. Rachinger and Cottrell found reasonable agreement with experiment for the compounds investigated;

however, Ball and Smallman [9] indicated that the above approach did not accurately predict the slip systems for NiAl or AuZn. Using the Bragg-Williams approximation for ordering energy, $kT_C/4$, and assuming that disordering occurs at the melting point of the compound, they calculated an ordering energy for NiAl of -0.04 eV. Since this value is less than the "critical" value determined by Rachinger and Cottrell, NiAl is predicted to exhibit <111> slip, which is incorrect. Therefore, Ball and Smallman addressed the problem of slip system prediction by using anisotropic elasticity theory to calculate the elastic energy and relative mobility of several dislocation configurations. Configurations with the lowest energy and highest mobility are expected to be most likely to operate. The elastic energy per unit length of dislocation, E, was determined by

$$E = \frac{kb^2}{4\pi} \ln\left(\frac{r}{r_0}\right)$$

where r and r_0 are the outer and inner cutoff radii, b is the Burgers vector and k is a function of the elastic moduli and the line direction of the dislocation. The mobility*, S, was estimated by

$$S = \frac{4\pi\zeta}{b} \exp\left(\frac{-2\pi\zeta}{b}\right)$$

where ζ is the dislocation width. ζ/b was estimated by

$$\frac{\zeta}{b} = \frac{kd}{2cb}$$

---

* "Mobility" is a misnomer, since higher values of S are considered less mobile [62].

where c is the shear modulus in the slip direction and d is the spacing between glide planes. That is, mobility increases with glide plane smoothness and ease of shear. Some results of Ball and Smallman's calculations are presented in Table 2-6.

Table 2-6. Elastic Energy and Mobility of Several Dislocation Configurations

<uvw>	{hkl}	character	E (ergs/cm)/10^4	S
111	$\bar{1}10$	screw/edge	13.9/29.3	0.98/0.42
110	$1\bar{1}0$	screw/edge	10.3/15.3	0.32/0.06
100	011	screw/edge	9.3/8.8	0.46/0.51
100	010	screw/edge	9.3/7.7	0.67/0.71

From these results it is obvious that dislocations with <100> Burgers vectors are of the lowest elastic energy and are therefore the most favorable to form. The <100>{011} and <100>{010} systems are competitive in this respect, although <100>{011} appears to be the more mobile of the two, and due to multiplication processes may be present in larger proportions. Regardless of slip plane, the <100> dislocations of edge or mixed [70] orientation are predicted to form more easily than the screw orientation. Slip by a/2<111> partial dislocations have not been considered in the above calculations because, as shown by both Ball and Smallman [9] and later by Potter [63], the total energy of such dislocations is still greater than that of the unit <100> dislocations due to the APB fault energy.

It is worth pointing out that all the early workers mentioned above [9, 63, 64] assumed the critical temperature for disordering (T_c) to be equal to the melting point (T_m) in determining the APB and ordering energy. Although this assumption seems reasonable, since long range order obviously cannot be maintained in a liquid, there is good reason to consider otherwise. First, from a thermodynamic point of view, the onset of melting only indicates that the liquid has a lower free energy than the solid, not that disordering is imminent. Second, there is experimental evidence [25] that some degree of short range

order is maintained in the liquid well above the melting point. Finally, the APB energy for NiAl calculated by Potter [63] based on $T_c = T_m$ for faulting on $<111>\{110\}$ was 223 ergs/cm^2. This is at strong variance with values determined both experimentally by TEM analysis [71] (at least 500 ergs/cm^2) and by first principles calculations [28, 72] (800 ergs/cm^2). Thus, NiAl is much less the "borderline" case of $<100>$ slip than originally thought.

Lautenschlager et al. [62] also examined the problem of slip system prediction in CsCl type compounds. They studied the effect of the atom size ratio, R_A/R_B, as well as the bonding type and crystal orientation (with respect to applied stress), on the observed slip system. Using a hard-sphere model, they determined that R_A/R_B has a strong effect on the slip plane roughness , as much better packing can be achieved when R_A/R_B tends toward 0.732. For example, the perpendicular displacement of the glide plane during $<100>\{011\}$ slip is 0.159a for $R_A/R_B = 0.732$ and 0.293a for $R_A = R_B$; for $<111>\{011\}$ slip these values are 0.209a and 0.063a, respectively. Therefore, $<111>$ slip is promoted when R_A and R_B are similar. The effect of bonding type (ionic, covalent or metallic) was observed to promote $<111>$ slip when metallic bonding dominates and $<001>$ otherwise. Crystal orientation, relative to the applied stress, affects the preferred slip system according to Schmid factor considerations, and thereby promotes $<111>$ Burgers vectors in general. The orientation effect is illustrated in Figure 2-10, after Lautenschlager [62].

For compounds such as NiAl, according to Lautenschlager et al., the bonding and orientation factors tend to cancel one another, and relegate the slip system choice to the R_A/R_B ratio. The estimation of the amount of local strain at the glide plane by a hard sphere model for each slip system provides criteria for predicting the most likely system to operate. By this approach, compounds with R_A/R_B tending to 1.000 will prefer $<111>$ slip and those with R_A/R_B tending to 0.732 will prefer $<100>$ slip, with the critical R_A/R_B ratio being about 0.95. For NiAl, R_A/R_B was estimated to be 0.847, which predicts $<100>\{011\}$, the experimentally observed system. Of course, accurate determination of

R_A/R_B for any intermetallic compound is difficult, as it depends on the known values for the atomic radii and the degree of charge depletion or accumulation. Further, the charge distribution has no requirement of sphericity, particularly in cases of strong, directional bonding. In fact, close examination of atom positions during <100>{011} slip of CsCl compounds reveals that this type of slip tends to maximize the continuous contact between unlike atoms.
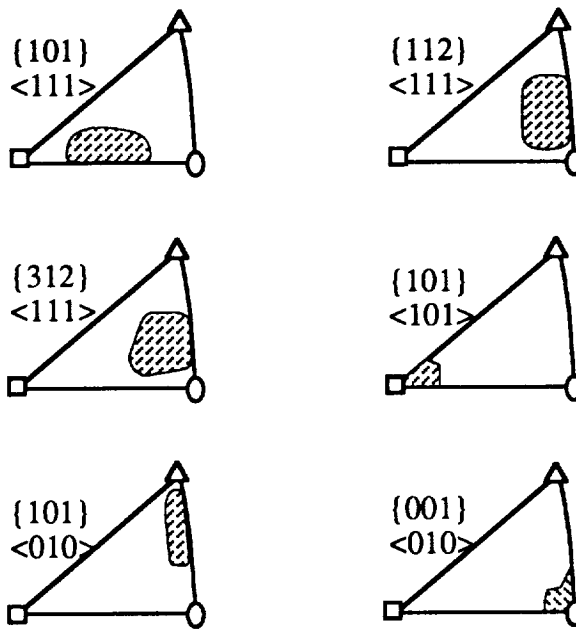

Figure 2-10. Influence of Crystal Orientation on B2 Slip Systems. Each slip system is favored in the shaded regions. After Lautenschlager et al. [62].

Implications of von Mises Criterion

The sole operation of <100>{011} slip can produce only three independent slip systems [12]. This number is insufficient to allow general plastic flow in a polycrystalline body, as five independent systems are required to produce the arbitrary shape change of each grain to maintain contact with adjacent grains [13]. Therefore, even though the critical resolved shear stress (CRSS) for <100>{011} slip is reasonably low [57], compressive

deformations as small as 1 percent have been shown to produce visible grain boundary fissures due to poor slip transfer to adjacent grains [69]. In tension, these fissures provide an easy path for intergranular fracture. This process is illustrated schematically in Figure 2-11. The lack of sufficient slip systems in NiAl has prompted research [14, 15, 16, 73] to alter the primary slip system from <100>{011} to <111>{110}, which has the required number of independent slip systems.

The combined operation of two slip system families can also provide five independent slip systems, when they cannot individually [74]. For example, combined operation of <100>{011} (three systems) and <110>{1T0} (two systems) produces five independent systems. This provides an alternative for satisfying the von Mises criterion without <111> slip, which would otherwise require a significant reduction in ordering energy.
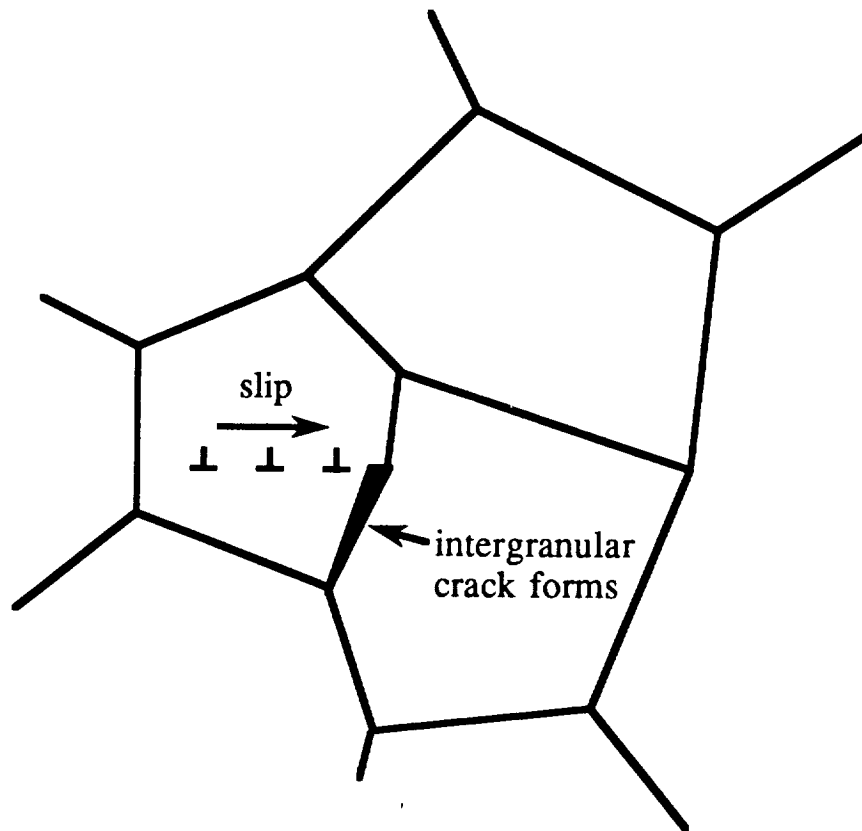

Figure 2-11. Effect of Insufficient Number of Independent Slip Systems on Plastic Deformation in Polycrystals

Fracture of NiAl

The tensile fracture mode of polycrystalline NiAl is intergranular (IG) at the stoichiometric composition [4, 49] and transgranular (TG) in off-stoichiometric compositions [15]. As described above, IG fracture in NiAl is a natural result of plastic flow on three independent slip systems with no other deformation mechanisms. This is due to a shape incompatibility between adjacent grains and the creation of IG cracks which coalesce and lead to catastrophic IG failure. However, for certain crack plane/grain boundary orientations, it is not unreasonable that TG failure (cleavage) will be favored. The TG failure in off-stoichiometric compositions is probably due to the difficulty of dislocation motion past constitutional point defects. The preferred TG cleavage plane has been reported to be {110} in stoichiometric NiAl [75].

Other arguments have been put forth to explain the presence of IG fracture in stoichiometric NiAl. The effect of certain embrittling agents, such as phosphorus or sulfur, which segregate to grain boundaries, is well-documented in ferrous metallurgy literature and has been considered to explain IG fracture in NiAl. Westbrook [76] investigated the effect of oxygen and/or nitrogen on the grain boundary hardness of AgMg and NiAl and concluded that these interstitials segregated to the grain boundary regions and increased the BDTT. However, more recent work by Zeller et al. [77] and George et al. [35] utilizing scanning Auger microscopy (SAM) has shown that grain boundaries in binary NiAl are free of any segregated impurities, including carbon, oxygen, boron or sulphur. This has been interpreted [35] as an indication that the grain boundaries in NiAl are intrinsically weak. In contrast, grain boundary structure simulations [78] seem to indicate that the boundaries should not be intrinsically brittle, provided there are no excess aluminum atoms at the boundary. Since off-stoichiometric NiAl alloys tend to fracture in a TG mode [15], it appears that grain boundaries are as strong as the bulk. Therefore, one would conclude that

the grain boundaries in NiAl are not intrinsically (structurally) weak, but become the site of Griffith defects when slip is activated.

Ternary Alloying Effects on Plastic Deformation

This section reviews the effects of ternary alloying additions to NiAl on plastic deformation and mechanical properties. Primarily single phase B2 alloys are considered. For convenience, microalloying (less than one atomic percent) and macroalloying additions are discussed separately.

Microalloying Additions

Boron. Boron has been found to prevent grain boundary fracture in Ni₃Al and to induce ductility in doing so. Based on this work, boron was also added to NiAl in hopes of achieving the same result [15, 35]. Law and Blackburn [15] added 0.25 percent boron to stoichiometric NiAl in both cast/extruded and powder/extruded forms and found no increase in ductility. In fact, the BDTT was elevated nearly 200K by the boron additions. The fracture mode was reported to shift from IG to TG, although whether this was due to an increase in grain boundary cohesiveness or the lack of plastic flow due to solid solution strengthening is not known. In a later study, George and Liu [35] added 30, 100 and 300 wppm (parts per million by weight) to cast and extruded NiAl alloys and compared them with binary NiAl. They found that boron did not impart any ductility to NiAl, although the fracture mode was reported to be TG with as little as 30 wppm while the percent elongation remained about two percent. George and Liu explained the change in fracture mode as being due to grain boundary strengthening by the boron, and did indeed find a significant segregation of boron to the grain boundaries. The boron additions also dramatically increased the strength of the alloys, about 4500 MPa/atomic percent boron. Similar ductility between the binary and NiAl+30 wppm alloys seems to indicate that the change in

fracture mode was due to a grain boundary effect and not simple yield strength elevation (lack of plastic flow). Strengthening of the grain boundaries by boron would make IG cracking more difficult, but would not necessarily facilitate slip transferral to adjacent grains or activate additional slip systems. Thus, NiAl with 30 wppm boron probably has smaller Griffith defects due to unaccommodated slip at the grain boundary. If the grain boundaries are truly strengthened, further cracking should take place along cleavage planes to produce the observed TG fractures. That is, the observation of grain boundary strengthening by boron addition does not imply that the boundaries are inherently brittle.

Carbon. Carbon is a common impurity in most commercial purity elemental nickel and, therefore, is probably present in nearly all NiAl alloys to some degree. George and Liu [35] intentionally added 300 wppm carbon to "high purity" NiAl and noted a strength increase similar to that of boron; no tensile elongation was measurable. The fracture mode for the carbon-containing alloy was IG and SAM analysis of the grain boundary surfaces showed that carbon does not segregate to the grain boundaries. (Recent re-analysis [79] of the published fractographs for this alloy by point counting has shown it to be mostly TG.)

Beryllium. In the same study, George and Liu also measured the effect of adding 500 wppm beryllium to NiAl. This alloy exhibited about 3 percent tensile elongation at room temperature and a slightly elevated yield strength (~15 percent greater than binary NiAl). Fracture occurred by IG separation and no beryllium appeared to segregate to the grain boundaries, which indicates that beryllium has little effect upon slip in NiAl aside from a small solid solution hardening effect.

Chromium, Zirconium and Titanium. These elements are known to be effective "getters" for interstitial elements such as carbon or oxygen. Field et al.. [18] added 0.05 and 0.2 atomic percent chromium to [001] oriented single crystals in an effort to measure the effect of chromium on dislocation type and character during compressive deformation. The chromium appeared to promote <111> slip relative to the binary; however, no APBs in the <111> dislocations were visible by TEM and thus no significant reductions in the

APB energy were apparent . As shown above, <111> slip in binary NiAl is the preferred slip system in this orientation in the absence of kinking, regardless of the presence of chromium, which makes any conclusions concerning slip somewhat tentative. It was suggested by Field et al. [18] that the ease of <111> dislocation activation was due to a gettering effect of the chromium, since Cr_7C_3 carbide precipitates were observed during TEM examination. To further investigate this effect, another NiAl alloy containing 0.45 percent Ti and 0.05 percent Zr (two very potent carbon scavengers) was prepared. This alloy behaved similarly to the chromium-containing alloys, although much greater strengthening was observed, perhaps due to the larger size of the Zr atoms. No solute softening was apparent, which may indicate a lack of gettering since the elements responsible for solid solution strengthening are removed from solution to form carbides. Therefore, the enhanced <111> activation was considered to be due to "differential proportional hardening," a general strengthening of all slip systems which decreases the relative differences in strength.

Zirconium was added to polycrystalline (cast and extruded) NiAl in a study by Bowman et al. [69] at the 0.05 percent (500 ppm) level. In this study, Zr was found to elevate the BDTT by about 300K and increase the strength significantly. No tensile ductility was observed and the fracture mode in the Zr-doped alloys was a combination of IG and TG. Extensive TEM examination determined that the operative slip system in both binary and Zr-containing alloys was <001>{110}. Therefore, Zr appears to have no effect on the operative slip system in NiAl.

Iron, Gallium and Molybdenum. A recent study by Darolia [3] indicated that 0.25 percent Fe increases the tensile ductility of [110] single crystals from two to nearly six percent at room temperature. Similar effects of 0.1 percent Ga and Mo were also measured, in which the ductilities were 4.5 and 2 percent, respectively. As shown in Table 2-4, typically one to two percent tensile elongation is measured in single crystals of NiAl in this orientation, which by comparison makes the results of Darolia quite striking. Since the

beneficial effect of these elements disappears at higher alloying levels, the mechanism(s) responsible is unknown at this time. However, since the slip system remains unchanged from <001>{110} [80] it is possible that the solute atoms assist in dislocation nucleation. This effect would likely increase the homogeneity of slip and therefore distribute deformation more evenly throughout the crystal instead of to confined slip bands.

Macroalloying Additions

To effect a change in the basic plastic deformation behavior of NiAl by adding a ternary addition, the addition must be readily soluble. The phase equilibria of a number of elements may be conveniently grouped according to the ternary element's position in the periodic table, Figure 2-12.

Al-Ni-X ternary phase(s)
NiAl-X pseudobinary eutectic
High solubility in NiAl and/or forms B2 aluminide

Figure 2-12. Portion of Periodic Table of the Elements Illustrating General Alloying Behavior of Ternary Additions to NiAl

The elements in Groups IIIB, IVB and VB (scandium, titanium, vanadium, yttrium, zirconium, niobium, lanthanum, hafnium and tantalum) form at least one ternary intermetallic compound with nickel and aluminum, usually the Heusler phase, Ni_2AlX, and are usually of limited solubility [81, 82, 83, 84, 85, 86, 87, 88]. Elements in Group VIIB (chromium, molybdenum, tungsten), and also rhenium, form "pseudobinary"

eutectic systems with NiAl and also have limited solubility in NiAl [16, 17, 84, 89, 90, 91, 92]. Vanadium also forms a pseudobinary eutectic with NiAl [84, 93], and is unique in that it is the only element known to fit into the first and second categories. The pseudobinary eutectic systems allow two phase equilibrium between NiAl and the BCC element and have potential for in situ ductile phase reinforcement. In fact, considerable research has gone into the development of directionally solidified pseudobinary eutectics such as NiAl-Cr and NiAl-Mo in which rods of alpha-Cr or alpha-Mo are distributed in a β-NiAl matrix [94]. The Group VIII elements (plus manganese and copper) display large solubility in NiAl and their B2 aluminides are often isostructural [73, 88, 95, 96, 97, 98, 99, 100, 101, 102]. This latter category offers considerable alloying potential.

Iron. Several studies have been conducted on single phase ternary NiAl+Fe alloys [15, 73, 103, 104, 105, 106, 107]. Iron additions are perhaps the most intuitively obvious, since FeAl can be ductile at room temperature, exhibits <111> slip [108], and is isostructural with NiAl [100]. Law and Blackburn [15] added from 10 to 30 percent iron to NiAl alloys containing a constant 48.5 percent aluminum and concluded the alloys were too brittle for further testing based on cracks observed during machining. Patrick et al. [73] produced a series of ternary alloys along the compositional tie-line from Ni-40Al to Fe-40Al, deformed them in compression at room temperature, and analyzed the dislocations by TEM. Their results indicated that more than 30 percent iron was necessary to effect a change in Burgers vector from <100> to <111>. In 1984, Inoue et al [107] reported a tensile ductility of five percent for single phase Ni-30Al-20Fe wire produced by rapid solidification processing (RSP). RSP induced a martensitic reaction, B2 → L2$_0$, and a very fine grain size of 4 microns. In the same study, Ni-30Al-30Fe processed in the same manner exhibited nil ductility. Two recent studies [103, 106] of Ni-30Al-20Fe demonstrated that cast and extruded material with a 25 μm grain size has essentially zero ductility and slips by the motion of <100> dislocations. In contrast, Kostrubanic et al. [104, 105] has shown that the addition of a fine dispersion of Y_2O_3 particles to Ni-35Al-

20Fe RSP ribbon by mechanical alloying and hot pressing can produce ambient toughness values as high as 34 MPa/m$^{0.5}$, as determined by four-point bending of notched specimens (ASTM E399). This is a substantial improvement over binary stoichiometric NiAl which has a toughness of about 6-8 MPa/m$^{0.5}$ [74, 98] and was considered to be due to the very fine grain size and induced plastic flow [105].

Chromium. Manganese and Gallium. During the course of a study of the effect of alloying on the microstructure and mechanical properties of cast polycrystalline NiAl-base alloys, Law and Blackburn [15] noted four compositions which were damage-tolerant enough to withstand electrostatic discharge machining (EDM) without extensive cracking: Ni-48.5Al, Ni-48.5Al-5Cr, Ni-44Al-5Mn and Ni-48Al-0.5Ga. After deforming compression specimens of these alloys to about 2 percent strain at room temperature, TEM analysis was conducted. Both the chromium- and manganese-containing alloys were determined to contain dislocations with <111> Burgers vectors. Slip in Ni-48.5Al-5Cr was reported to occur on {112} planes within well-defined slip bands among spherical alpha-chromium precipitates. These dislocations were reportedly of screw character and were arranged in dipoles within the bands. In Ni-44Al-5Mn, <111>{112} slip was reported although the dislocations were not confined to slip bands. In this case, the dislocations were primarily edge in nature. Analysis of the binary and gallium-containing alloys deformed at 300K revealed only <100>{011} slip. Some of the results of Law and Blackburn are summarized in Table 2-7. In spite of the reported change in slip system for the chromium- and manganese-containing alloys, no tensile ductility was apparent at 300K. The low mobility of <111> dislocations was offered as a possible explanation for this lack of ductility.

In a related study [16], directionally-solidified Ni-43Al-5Cr was also reported to exhibit <111> slip. However, since the growth direction of the ingot was [101], as was as the compression axis of the machined specimens, the resolved shear stress on the <100>{011} systems were low compared with those on the <111>{112} systems. In this

manner, <100> slip was discouraged by at least a factor of two, based on Schmid factor comparisons of the two most favored <100> and <111> containing systems. Although it can be argued that <111> slip was made less difficult (recall that a factor of six was noted above for binary NiAl), no actual preference for <111> slip over <100> slip was demonstrated.

Table 2-7. TEM Results of Law and Blackburn [15] for Polycrystalline NiAl-base Ternary Alloys Deformed at 300K

Composition (at.%)	Slip System	Character
Ni-48.5Al	<001>{110}	edge
Ni-48Al-0.5Ga	<001>{110}	edge
Ni-46.1Al-2.4Ga	<001>{110}	edge
Ni-48.5Al-5.2Cr	<$\bar{1}$11>{1$\bar{1}$2}	screw
Ni-43.7Al-4.9Mn	<$\bar{1}$11>{1$\bar{1}$2}	edge

Field et al [18] evaluated the effect of chromium additions on slip systems and mechanical properties in [100] oriented single crystals at room-temperature. As noted above, [100] oriented crystals slip by <111> dislocations in binary NiAl in the absence of kinking. In Ni-49Al-6Cr and Ni-48Al-2Cr alloys, substantial precipitation of alpha-chromium was observed. Chromium and NiAl have very similar lattice parameters, and fine-scale solid state precipitation produces semicoherent interfaces which contain interfacial nets of dislocations to accommodate the strain [109, 110]. These nets appear to be of two types, square and hexagonal. Walter and Cline [109] determined the square nets to consist of orthogonal <100> dislocations. Field et al. [18] showed the hexagonal nets to consist of <100> and 1/2<111> dislocations and speculated that these arrays may serve as sources for <111> dislocations. Although <111> dislocations were observed in the microstructure, no conclusive evidence was apparent to support this idea. Further investigation of the slip bands of <111> dislocations indicated they were being generated from Cr_7C_3 precipitates, which have an orientation relationship with the matrix of

$$[100]_{ppt} \parallel [011]_{matrix}$$

$$(001)_{ppt} \parallel (11\bar{1})_{matrix}$$

This implied that <111> dislocations were more easily generated at the carbide/matrix interface than other sources, but says little about true alteration of the slip system from that observed in binary NiAl. The occurrence of the Cr_7C_3 phase is curious, since $Cr_{23}C_6$ is the carbide phase in equilibrium with alpha-chromium in a binary system [111]. This may be due to the relative ease of nucleation of the Cr_7C_3 phase for the above orientation relationship. In the same study, the results of alloys containing lower levels of chromium indicated that a general solid solution strengthening makes <111> slip relatively more favorable than in the binary. No definitive evidence of the preference of <100> slip over <111> slip in any orientation other than [100] was shown.

Other Elements. In addition to those already mentioned, Law and Blackburn [15] also examined the effects of additions of cobalt, beryllium, titanium, niobium, tantalum, silicon, vanadium and zirconium. However, none of the ternary alloys containing these additions was reported to demonstrate any ductility at room temperature, nor were any detailed examinations of slip phenomena performed. Darolia et al. [14] studied the effect of up to 10 percent vanadium, substituted for aluminum, on the slip and mechanical properties in [100] oriented single crystals. They determined that vanadium causes significant solid solution hardening and also noted the presence of Ni_2AlV (Heusler, $L2_1$) precipitates which are expected to produce further strengthening. None of the alloys exhibited measurable room-temperature ductility and TEM analysis revealed only <100> dislocations.

Prediction of Alloying Effects on Plastic Deformation of NiAl

Generally, two approaches to predicting the effect of alloying on plastic deformation have been utilized, semi-empirical and theoretical. Both acknowledge the high ordering energy of NiAl, which is directly related to the high APB energy. These high energies promote nickel-aluminum bonds and likewise resist like-pair bonds, which is the reason for the difficulty of <111>{110} slip and ultimately, the reason for the operation of only three independent slip systems. These approaches endeavor to make <111> slip easier by substituting elements on the B2 NiAl lattice which will lower the ordering energy of the compound.

Phenomenological Approaches. The calculated and measured ordering energies for a number of B2 aluminides show a steady reduction in magnitude [112, 113]

$$NiAl > CoAl > FeAl > MnAl > CrAl > VAl$$
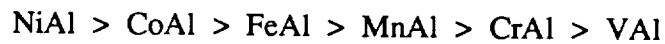
Therefore, it is logical to add elements such as vanadium, chromium or manganese to NiAl, substituted for nickel, to try to promote <111> slip. The relationship between ordering energy (or heat of formation) and slip system has been demonstrated by Cotton et al. [114], in which lower ordering energies correspond to <111> slip while higher ordering energies correspond to <100> slip, Figure 2-13. Another semi-empirical approach is to choose atoms for substitution based on their respective size and alter the mean atomic radii ratio (R_{Ni}/R_{Al}). Then, as described by Lautenschlager et al. [62], when R_{Ni}/R_{Al} tends to 1.000, <111> slip will be preferred. For instance, aluminum is a much larger atom than nickel. To bring R_{Ni}/R_{Al} nearer to 1.000, one should substitute larger atoms for nickel. Law and Blackburn [15] considered both of these approaches in devising their alloying schemes. In the latter case, they added Be for aluminum in an attempt to bring the mean

R_{Ni}/R_{Al} nearer to 1.000. As already noted, none of the alloys investigated by Law and Blackburn displayed any measurable tensile ductility at room temperature, probably because of solid solution hardening.

Theoretical-Computational Approaches. Quite recently, first-principles calculations based on interatomic potentials, combined with the use of high-speed supercomputers, have allowed the *a priori* determination of material properties. Calculations for materials for which some properties are already known, such as NiAl, allow a check for accuracy. Hong and Freeman [29, 72, 115] employed all-electron self-consistent total-energy linear-muffin-tin-orbital calculations using a super cell approach to determine the $1/2<111>\{110\}$ and $1/2<111>\{112\}$ APB energies for binary and ternary NiAl alloys. For binary stoichiometric NiAl they calculated energies of about 800 mJm^{-2} for both cases, a result which is consistent with the experimental results of Vessyiere and Noebe [71] . The substitution of chromium for aluminum, or vanadium for nickel, is predicted to decrease the calculated APB energy to 250 mJm^{-2}. However, the supercell models employed in these calculations assumed 17 percent solubility; as already mentioned, the solubilities for these elements are quite low (less than two percent at 300K). Fu and Yoo [28] also determined the $<111>\{110\}$ APB energy for binary NiAl using total energy calculations and arrived at a value of 810 mJm^{-2}. Similar to Hong and Freeman, they also suggested that substitutions of less electropositive 3d transition elements for aluminum would decrease the APB energy. In unpublished work, Hahn and Vedula [116] examined the effect of substitution of a large number of ternary elements on the calculated ordering energy, using the pseudopotential method. Their results indicated that the substitution of rhenium, vanadium or silicon for nickel should decrease the ordering energy of NiAl.

The phenomenological and theoretical models discussed above ignore the effect of solid solution hardening. For a substitutional element to effect a basic change in the bonding of NiAl, it is reasonable that substantial amounts must be soluble, based on the information shown in Figure 2-13. As a first approximation, a rule-of-mixtures may be

applied to estimate the amount of solute required to place the alloyed NiAl compound within the region of <111> slip. This line of reasoning would require at least half the nickel to be replaced with another transition element, a substantial amount. If such additions cause the yield strength to be increased above the fracture strength by solid solution hardening before the ordering energy is effectively decreased, the alloy will not be able to undergo any significant deformation prior to fracture and their purpose will be defeated.
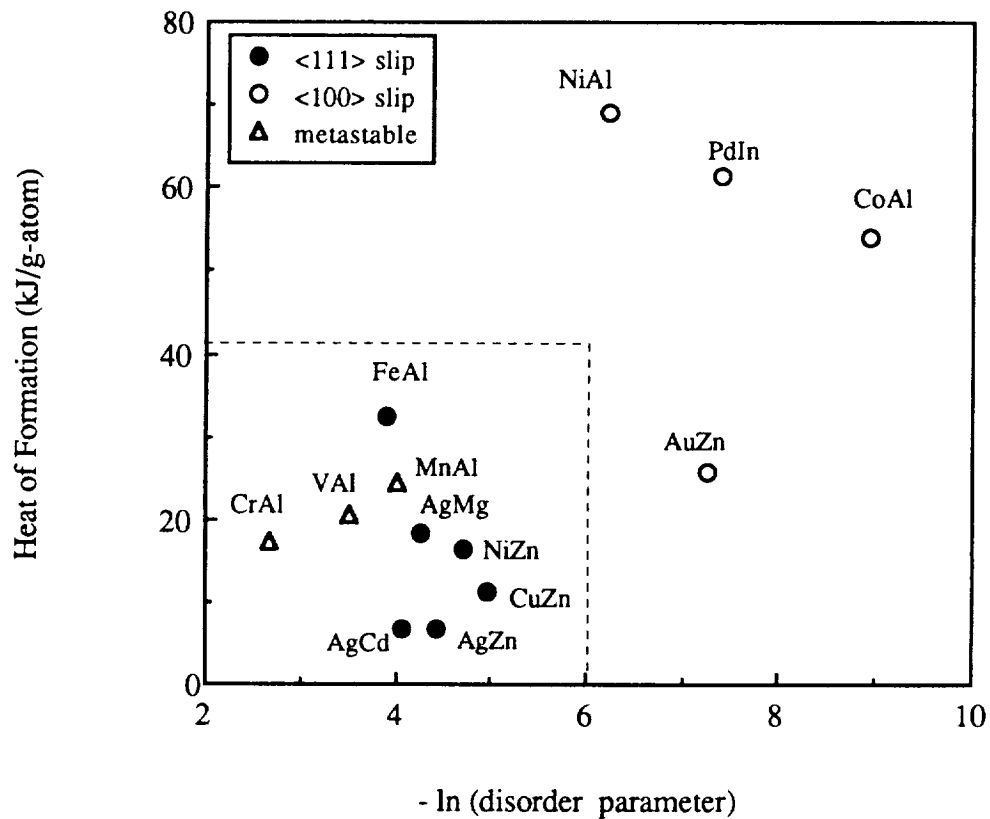

Figure 2-13. Relationship Between Heat of Formation, Degree of Disorder and Observed Slip System at 300K. Note that higher order and larger heats of formation correspond to <100> slip [114].

Another important factor which has not been considered in current theoretical models is site preference of the ternary addition. If the alloying addition is substituted

compositionally for a particular site (say nickel), but instead prefers the other site (say aluminum), then the intended effect has not been realized. Further, such a case would lead to nickel vacancies and the associated hardening. Therefore, not only must the substitutional addition decrease the ordering energy, it must be adequately soluble, an impotent hardener, and exhibit the proper site preference in the NiAl lattice.

CHAPTER 3
EXPERIMENTAL PROCEDURE

The materials used in this study were obtained in several forms: homogenized arc-melted (HAM) castings, as-arc-melted (AM) castings, extruded vacuum-induction-melted (XVIM) castings and extruded atomized powder (XAP). The different production methods are described separately below. The experimental work was performed while in residence at the NASA - Lewis Research Center (LRC) in Cleveland, Ohio. Compositions are given in atomic percent, e.g. Ni-45Al-5Cr indicates 45 atomic percent aluminum, 5 atomic percent chromium and 50 atomic percent Ni.

Materials

HAM and AM Castings

The nominal and analyzed compositions of the 15 castings used in this study are plotted in Figure 3-1. The castings were produced by nonconsumable arc melting 0.070 kg of constituent elements (99.95 percent nickel, 99.999 percent aluminum, 99.99 percent chromium, by weight) in a water-cooled copper bowl under argon to produce buttons, Figure 3-2, and then inverting and remelting twice more to insure homogeneity. Subsequent weighing of the buttons indicated weight losses were generally less than 0.1 percent. The buttons were cast into a copper mold of approximate dimensions 50 mm x 13 mm x 13 mm to produce somewhat rectangular castings with a small "buttonhead" to reduce pipe shrinkage. The castings were subsequently homogenized by heating under slow-flowing commercial purity argon for 24 hours at 1400°C, utilizing heating and cooling rates of 5K per minute. The AM castings were analyzed in the as-cast state.

XVIM and XAP Extrusions

Five compositions were produced by this processing route, to coincide with five of the HAM casting compositions. 1 kg charges of constituent elements were melted together under vacuum by induction heating to produce 0.15 m by 0.05 m diameter castings. One composition, Ni-45Al-5Cr, was vacuum atomized to produce powder by Homogeneous Metals, Inc. The castings and resulting atomized powder were enclosed in 1018 steel cans by tungsten-inert-gas welding which were subsequently evacuated and sealed by electron beam welding. Each canned alloy was heated at 1127°C for four hours prior to extrusion in a Loewy vertical hydraulic 340 ton press at an extrusion ratio of 16:1.
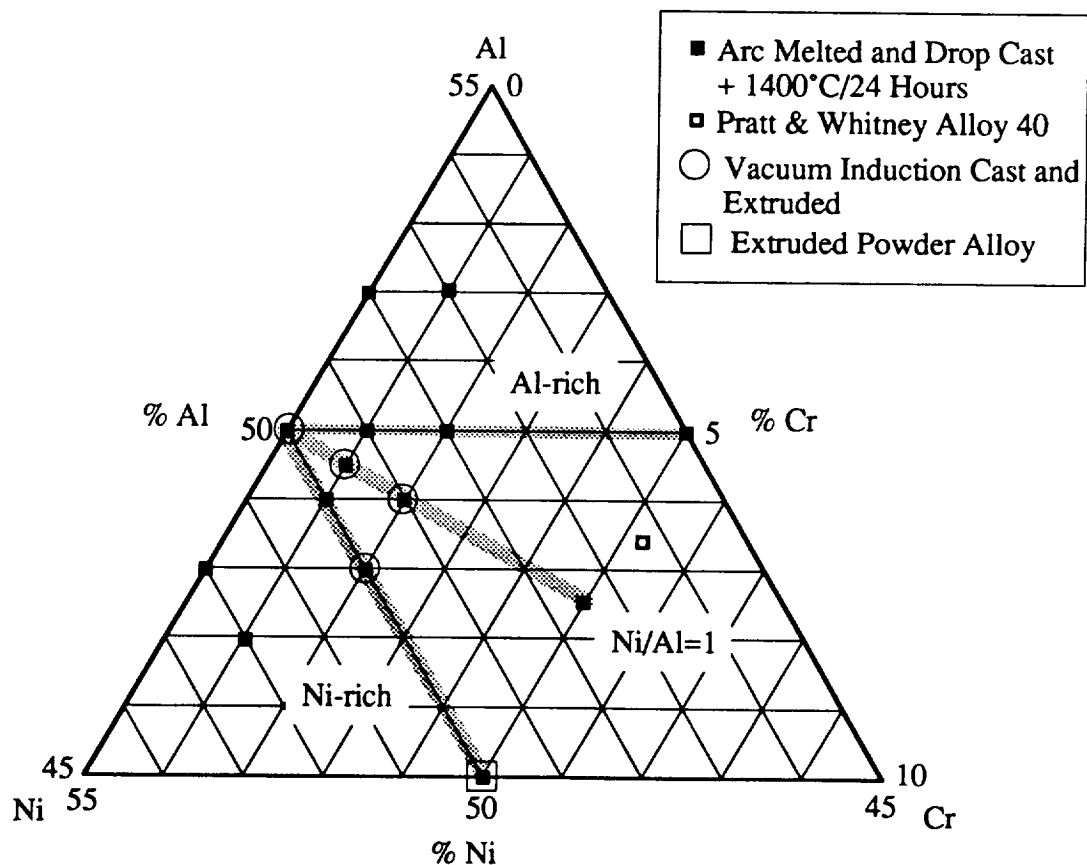
Figure 3-1. Ternary Diagram of Alloy Compositions in Current Study

Prior to further investigation, the extrusions were cut into 0.05 m lengths and the steel can removed chemically by immersion in an aqueous solution of 50 percent nitric acid with a small amount of sulfuric acid for 1 hour at room temperature.

Other Materials

During the course of the investigation it was necessary to obtain some alloys which, although not an intrinsic part of the original study, were necessary to resolve particular questions. These include the following: (1) a portion of a vacuum-induction-melted Ni-48.5Al-4.2Cr casting produced at United Technologies - Pratt and Whitney which was originally investigated in reference [15] (courtesy Dr. S. Russell); (2) three NiAl single crystals in [100], [111] and [123] orientations from LRC (courtesy R.D. Noebe) for microhardness determination only; (3) HAM Ni-43Al and Ni-43Al-5Cr castings in response to discussions with D.B. Miracle and his work referenced in [16]; (4) two series of five HAM castings containing 0, 0.25, 0.50, 0.75 and 1 atomic percent chromium (Ni/Al ratio = 1), to establish the effect of constituent nickel reported to contain very low interstitial levels (high-purity nickel provided courtesy of Dr. S. Chumley, Ames Research Laboratory, Ames, Iowa) and (5) seven other additional HAM castings for microhardness determination only, to establish trends indicated by the original 15 compositions described above.

Optical Microscopy

Transverse cross-sections of the castings and extrusions were removed by abrasive wheel cutting for optical metallographic analysis and microhardness testing. The slices were metallographically prepared used standard mounting and grinding procedures, polished through 0.05 μm alumina media and then etched with saturated molybdic acid
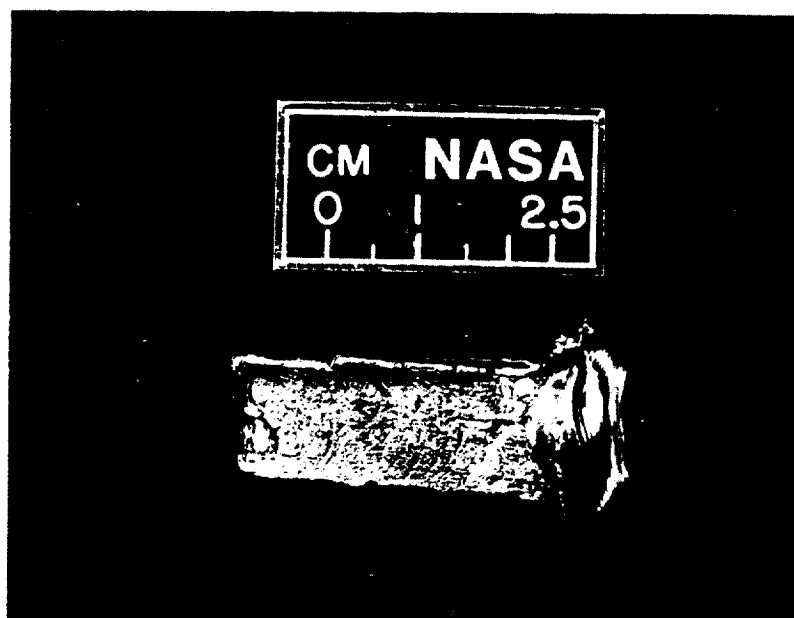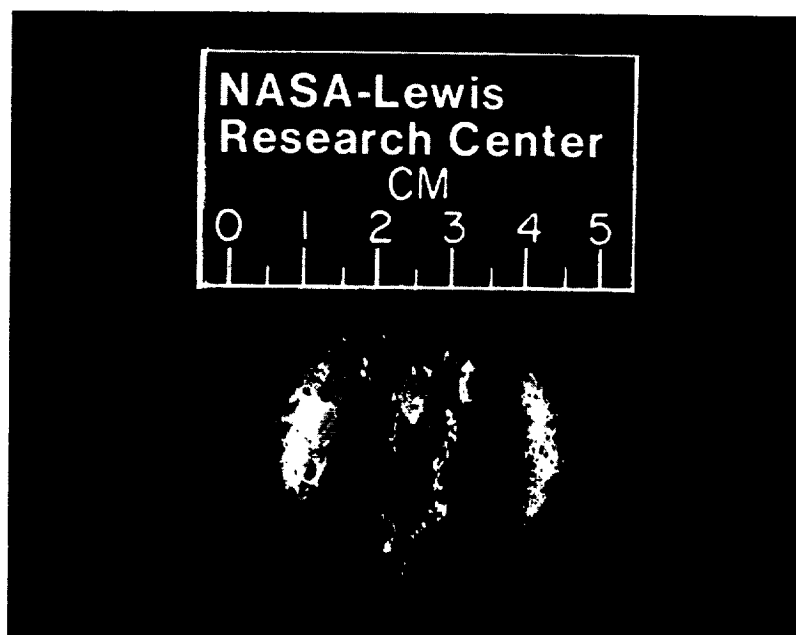
Figure 3-2. Arc-Melted Button and Casting of Binary NiAl

(0.100 kg MoO_3, 50 ml HF and 150 ml H_2O) to reveal the microstructure. Light optical micrographs were recorded for each alloy, with the exception of the binary stoichiometric Ni-50Al due to its extreme resistance to etching. Both bright field (BF) and differential interference contrast (DIC) were used to illuminate particular microstructural features.

Mechanical Property Testing

Compression Testing

Castings. The body of each casting was sent to Ultracut, Inc., West Palm Beach, Florida, for electrostatic discharge machining (EDM) of cylindrical compression test specimens, Figure 3-3 and 3-4. Approximately 16 compression specimens were obtained from each casting, with the exception of Ni-52Al-1Cr from which none could reliably be produced due to its extreme brittleness. The compression specimens were specified to be 6.0 ± 0.1 mm in length by 3.0 ± 0.01 mm diameter, as this is a convenient diameter for subsequent TEM specimen preparation. Following EDMing, a longitudinal burr remained on each compression specimen, as well as a gray oxide. The burr was removed by lightly grinding on 400 grit SiC paper; the specimen ends were briefly abraded to remove the oxide layer. Parallelism of the ends was checked during specimen measurement by placing the specimen in a micrometer and examining for light visibility between the specimen and micrometer platens.

Extrusions. Compression specimens of identical dimensions were produced from the extrusions by centerless grinding to final dimensions. This method produces a smoother surface than that associated with EDMing. Thus, the properties derived from the extrusions were more reproducible than those of the castings for a given alloy.

Compression tests were conducted primarily to introduce a small amount of deformation into the alloys for the purpose of dislocation analysis. Since preliminary

Casting

~ 25

~ 15 mm

~ 15 mm

Rod

3 mm +-
0.05 mm

Specimen

3 mm +-
0.05 mm

6 mm +-
0.1 mm

ends must be flat
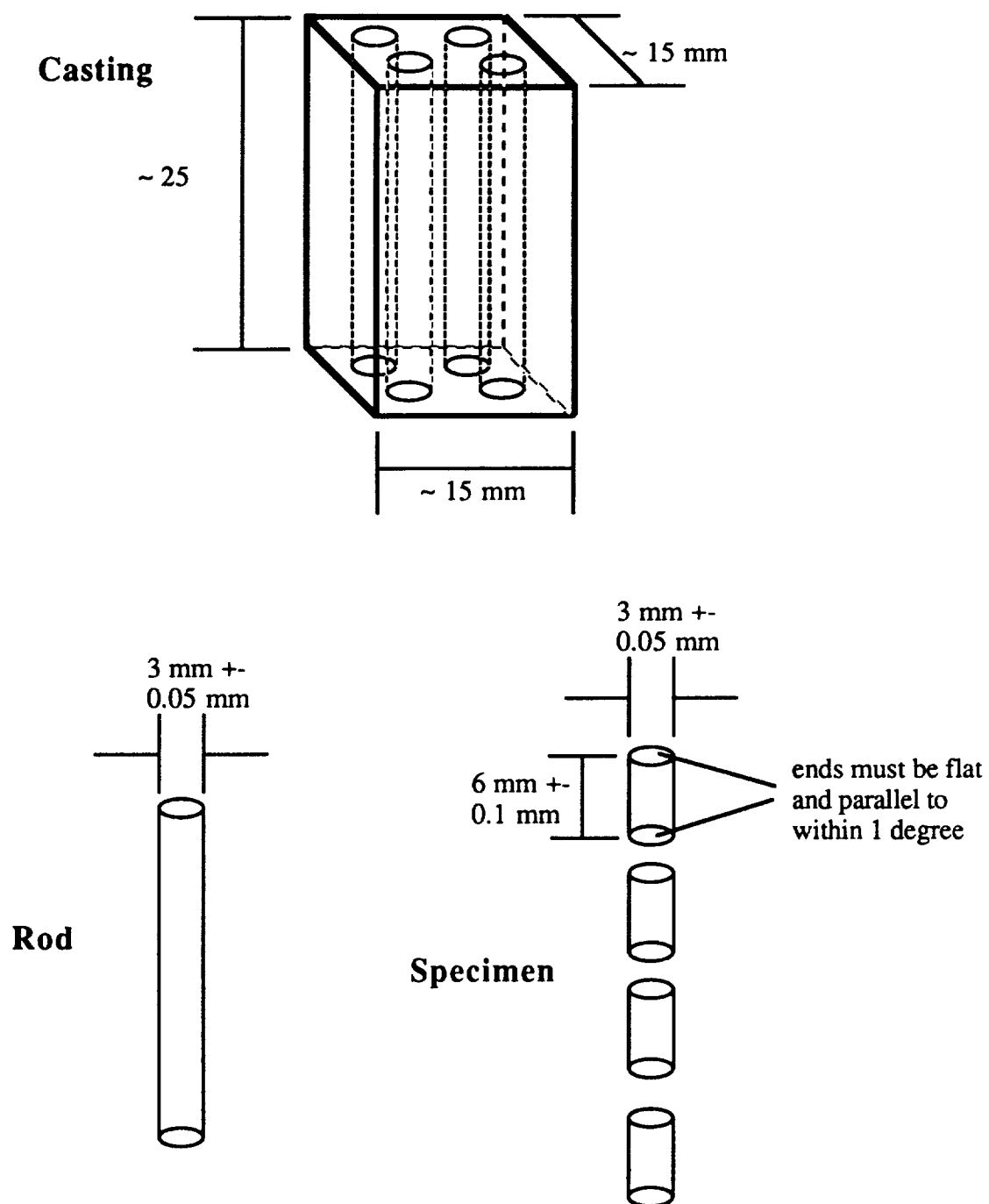and parallel to
within 1 degree

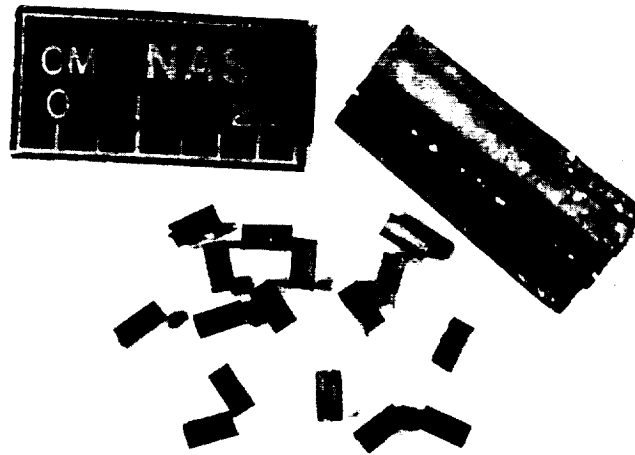Figure 3-3. Schematic Drawing of Compression Test Specimens

Figure 3-4. Electrostatic Discharge Machined Compression Specimens

research indicated that strains in excess of about one percent produce dislocation densities too high for individual dislocation analysis, the deformation strain was generally limited to 0.5 percent. In addition, at least four tests to failure were conducted for each cast and homogenized composition to allow determination of 0.2 percent offset yield (CYS) and ultimate compressive strengths (UCS) and strain-to-fracture (ε_p). All tests were conducted at a temperature of 300K in an Instron load frame, at a chart speed of 2.117 x 10^{-4} m per sec (0.5 inches per minute) and a crosshead speed of 8.47x10^{-7} m per sec (0.002 inches per minute). The nominal strain rate was 10^{-4} m/m. Boron nitride was used to lubricate the specimen ends prior to each test and preload of approximately 10 kg was applied before initiating crosshead travel. Following each test, the strain in each specimen designated for TEM specimens was measured directly from the reduction in length by micrometer. In specimens intended for mechanical property determination only, failure was considered to have occurred upon observation of the first discontinuity in the load-displacement curve,

regardless of any subsequent increase in load. The test was usually terminated after observation of the second load drop. In data reduction, only engineering stress and strain were reported, due to the small strains-to-failure generally observed.

Tensile Testing

Buttonhead type tensile specimens of dimensions shown in Figure 3-5 were machined from the extrusions by centerless grinding and electropolishing to remove surface defects. The same Instron load frame used for the above compression specimens was used for testing and the data were reduced in similar fashion. In addition, limited elevated temperature tests were conducted to determine the brittle-to-ductile-transition-temperature (BDTT) of each of the five extrusion alloys.

Microhardness Testing

All microhardness determinations were conducted on a Buehler Micromet II microhardness testing machine using a Vickers indenter. The indenter load was chosen to be 0.5 kg, with a load duration of 15 s. Prior to each testing session the machine was calibrated using standard hardness test blocks of hardened steel. Specimens were metallographically prepared prior to testing and either 10 or 15 indentations were made in each, sampling at least five different grains. Each indentation was optically examined for cracking or subsurface defects prior to measurement; any such defective indentations were ignored. The resulting compilation of hardness values were averaged for each alloy.

Transmission Electron Microscopy (TEM)
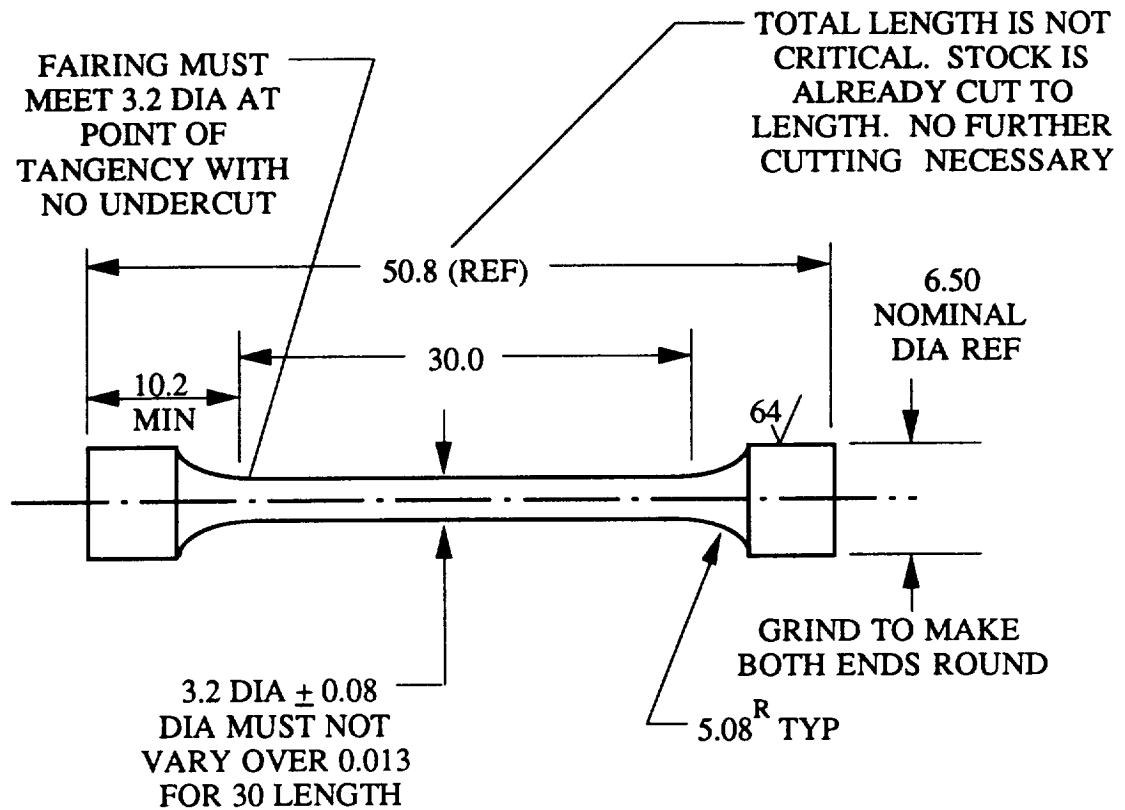
Specimen Preparation

Compression specimens were sliced into disks 300 μm thick with a low-speed Buehler saw using 250 μm thick SiC blades with water as a lubricant and then wet ground

by hand on 600 grit SiC paper to approximately 150 μm in thickness. Each disk was then jet-polished to perforation in a solution of 62 ml perchloric acid, 100 ml butyl cellusolve, 137 ml H_2O and 700 ml ethanol, at 0°C, 32 V and 150 mA using a Struers TENUPOL-3 polishing unit. The pumping speed of the jets was as slow as possible to minimize bending damage in the thin area.

Microstructural Characterization and Dislocation Analysis

All observations were made on a JEOL 100C transmission electron microscope (TEM) operated at an accelerating voltage of 120 kV on a double-tilt stage allowing ± 60° and ± 30° tilts. Both extruded and cast material were studied by TEM. Representative micrographs were recorded and the presence of second phases were noted and identified using electron diffraction analysis. In addition, the association of dislocations with particular microstructural features, such as grain boundaries and precipitates, was noted. The Burgers vectors of dislocations was determined by the "invisibility criterion" (zero contrast) as described by Hirsch, Howie and Whelan [116] by recording bright field images of dislocations illuminated by various diffracting vectors. In general, 25 to 100 dislocations could be imaged in one field of view at 20,000 to 50,000 magnifications (X). Enlarged prints were produced from the images which allowed the determination of the slip vector for a large number of dislocations within a given grain. For most compositions, at least three different grains were analyzed in foils from at least two different specimens to achieve a representative sample of Burgers vectors and help eliminate errors in analysis and orientation effects. Because of the elastic anisotropy in NiAl and extended dilation around the edge components of dislocations, some residual contrast sometimes remained in spite of satisfying the invisibility criterion. With practice, it was possible to identify the visibility conditions with little ambiguity. To insure the accuracy of the analyses, typically six different imaging conditions were recorded, as opposed to the minimum of three. Selected

specimens were analyzed in further detail to determine dislocation line direction, character and slip plane, in addition to Burgers vector, by appropriate stereographic techniques [10].

FAIRING MUST MEET 3.2 DIA AT POINT OF TANGENCY WITH NO UNDERCUT

TOTAL LENGTH IS NOT CRITICAL. STOCK IS ALREADY CUT TO LENGTH. NO FURTHER CUTTING NECESSARY

50.8 (REF)

6.50 NOMINAL DIA REF

30.0

10.2 MIN

64/

3.2 DIA ± 0.08 DIA MUST NOT VARY OVER 0.013 FOR 30 LENGTH

GRIND TO MAKE BOTH ENDS ROUND

5.08^R TYP

NOTE

1. ALL DIAMETERS MUST BE CONCENTRIC AND TRUE WITHIN 0.013

2. $^{16}/\vee$ UNLESS OTHERWISE NOTED

3. MATERIAL IS EXTREMELY BRITTLE. HANDLE AND MACHINE WITH CAUTION

4. ALL DIMENSIONS IN MILLIMETERS

Figure 3-5. Tensile Test Specimen Produced from Extrusions by Centerless Grinding

ALCHEMI

A determination of the site preference of chromium on the B2 NiAl lattice was made by axial Atom Location by Channelling Enhanced Microanalysis (ALCHEMI) [117, 118], via the TEM, of extruded Ni-49.5Al-1Cr along the [110] zone axis. This alloy was chosen because the chromium was entirely in solid solution and thus, interference from alpha-chromium precipitates could not occur. The technique is described in detail by Otten [117], however, it basically consists of acquiring X-ray spectra while the electron beam is aimed exactly along the [110] crystal axis (the [100] direction would do just as well). The resulting spectrum is compared with another spectrum acquired slightly off (about two degrees) the [110] axis along a high index direction. Because of the tendency for a standing electron wave to develop in the [110] direction, columns of atoms of one type, e.g. nickel, will be excited to a greater degree than the other, in this case, aluminum, and this will be reflected in the x-ray spectrum relative to the off-axis analysis. If chromium displays a site preference, its peak intensity will be augmented or diminished according to the degree of site preference.

X-ray Diffraction Analysis (XRD)

The lattice parameters of the alloys were determined by XRD on a Scintag PAD V diffractometer with powders produced by crushing samples of the castings. Copper K^α radiation was used. Because of the similarity in the lattice parameters of the B2 and A2 phases in the two-phase alloys, deconvolution of the peaks was not always possible and may have influenced the results.

CHAPTER 4
RESULTS

The results of the experiments described in the previous section are presented below in similar order. Justification for the particular experiments chosen and critical evaluation of the data are reserved for the discussion.

Alloy Compositions

The nominal and analyzed compositions of the materials in this study are summarized in Tables 4-1, 4-2 and 4-3. Table 4-1 pertains only to HAM castings with the exception of Ni-48.5Al-5.2Cr, which was also studied in the AM state. The analyzed compositions of the castings appeared to indicate higher aluminum contents and slightly lower nickel and chromium contents than intended. However, based on the very small casting weight losses measured, and the fact that the aluminum content appears to have increased (unlikely), it is probable that the chemical analysis is in error and the nominal compositions are reasonable measures of the true compositions. The extrusion compositions appear very near to their nominal compositions, Table 4-2.

Optical Microscopy

Representative light optical micrographs of the castings and extrusions are presented below in Figures 4-1 through 4-10 and 4-11 through 4-15, respectively.

HAM Microstructures

The structures of the cast and homogenized binary alloys, Ni-48Al, Ni-50Al and Ni-52Al, were single phase and coarse grained, as shown in Figures 4-1 and 4-2. While

Ni-50Al appeared to cast well and contained few defects, the other two binary alloys contained a large number of cracks which were usually intergranular. Alloys containing one percent chromium were generally single phase (Figure 4-3), with occasional fine precipitation. Based on available ternary phase diagrams, any second phase precipitation in this system is expected to be alpha-chromium. Both XRD and TEM analysis confirmed this to be true, as discussed below. Alloy Ni-48Al-2Cr was very similar to the one percent chromium alloys, as shown in Figure 4-4. These alloys also displayed a significant degree of cracking and shrinkage pores. In contrast to Ni-48Al-2Cr, Figures 4-5 and 4-6 show the microstructures of Ni-49Al-2Cr and Ni-50Al-2Cr to contain fine, intragranular precipitation. The precipitates in these alloys were often aligned in smoothly curving arcs. The precipitation in Ni-50Al-2Cr appeared to be of a slightly larger mean size than that in the Ni-49Al-2Cr. The precipitation in the alloys containing five percent chromium was marginally coarser than in the alloys containing two percent chromium, and was less homogeneously distributed, Figures 4-7 through 4-9. The alignment of precipitates was less pronounced in the Ni-45Al-5Cr and Ni-47.5Al-5Cr alloys, but was well-developed in the Ni-50Al-5Cr alloy. In these latter alloys, the grain boundaries were often delineated by allotriomorphs and a surrounding precipitate free zone, Figure 4-9. The microstructure of the Ni-48.5Al-5.2Cr alloy was very similar to Ni-50Al-5Cr and is shown in Figure 4-10.

XVIM and XAP Microstructures

The optical microstructures of the extrusions are shown in Figures 4-11 through 4-15. The binary Ni-50Al and the Ni-49.5Al-1Cr alloys both contain fully recrystallized structures of fairly equiaxed grains which have undergone dynamic recrystallization and grain growth. The Ni-49Al-2Cr and Ni-48Al-2Cr alloys are similar, but have retained partially recrystallized regions containing fine subgrains and a generally finer structure. The highest chromium alloy, Ni-45Al-5Cr, displayed the finest grain structure and was

fully recrystallized. In all the chromium-containing alloys, stringers of second phase could be discerned extending in the extrusion direction.

Table 4-1. Nominal and Analyzed Compositions (Atomic Percent or Wppm) of Cast and Homogenized Alloys in Current Study

Alloy #	Nominal % Ni	Nominal % Al	Nominal % Cr	Analyzed % Ni	Analyzed % Al	Analyzed % Cr	Analyzed % Fe	Analyzed % Cu	wppm C	wppm N	wppm O	% Wt. Loss
1	52	48	0	51.3	48.7	na	nd	nd	60	nd	74	-0.11
2	50	50	0	48.8	51.2	na	nd	nd	58	nd	76	-0.07
3	48	52	0	47.0	53.0	na	nd	nd	48	nd	60	-0.09
4	52	47	1	51.0	48.2	0.83	nd	nd	50	nd	87	-0.19
5	50	49	1	48.7	50.4	0.90	nd	nd	58	nd	46	-0.18
6	49.5	49.5	1	48.6	50.5	0.82	nd	nd	56	nd	59	-0.32
7	49	50	1	48.2	51.0	0.82	nd	nd	57	nd	25	-0.22
8	47	52	1	45.4	53.7	0.89	nd	nd	56	nd	27	-0.17
9	50	48	2	48.8	49.5	1.7	nd	nd	57	nd	36	-0.20
10	49	49	2	48.1	50.3	1.6	nd	nd	50	35	86	-0.14
11	48	50	2	47.0	51.3	1.7	nd	nd	64	31	56	-0.41
12	50	45	5	49.7	46.1	4.2	nd	nd	59	10	97	-0.33
13	47.5	47.5	5	46.5	49.4	4.1	nd	nd	55	nd	43	-0.20
14	45	50	5	44.1	51.7	4.7	nd	nd	116	138	148	-0.24
15	46.2	48.5	5.2	44.2	50.2	4.7	0.84	nd	240	31	45	na

nd = not detected (less than 0.2 wppm)
na = not analyzed

Table 4-2. Nominal and Analyzed Compositions (Atomic Percent or Wppm) of Extruded Alloys in Current Study

Extrusion #	Billet Type	Nominal % Ni	Nominal % Al	Nominal % Cr	Analyzed % Ni	Analyzed % Al	Analyzed % Cr	Analyzed % Fe	wppm C	wppm N	wppm O
L-2692	VIM Cast	50	50	0	50.2	49.8	na	na	82	nd	42
L-2661	VIM Cast	49.5	49.5	1	49.7	49.3	0.94	na	110	na	35
L-2663	VIM Cast	49	49	2	49.2	49.9	1.9	na	79	na	38
L-2659	VIM Cast	50	48	2	50.1	48.0	1.9	na	70	na	42
L-2614	Powder	50	45	5	50.9	44.6	4.4	0.08	21	nd	120

nd = not detected (less than 0.2 wppm)
na = not analyzed

Table 4-3. Compositions of Additional Alloys (Atomic Percent or Wppm)

Alloy Identification	Nominal			Analyzed						
	% Ni	% Al	% Cr	% Ni	% Al	% Cr	% Fe	wppm C	wppm N	wppm O
P&W Alloy 40	47.3	48.5	4.2	47.2	48.7	4.0	0.09	94	8	24
[100] NiAl SC	50	50	0	na	na	na	na	na	na	na
[111] NiAl SC	50	50	0	na	na	na	na	na	na	na
[123] NiAl SC	50	50	0	na	na	na	na	na	na	na
Ni-43Al	57	43	0	57.0	42.9	0	0.09	58	58	116
Ni-43Al-5Cr	52	43	5	52.4	43.6	3.94	nd	56	125	116
CP NiAl	50	50	0	na	na	na	na	60	42	111
CP NiAl+0.25Cr	49.88	49.88	0.25	na	na	na	na	na	na	na
CP NiAl+0.50Cr	49.75	49.75	0.50	na	na	na	na	na	na	na
CP NiAl+0.75Cr	49.63	49.63	0.75	na	na	na	na	na	na	na
CP NiAl+1.0Cr	49.50	49.50	1.0	na	na	na	na	na	na	na
HP NiAl	50	50	0	na	na	na	na	56	nd	116
HP NiAl+0.25Cr	49.88	49.88	0.25	na	na	na	na	na	na	na
HP NiAl+0.50Cr	49.75	49.75	0.50	na	na	na	na	na	na	na
HP NiAl+0.75Cr	49.63	49.63	0.75	na	na	na	na	na	na	na
HP NiAl+1.0Cr	49.50	49.50	1.0	na	na	na	na	na	na	na
Ni-49.25Al-1.5Cr	49.25	49.25	1.5	na	na	na	na	na	na	na
Ni-48.25Al-3.5Cr	48.25	48.25	3.5	na	na	na	na	na	na	na
Ni-51.5Al-2.5Cr	46	51.5	2.5	na	na	na	na	na	na	na
Ni-46Al-2.5Cr	51.5	46	2.5	na	na	na	na	na	na	na
Ni-46.5Al-3.5Cr	50	46.5	3.5	na	na	na	na	na	na	na
Ni-50Al-3.5Cr	46.5	50	3.5	na	na	na	na	na	na	na
Ni-46Al	54	46	0	na	na	na	na	na	na	na

nd = not detected (less than 0.2 wppm)
na = not analyzed

Mechanical Properties

Compression Tests

HAM Castings. The room-temperature compression test results are given in Table 4-4 and Figure 4-16. Typical stress-strain curves are shown in Appendix A. Because of the error involved in measuring the mechanical properties of cast material due to the large grain size (relative to specimen size) and casting inhomogeneities, comparisons should be

made with caution. However, several observations may be made. First, compositions for which the nickel-to-aluminum ratio is unity correspond to a minimum in strength, regardless of chromium content. Second, substantial strengthening (about three times) occurs between zero and one percent chromium for all three series of alloys. An interesting result in Figure 16b is that chromium, when substituted at low levels for nickel, hardens NiAl in a manner similar to nickel in the binary alloy. Finally, alloys with chromium levels beyond one percent demonstrate almost no additional strengthening when the nickel-to-aluminum ratio is one, and moderate strengthening otherwise.

Table 4-4. Results of Compression Tests of HAM Castings at 300K (error = std. dev.)

Alloy	0.2% CYS (MPa)	UCS (MPa)	Plastic Strain (%)	# tests
Ni-48Al	462 ± 25	527 ± 34	0.4 ± 0.3	8
Ni-50Al	148 ± 29	468 ± 171	12 ± 10	8
Ni-52Al	834 ± 186	867 ± 238	0.35 ± 0.2	7
Ni-47Al-1Cr	543 ± 72	606 ± 64	0.73 ± 0.4	8
Ni-49Al-1Cr	450 ± 56	534 ± 68	0.5 ± 0.2	9
Ni-49.5Al-1Cr	403 ± 100	457 ± 70	0.9 ± 0.8	9
Ni-50Al-1Cr	461 ± 97	514 ± 92	0.5 ± 0.4	8
Ni-52Al-1Cr	no data	246	no data	2
Ni-48Al-2Cr	461 ± 49	500 ± 49	0.5 ± 0.2	8
Ni-49Al-2Cr	440 ± 42	560 ± 49	0.7 ± 0.3	9
Ni-50Al-2Cr	571 ± 81	599 ± 69	1.0 ± 0.8	8
Ni-45Al-5Cr	753 ± 69	870 ± 63	0.6 ± 0.1	8
Ni-47.5Al-5Cr	453 ± 68	608 ± 9	1.3 ± 1.5	7
Ni-50Al-5Cr	816 ± 151	885 ± 94	0.2 ± 0.3	7

Extrusions. The compressive yield strengths for the XVIM and XAP extrusions are given below in Table 4-5. Values for strain-to-failure and fracture strength were not recorded for the extrusions. Plotting the yield strengths of the castings versus the extrusions for identical alloy compositions, Figure 4-17, shows that the relative differences in strength between alloys is consistent for both processing routes, although the extruded material is generally about 40 MPa stronger.
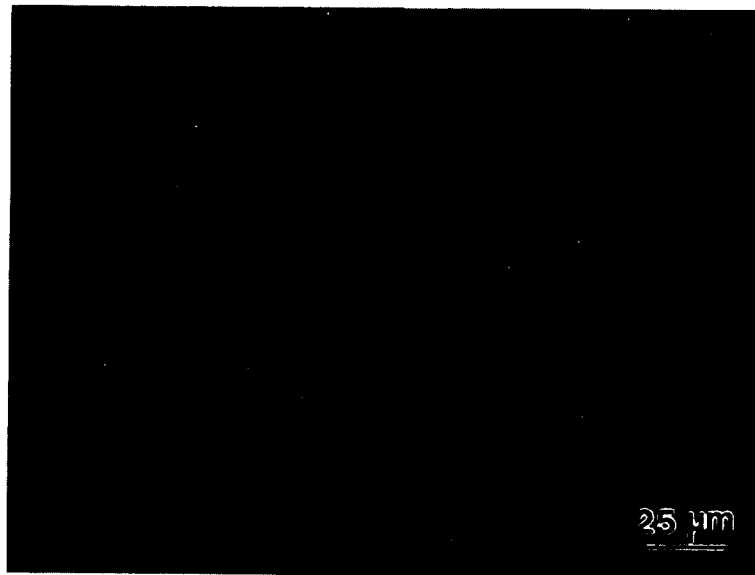
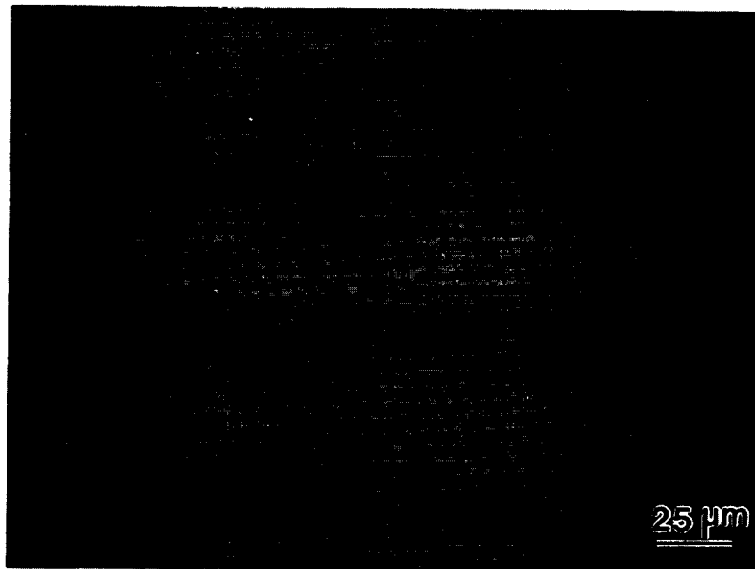Figure 4-1. Optical Microstructure of Ni-48Al HAM Casting

Figure 4-2. Optical Microstructure of Ni-52Al HAM Casting

Figure 4-3. Optical Microstructure of Ni-49Al-1Cr HAM Casting

Figure 4-4. Optical Microstructure of Ni-48Al-2Cr HAM Casting
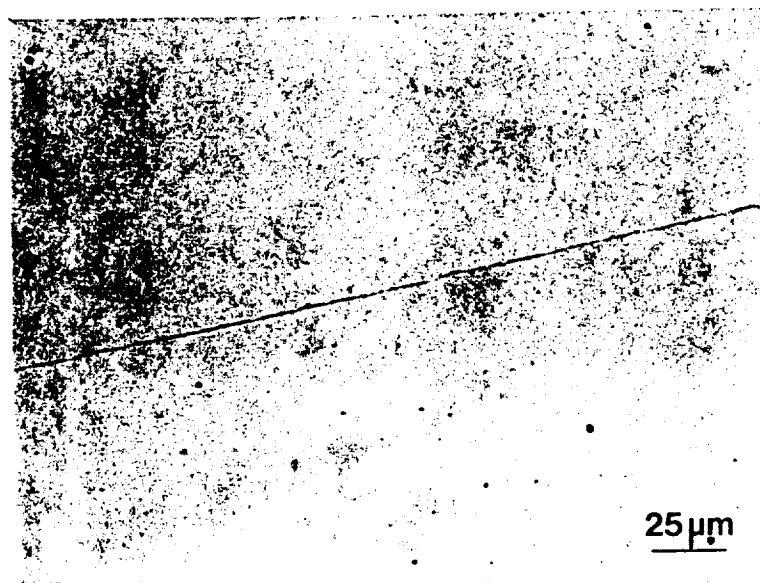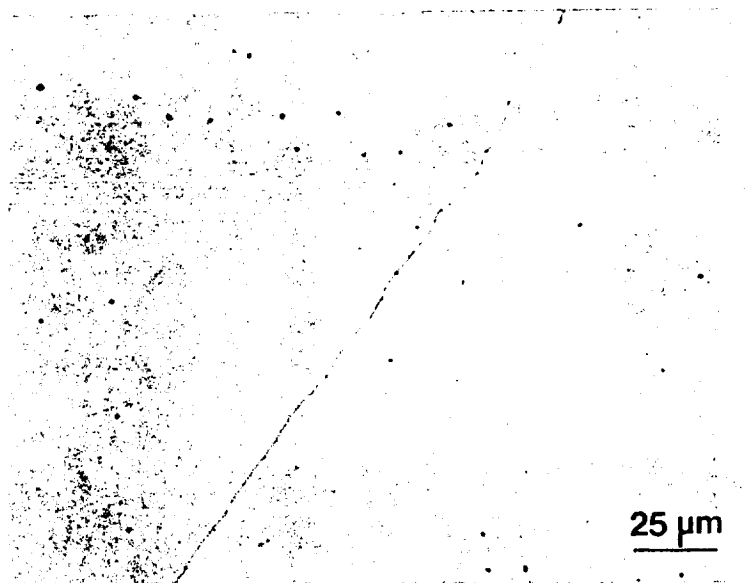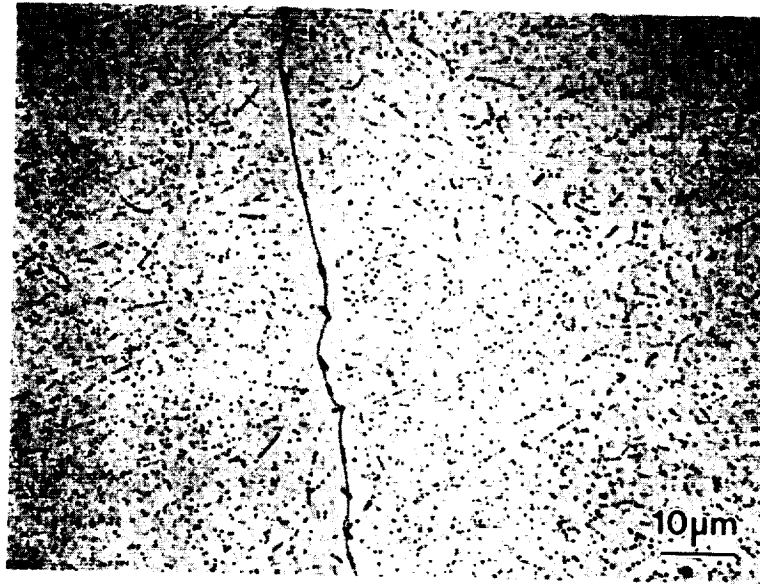
55
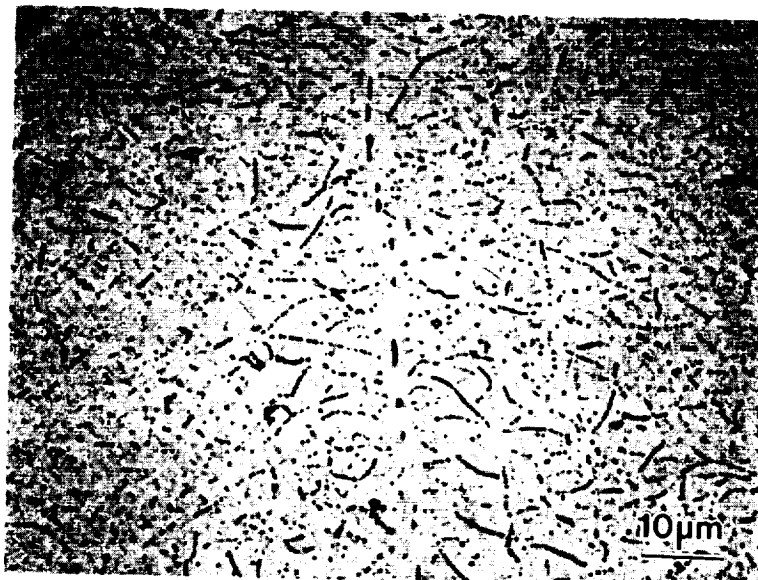
Figure 4-5. Optical Microstructure of Ni-49Al-2Cr HAM Casting

Figure 4-6. Optical Microstructure of Ni-50Al-2Cr HAM Casting
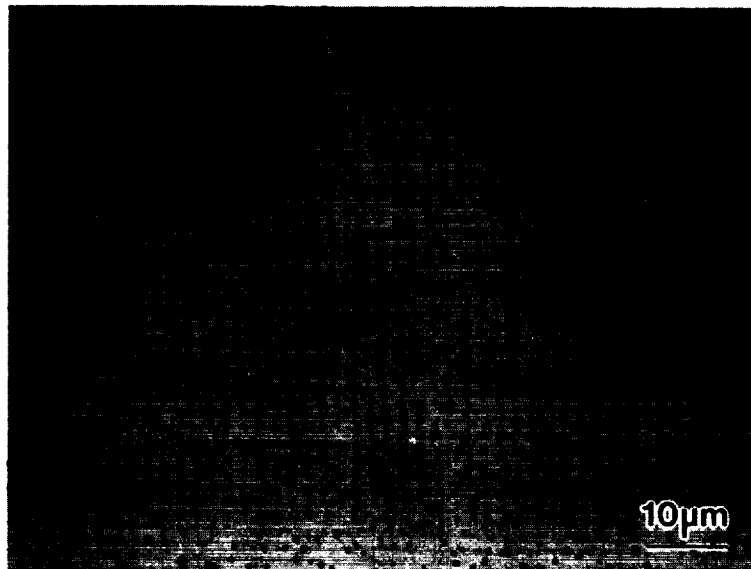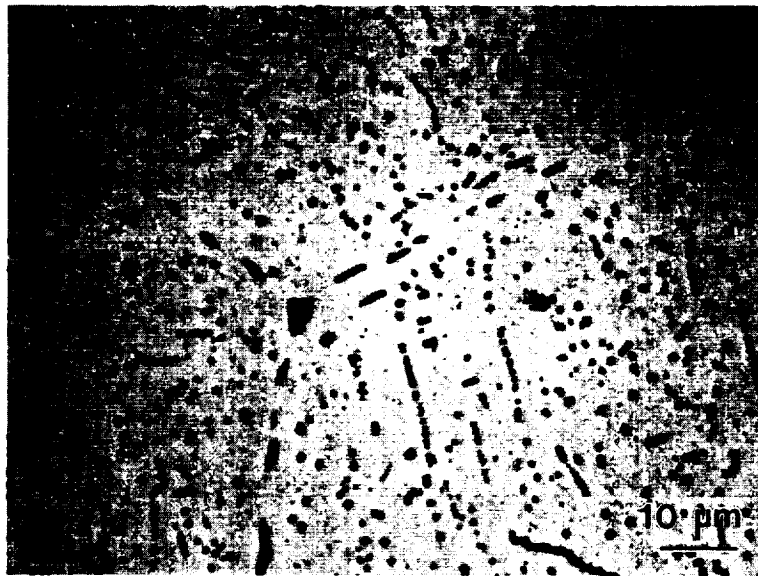
56

ORIGINAL PAGE
BLACK AND WHITE PHOTOGRAPH

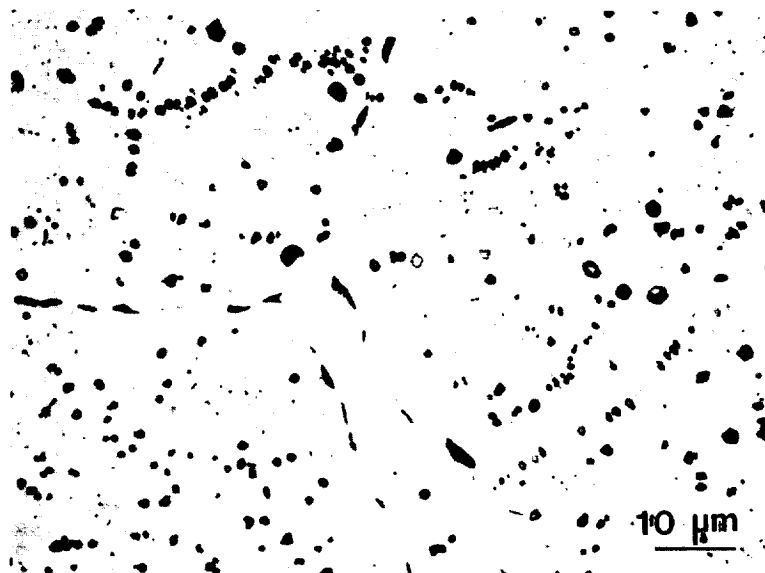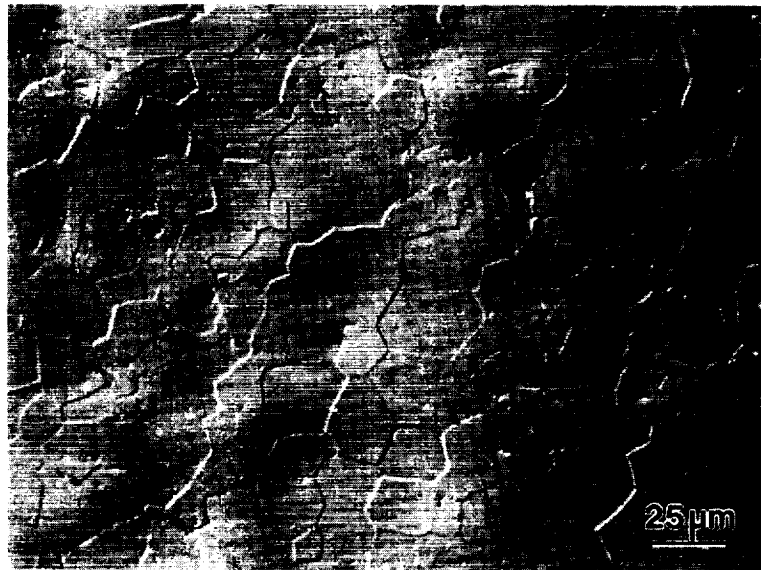Figure 4-7. Optical Microstructure of Ni-45Al-5Cr HAM Casting
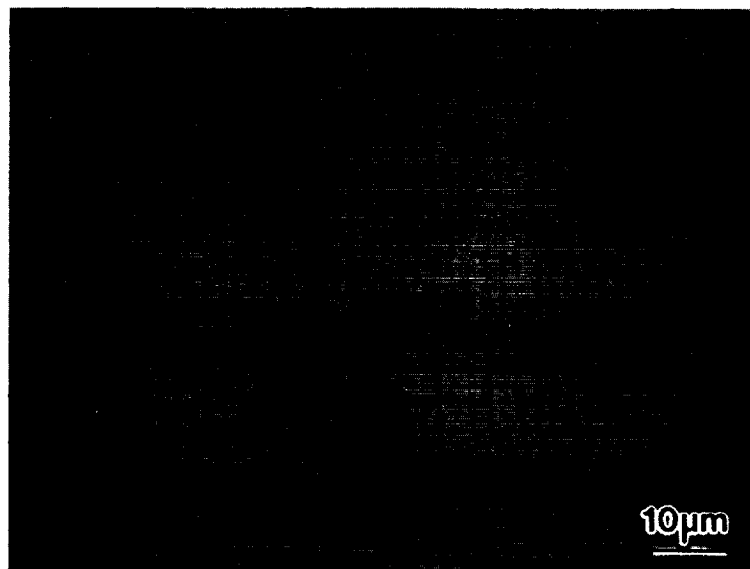
Figure 4-8. Optical Microstructure of Ni-47.5Al-5Cr HAM Casting

Figure 4-9. Optical Microstructure of Ni-50Al-5Cr HAM Casting

Figure 4-10. Optical Microstructure of Ni-48.5Al-5.2Cr HAM Casting

ORIGINAL PAGE
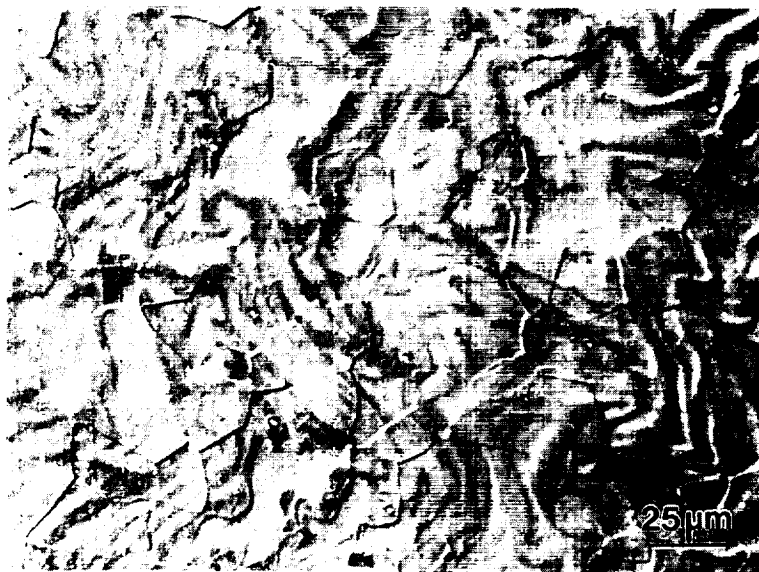BLACK AND WHITE PHOTOGRAPH

(a)

(b)

Figure 4-11. Optical Microstructure of Ni-50Al XVIM Extrusion (a) Longitudinal; (b) Transverse

(a)

(b)

Figure 4-12. Optical Microstructure of Ni-49.5Al-1Cr XVIM Extrusion (a) Longitudinal;
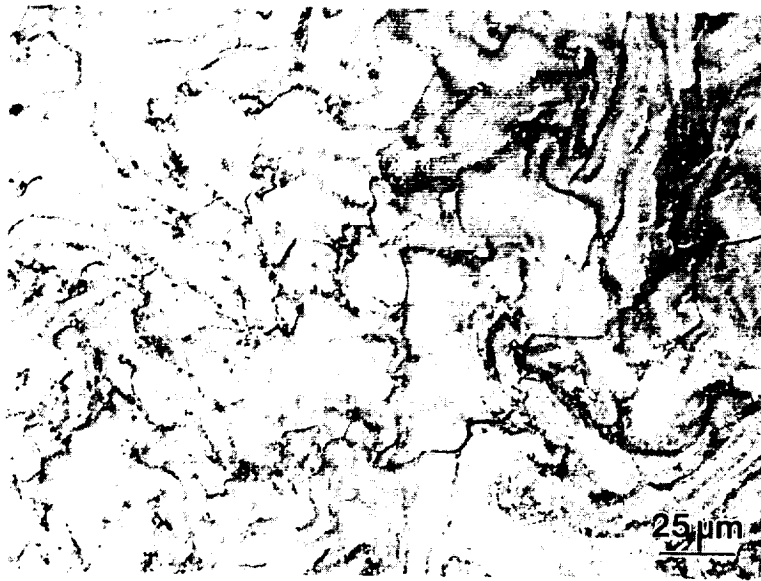(b) Transverse

(a)
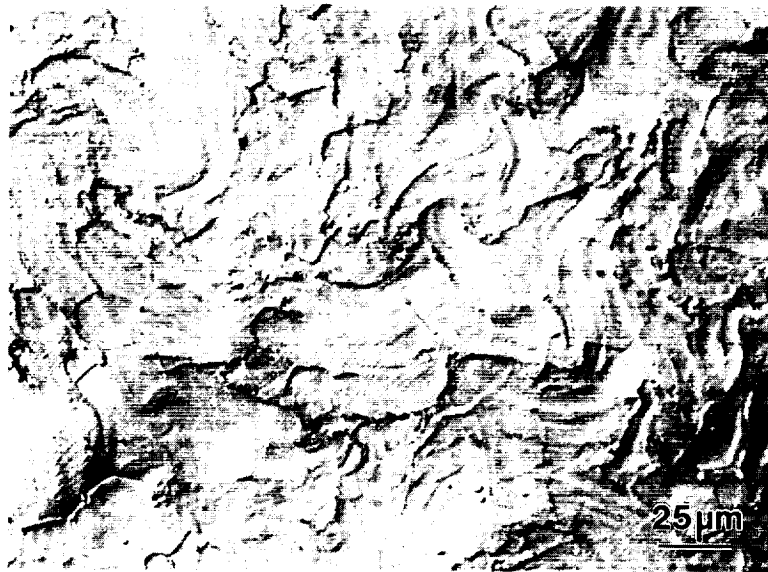
(b)

Figure 4-13. Optical Microstructure of Ni-48Al-2Cr XVIM Extrusion (a) Longitudinal; (b) Transverse

(a)

(b)

Figure 4-14. Optical Microstructure of Ni-49Al-2Cr XVIM Extrusion (a) Longitudinal; (b) Transverse

62
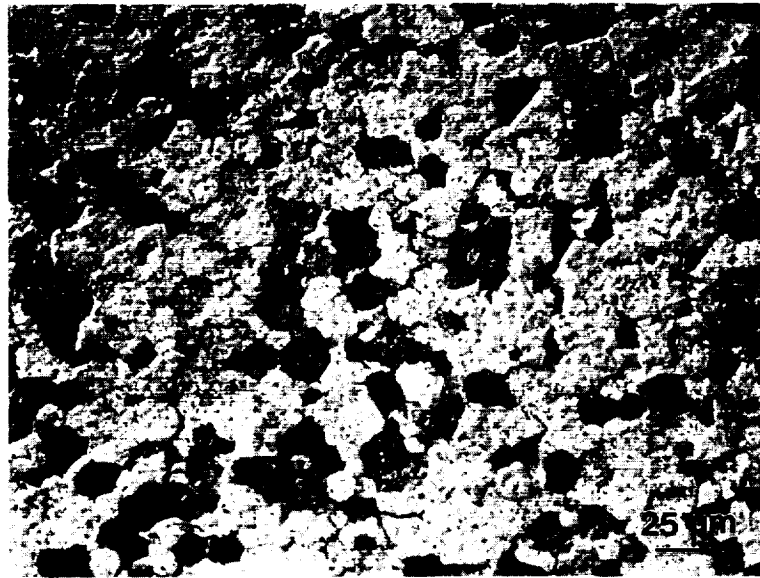
(a)

(b)

Figure 4-15. Optical Microstructure of Ni-45Al-5Cr XVIM Extrusion (a) Longitudinal; (b) Transverse

(a)

0.2% CYS (MPa) vs Atom Percent Chromium

□ Cr for Al
△ Cr for Ni
○ Ni/Al =1

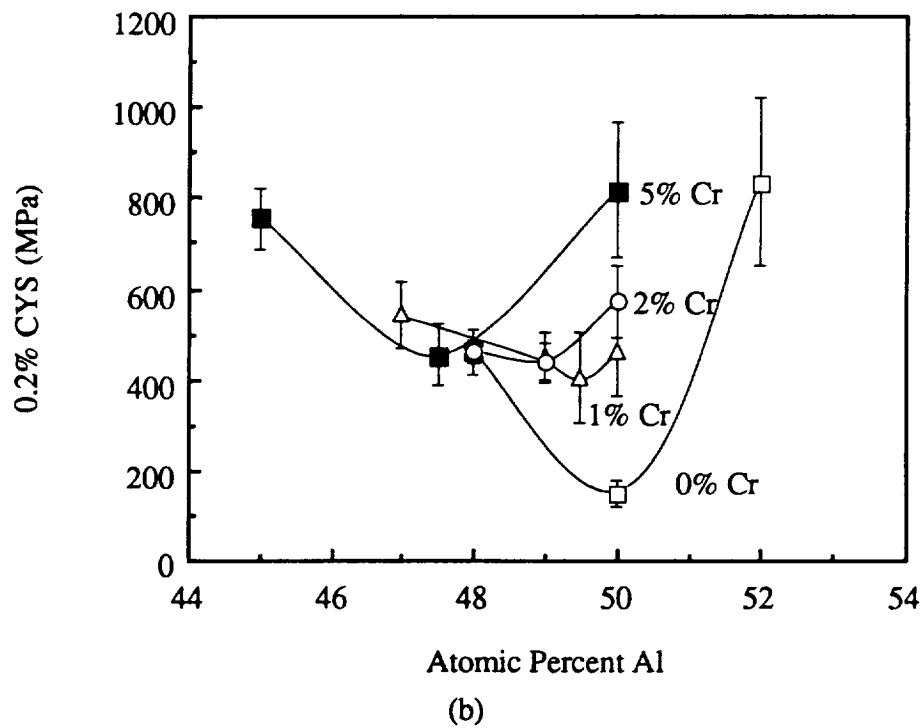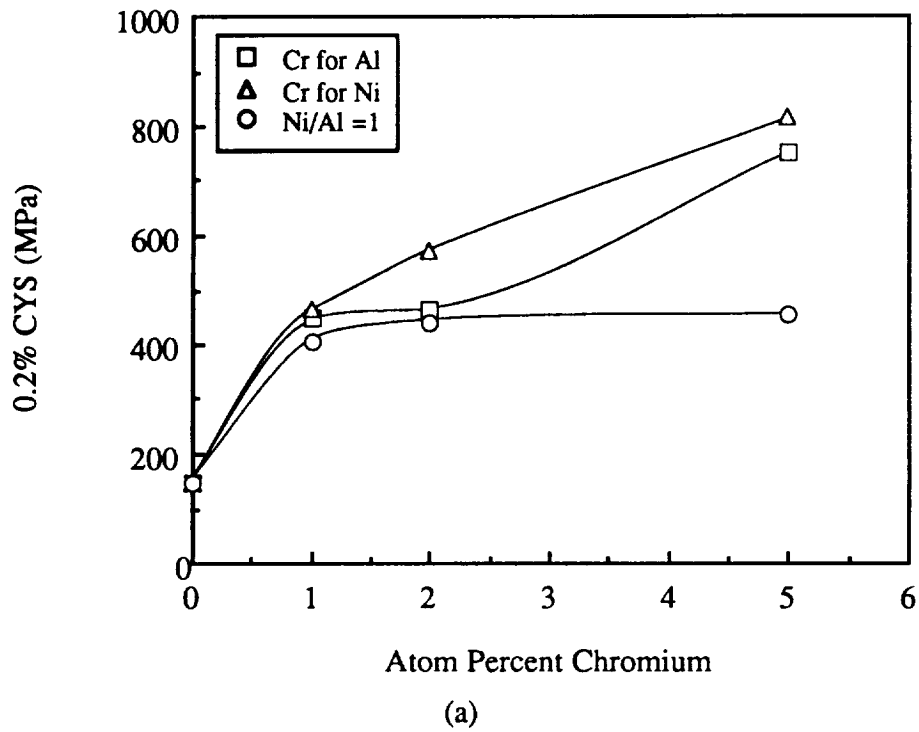**(b)**

0.2% CYS (MPa) vs Atomic Percent Al

5% Cr
2% Cr
1% Cr
0% Cr

Figure 4-16. 0.2 Percent Compressive Yield Strength at 300K of HAM Castings as a Function of (a) Chromium Content; (b) Aluminum Content

strength and increases the dependence of strength on temperature. The elongations as a function of temperature indicate that chromium elevates the BDTT about 150K relative to binary stoichiometric NiAl. Comparison of the tensile ductilities for Ni-49.5Al-1Cr and Ni-49Al-2Cr indicates the nickel-to-aluminum ratio has a stronger influence on the BDTT than does the chromium content. This influence is suggested because the nickel-to-aluminum ratio for these two alloys is equal to one while their chromium contents differ by a factor of two; yet their BDTTs are both about 750K. Ni-48Al-2Cr and (nickel-to-aluminum ratio equal to 1.04) and Ni-45Al-5Cr (nickel-to-aluminum ratio equal to 1.11) display respectively higher BDTTs than Ni-49.5Al-1Cr and Ni-49Al-2Cr.

Microhardness Tests

The measurement of microhardness was considered an alternative route to estimating yield strength variations for a number of extra compositions beyond the original 15 alloys. A reasonably good relationship between microhardness and yield strength was initially established, as shown in Figure 4-19.

The Vickers microhardness as a function of chromium content is plotted in Figure 4-20 in three curves representing substitutions for nickel only, aluminum only, and evenly for both. The hardening response at chromium levels below one percent is very flat and similar for all three substitutional schemes, roughly 265 kg/mm^2. At about one percent chromium the hardness increases sharply for all three curves, the most marked change occurring when chromium is substituted for nickel and the least marked when chromium is substituted for both elements. Beyond one percent chromium the curves separate, with the smallest degree of hardening occurring when chromium is substituted equally for both nickel and aluminum, and the greatest degree of hardening occurring when substituted for nickel. Comparison of the hardness and compressive yield strength values of the HAM

castings, Figures 4-20 and 4-16, shows that yield strength is more sensitive to property changes than hardness.

The flat hardening response at chromium levels below one percent prompted a study of the effect of interstitial purity levels on the hardness of low-chromium nickel aluminide alloys. The hardness of two series of alloys containing from zero to one percent chromium, all other variables being the same, are plotted in Figure 4-21 as a function of chromium content. This data indicates the source of constituent nickel used to cast the nickel aluminide alloys has a strong influence on the hardness, and probably other mechanical properties as well. A student's t test was performed to check for the statistical significance of the difference between the means of the hardness of the two binary alloys. They were found to be significantly different to at least 99 percent confidence. Interestingly, this apparent dependence on purity was not reflected in the interstitial analyses shown in Table 4-3, except in regard to nitrogen content, an unlikely contaminant.
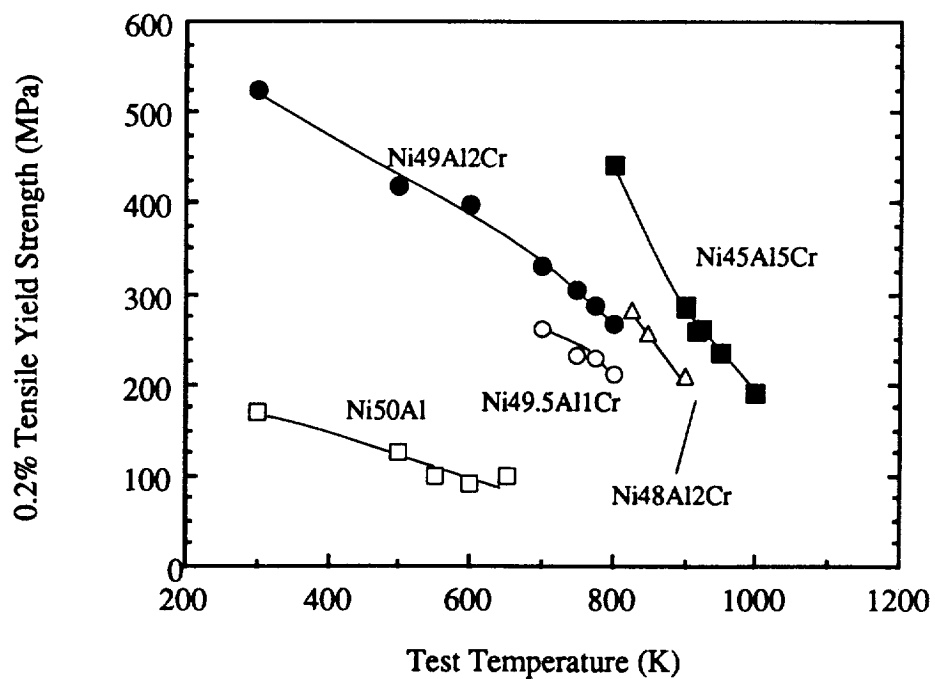
Figure 4-18. Tensile Properties of Extruded Alloys as a Function of Test Temperature
(a) 0.2% Tensile Yield Strength
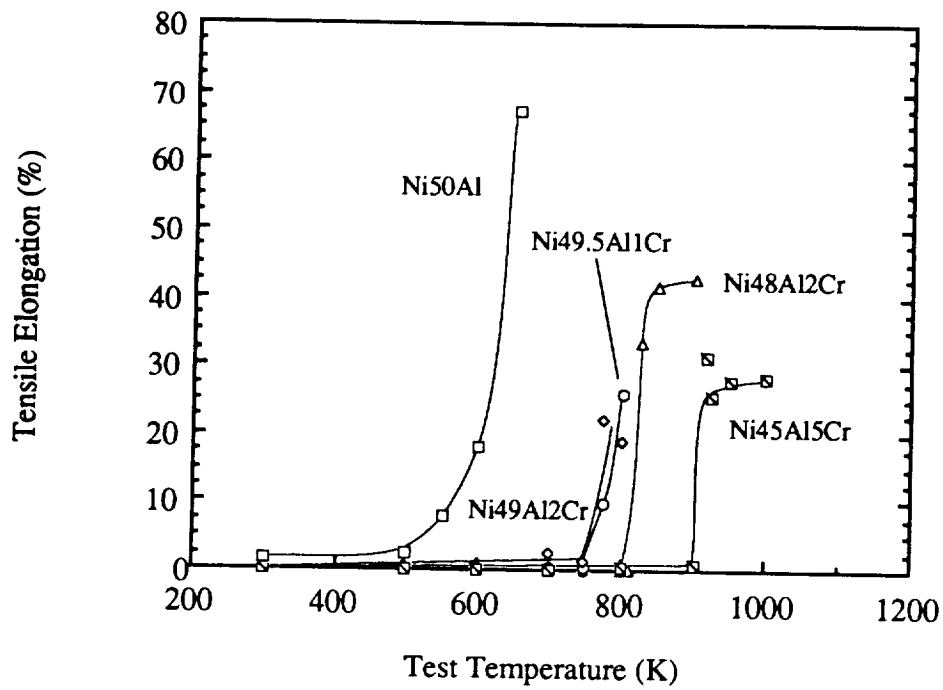
Figure 4-18--continued. (b) Tensile Elongation
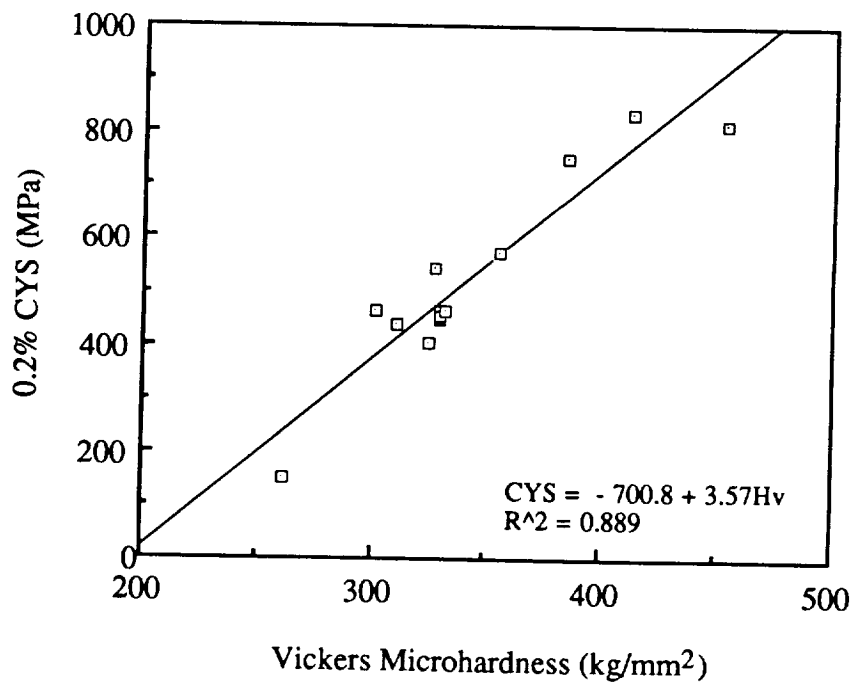
Figure 4-19. Relationship Between Microhardness and CYS for HAM Cast Alloys
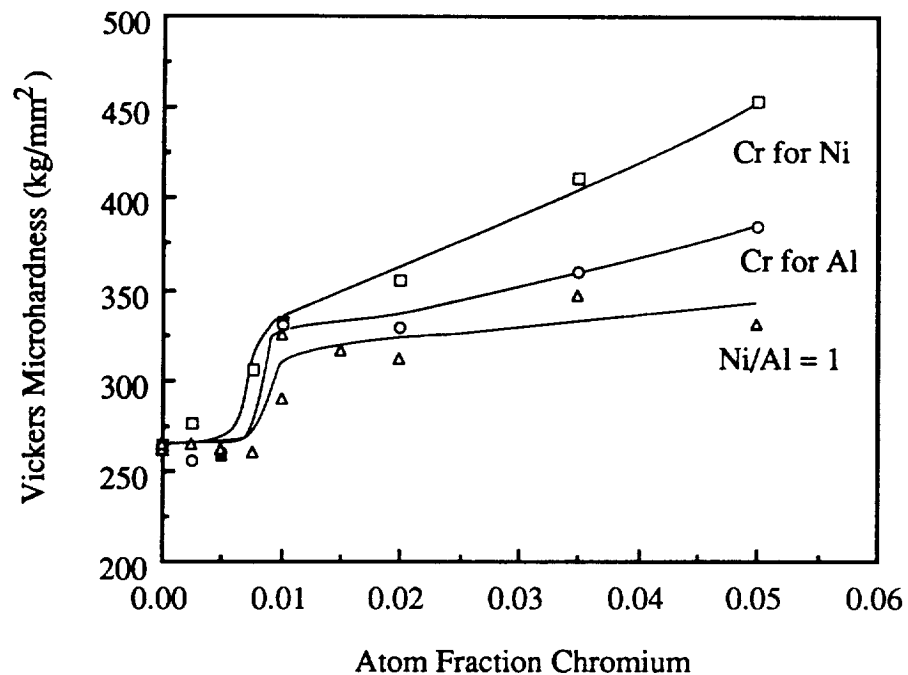
Figure 4-20. Vickers Microhardness of Cast and Homogenized NiAl+Cr Alloys as a
Function of Chromium Content

Further analysis of the as-received constituent nickel did not reveal any significant

differences in interstitial or metallic impurity content. These results are in Table 4-6.

Table 4-6. Chemical Analysis of As-Received Nickel Shot (Wppm)

	NASA - LRC							LECO			
Nickel	Ni	Al	Fe	Cu	Si	C	N	O	C	N	O	S
Commercial	bal	nd	nd	<0.2	<0.1	97	<10	56	69	<2	57	<2
Purified	bal	nd	nd	<0.2	<0.1	84	<10	47	76	<2	42	<1

nd indicates less than 0.05 wppm

The hardness dependence upon aluminum content at constant chromium levels is

plotted in Figure 4-22 for the cast and homogenized alloys. The expected hardness

minimum at the stoichiometric composition is obvious in the binary alloy, but less

pronounced in the ternary alloys which demonstrate less of an increase for nickel-rich compositions. This is especially true of the one percent chromium alloys.

A better understanding of the overall dependence of hardness upon composition may be achieved by a three-dimensional (3D) plot of the hardness surface as a function of aluminum and chromium content. Such a plot is shown in Figure 4-23. The 3D plot makes it clear that hardness minima reside along a "valley" in which the nickel-to-aluminum ratio is equal to one. It is also shown that aluminum-rich compositions are substantially harder than nickel-rich compositions, regardless of chromium content. A small minimum in hardness appears to occur at the Ni-49Al-2Cr composition, however, this minimum probably falls within the data scatter.
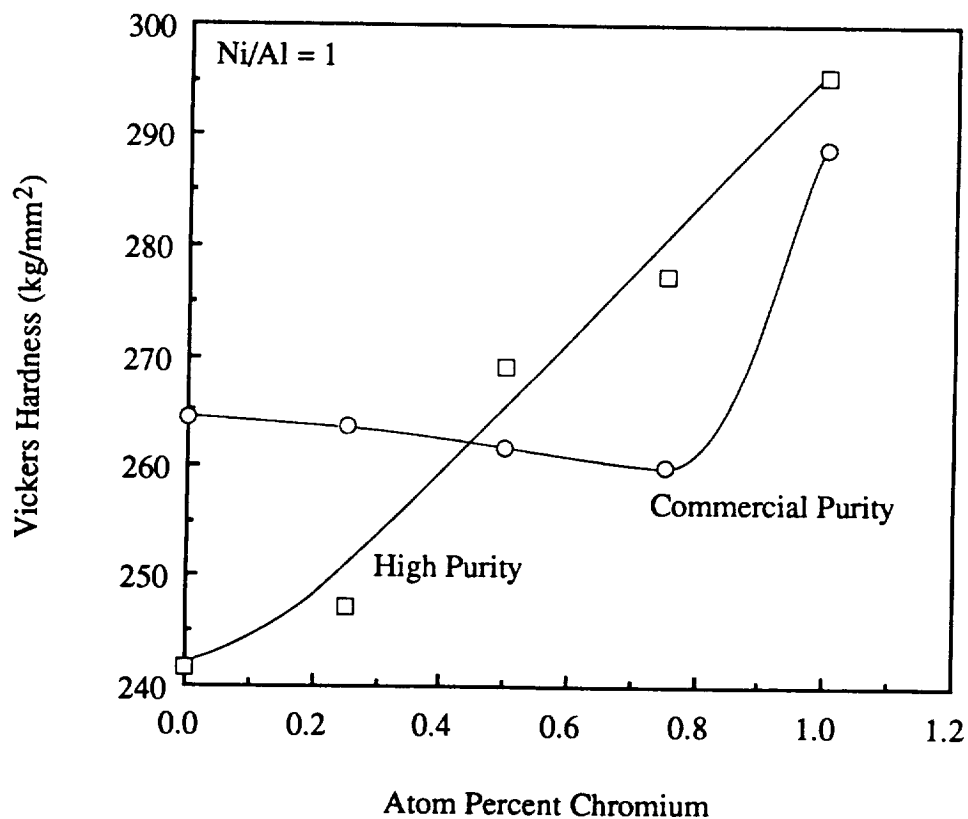
Figure 4-21. Comparison of Hardening Responses of Low-Chromium NiAl+Cr Alloys Produced from Commercial Purity and High Purity Nickel Sources.
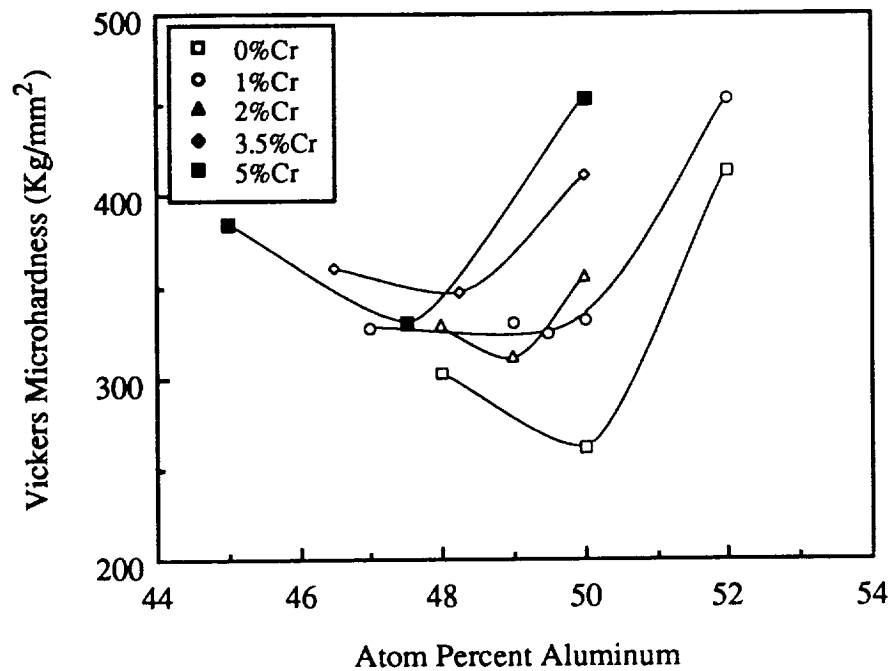
Figure 4-22. Vickers Microhardness of Cast and Homogenized NiAl+Cr Alloys as a
Function of Aluminum Content

Transmission Electron Microscopy

HAM and AM Castings

Typical microstructures are shown in Figures 4-24 through 4-36, while Figure 4-37 shows the microstructure of Pratt and Whitney alloy 40. All the cast alloys contained very large grains (hundreds or thousands of microns) such that few grain boundaries were encountered during TEM analysis. Prior to room temperature deformation, very few dislocations were found. The deformed binary alloys were single phase, with only Ni-50Al containing significant numbers of dislocations which were determined to be of <100> Burgers vectors. These dislocations were generally homogeneously distributed after 0.3 percent deformation, and appeared to be in the form of elongated loops or short segments. The short segments often contained one sharp bend which separated otherwise straight lengths. An example dislocation structure of Ni-50Al is shown in Figure 4-24.

Figure 4-23. Three-Dimensional Plot of Microhardness of Cast and Homogenized
NiAl+Cr Alloys as a Function of Composition

Alloys Ni-47Al-1Cr and Ni-49Al-1Cr were single phase. The extreme brittleness of Ni-47Al-1Cr prevented sufficient deformation to produce a workable dislocation density. Ni-49Al-1Cr, on the other hand, contained a moderate number of dislocations and tangles, similar to Ni-50Al. Ni-50Al-1Cr containe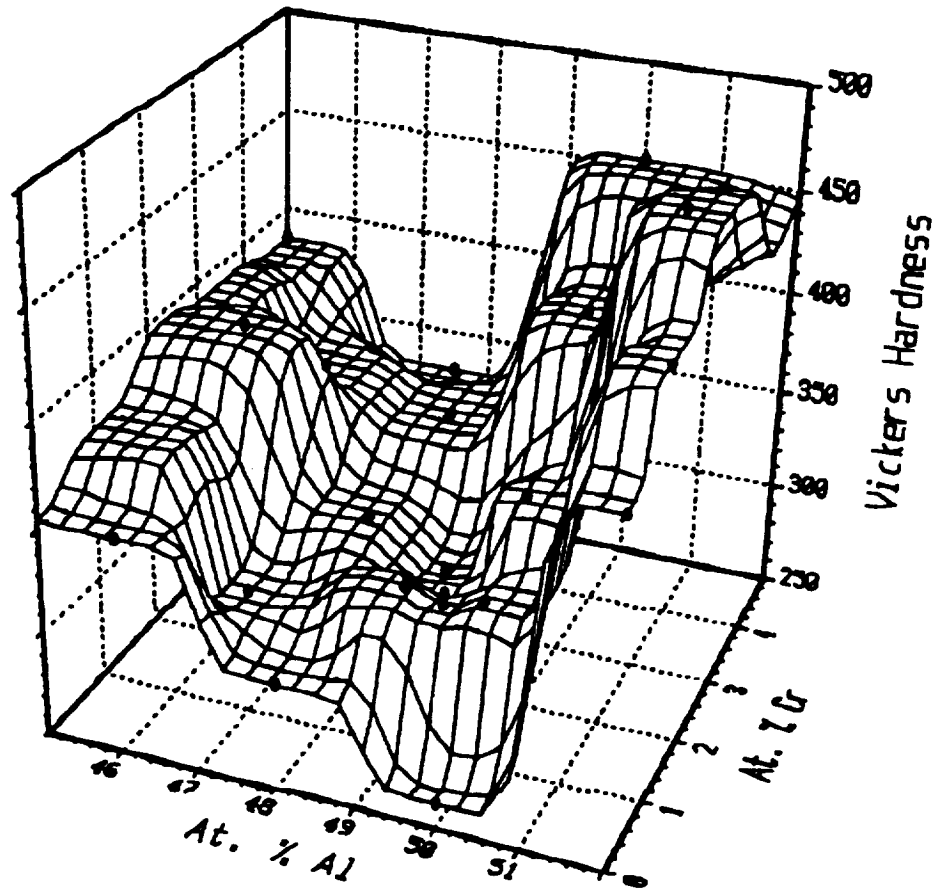d spherical precipitates of alpha-chromium of approximately 10 nm diameter. Occasionally, rods of alpha-chromium were encountered of similar diameter. Both forms of precipitation were usually associated with what appeared to be prismatically punched dislocation loops and associated loose tangles at the precipitate/matrix interface. In the matrix, bent dislocation segments were observed along with very small dislocation loops. The vast majority of dislocations analyzed contained <100> Burgers vectors. An example of this microstructure and the accompanying dislocation analysis are shown in Figure 4-25.

Ni-48Al-2Cr, Ni-49Al-2Cr and Ni-50Al-2Cr all contained spherical precipitates of alpha-chromium, as shown in Figures 4-26 through 4-28. The precipitation in Ni-48Al-2Cr appeared to be of a narrow size distribution centered around 100 nm, while the precipitation in the latter two alloys tended to be bimodal, either 25 or 250 nm in diameter. In some regions, a rod-like form of alpha-chromium was encountered. Larger precipitates were often associated with dislocation tangles, Figures 4-27 and 4-28, while the smaller precipitates appeared to pin matrix dislocations, Figure 4-26. The "double-arced" strain contrast displayed by the precipitates in Figures 4-27a and 4-28a indicates the precipitates are coherent. As for the above alloys, sharply bent dislocation segments were often observed within the matrix, and in the Ni-48Al-2Cr and Ni-49Al-2Cr alloys, dislocation loops were noted. All the dislocations analyzed in these alloys contained <100> Burgers vectors. Such an analysis is shown in Figure 4-26.

The alloys containing five percent chromium, Ni-45Al-5Cr, Ni-47.5Al-5Cr and Ni-50Al-5Cr, exhibited substantial precipitation of alpha-chromium particles, Figures 4-29 through 4-33. Precipitation in the first two alloys was generally bimodal in size, with the finer precipitation of about 10 to 25 nm diameter and coarser precipitation of about 250 nm

diameter. While the finer precipitates were spherical, the coarser precipitates were often irregular in morphology and were probably partially dissolved interdendritic chromium resulting from incomplete homogenization (Figure 4-31). The alpha-chromium precipitates in Ni-50Al-5Cr tended to be one of three different sizes: (1) fine, aligned spheres (about 15 nm in diameter), (2) small spheres or rods (about 200 nm in diameter) containing interfacial dislocation networks, and (3) large, aligned second phases of approximately square cross section with rounded edges which were also associated with interfacial misfit dislocation networks (about 1200 nm in width), Figure 4-32. The orientation relationship between the precipitates and the matrix was determined to be cube-on-cube, i.e., $<100>_\alpha\{001\}_\alpha$ // $<100>_\beta\{001\}_\beta$, Figure 4-33. Pinning of matrix dislocations by the finest precipitates was observed for all three alloys. In every case, the Burgers vector of the dislocations was determined to be of the $<100>$ type, an example of which is shown for Ni-47.5Al-5Cr in Figure 4-30.

TEM analysis of the Ni-48.5Al-5.2Cr alloys was performed for both the AM and HAM castings, and also for the material obtained from Pratt and Whitney. Although this alloy was reported to contain 5.2 percent chromium [16], documentation obtained with the alloy indicated it contained 4.2 percent chromium, as confirmed by chemical analysis in Table 4-3. The AM Ni-48.5Al-5.2Cr alloy microstructure is shown in Figures 4-34 and 4-35, and indicates that substantial segregation occurred during solidification. Figure 4-34 shows interdendritic alpha-chromium in the form of small, dense particles; identification by convergent beam electron diffraction analysis showed these to be $Cr_{23}C_6$ carbides. Away from the interdendritic regions, alpha-chromium precipitation was observed to consist of a relatively homogeneous dispersion of fine, spherical particles, Figure 4-35. Plastic deformation in these regions occurs in the form of concentrated slip bands of $<100>$ dislocations; no dislocations with $<111>$ Burgers vectors were found.

Upon homogenization, the interdendritic alpha-chromium was eliminated and a precipitate dispersion of a wide size distribution is produced (1 to 500 nm diameter), as

shown in Figure 4-36. These precipitates are spherical and are occasionally aligned into short rows. Dislocation networks decorate the precipitate/matrix interface for the larger precipitates, which are sometimes also the site of loose tangles. All precipitates appear to participate in dislocation pinning. Unlike the AM castings, no slip bands were observed after deformation. As in other alloys previously mentioned, most of the matrix dislocations have the peculiar sharp bend separating otherwise straight lengths.

Figure 4-37 shows the microstructure of the Pratt and Whitney alloy (Ni-48.5Al-4.2Cr). The precipitation in this alloy was very dense, of a wide size distribution, and was often aligned into closely-packed rows. The microstructural homogeneity was intermediate to the AM and HAM Ni-48.5Al-5.2Cr structures, Figures 4-34 to 4-36. No slip bands were observed, although dislocation tangles tended to concentrate along the rows of larger precipitates. Otherwise, the dislocation distribution was homogeneous. Some dislocation loops were also observed. The majority of the dislocations produced by 300K deformation were of the <100> type, contrary to published results on this material [15, 16].

Microstructures of XVIM and XAP Extrusions

In general, the extruded microstructures were fine-grained, typically 10 to 20 μm in diameter, and displayed a <111> fiber texture which was evident during analysis of the TEM foils. In other respects the structures differed as described below.

Ni-50Al. The as-extruded microstructures were generally featureless with the exception of a moderately low density of <100> dislocations, Figure 4-38a. Most of these dislocations consisted of short segments containing two straight lengths connected by a sharp bend, as observed in the cast and homogenized material. Occasionally, small elongated loops or partial loops were noted. Room-temperature plastic deformation (0.55 percent) increased the dislocation density, causing loose tangles, Figure 4-39; the same

sharply bent configurations were observed as above. The vast majority of the dislocations analyzed contained <100> Burgers vectors, usually on {011} planes.

Ni-49.5Al-1Cr. This alloy was similar to the binary in the as-extruded state. No second phase was observed and the dislocation density was relatively low. Upon room-temperature deformation (0.6 percent), marked differences were noted in comparison to the binary. As shown in Figures 4-40 and 4-41, deformation occurred primarily by the propagation of concentrated slip bands with <100> Burgers vectors emanating from the grain boundaries. These slip bands were usually planar and quite straight, however, the intersection of two bands sometimes caused deviation, as indicated by the curved slip band in Figure 4-41. Figure 4-40 provides evidence that the slip bands are nucleated at grain boundaries (not merely terminating there) by the observation of half-loops extending from the grain boundary at the initiation site of the slip bands. Dense slip bands, such as shown in Figure 4-40, contained a considerable number of small dislocation loops with <100> Burgers vectors. It was not clear whether the bands propagated by dislocation multiplication or by the glide of mobile dislocations.

Ni-48Al-2Cr and Ni-49Al-2Cr. These two alloys were essentially identical in their microstructures and dislocation substructure. Dense, homogeneous precipitation of 25 nm diameter alpha-chromium particles were observed throughout the microstructures. Larger $Cr_{23}C_6$ carbides were also commonly observed (about one or two per grain) and appeared to serve as nucleation sites for slip bands of <100> dislocations during extrusion, as shown in Figures 4-42 and 4-43. When deformed at room temperature, numerous parallel slip bands were observed to nucleate at grain boundaries and extend into the grain centers, Figures 4-44 and 4-45. Small dislocation loops, 10 to 20 nm in diameter, were usually associated with all but the most diffuse slip bands, and appeared to be Orowan type loops surrounding the fine precipitates. A typical Burgers vector analysis of the matrix dislocations is shown in Figure 4-46 for Ni-48Al-2Cr.

Ni-45Al-5Cr. The as-extruded microstructure of this alloy is shown in Figure 4-47. The alpha-chromium precipitation appears to be of a higher volume fraction, although the typical precipitate diameter is similar to the other alloys. The dislocation density is low, with few dislocation interactions visible. The sharp bending of short segments, obvious in other alloys, is less prominent in this alloy. Room temperature deformation (about 0.6 percent) significantly increases the dislocation density, Figure 4-48. However, the deformation appears more homogeneous compared to the other alloys, with few slip bands. Dislocation pinning by the precipitates is observed, as are dislocation loops, which occasionally surrounded the precipitates. Nearly all dislocations analyzed contained <100> Burgers vectors.

Chromium Solubility and Site Preference in NiAl

Based on the above results, the solubility of chromium in NiAl for the given processing conditions may be determined. A portion of the ternary nickel-aluminum-chromium diagram is presented in Figure 4-49 with the trace of the solvus surface indicated based on the microstructural results of the ternary alloys. This diagram indicates that the solubility of chromium is higher for nickel-rich alloys. ALCHEMI results, taken with the extruded Ni-49.5Al-1Cr alloy along the [110] zone axis, support the microstructural data by indicating a strong preference of chromium for the aluminum site in NiAl. These results are plotted in Figure 4-50, which shows the intensity of the primary K-alpha X-ray peaks as a function of deviation angle of the zone axis from the primary beam. Since the chromium peak intensity tends to mimic the aluminum peak intensity, i.e. it decreases with increasing deviation angle, a strong site preference for aluminum is shown. It is not known whether nickel vacancies are created by this site preference for alloys in which the combined chromium and aluminum contents exceed the nickel content.

77

Figure 4-24. Bright Field TEM Micrograph of <100> Dislocations in HAM Cast Ni-50Al
Deformed 0.3 Percent at 300K

ORIGINAL PAGE
BLACK AND WHITE PHOTOGRAPH
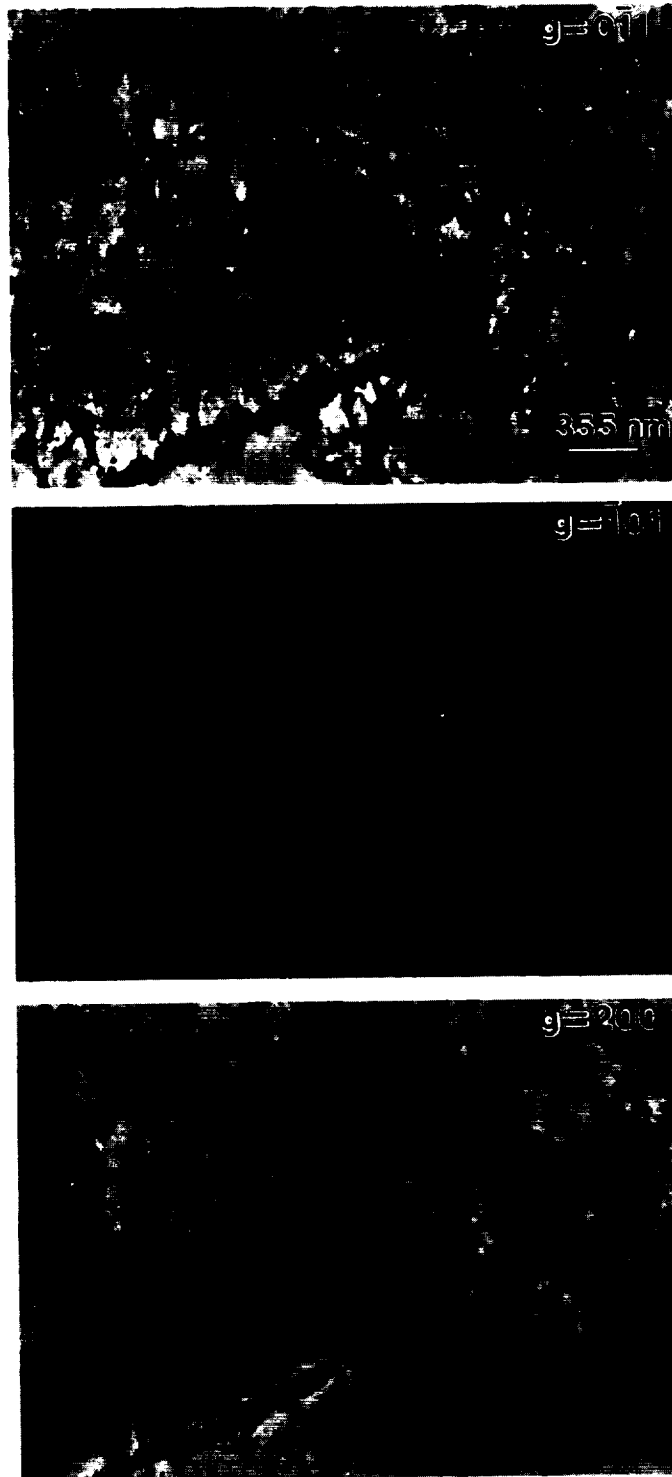
Figure 4-25. TEM Dislocation Analysis Indicating <100> Dislocations in HAM Cast
Ni-50Al-1Cr Deformed 0.3 Percent at 300K
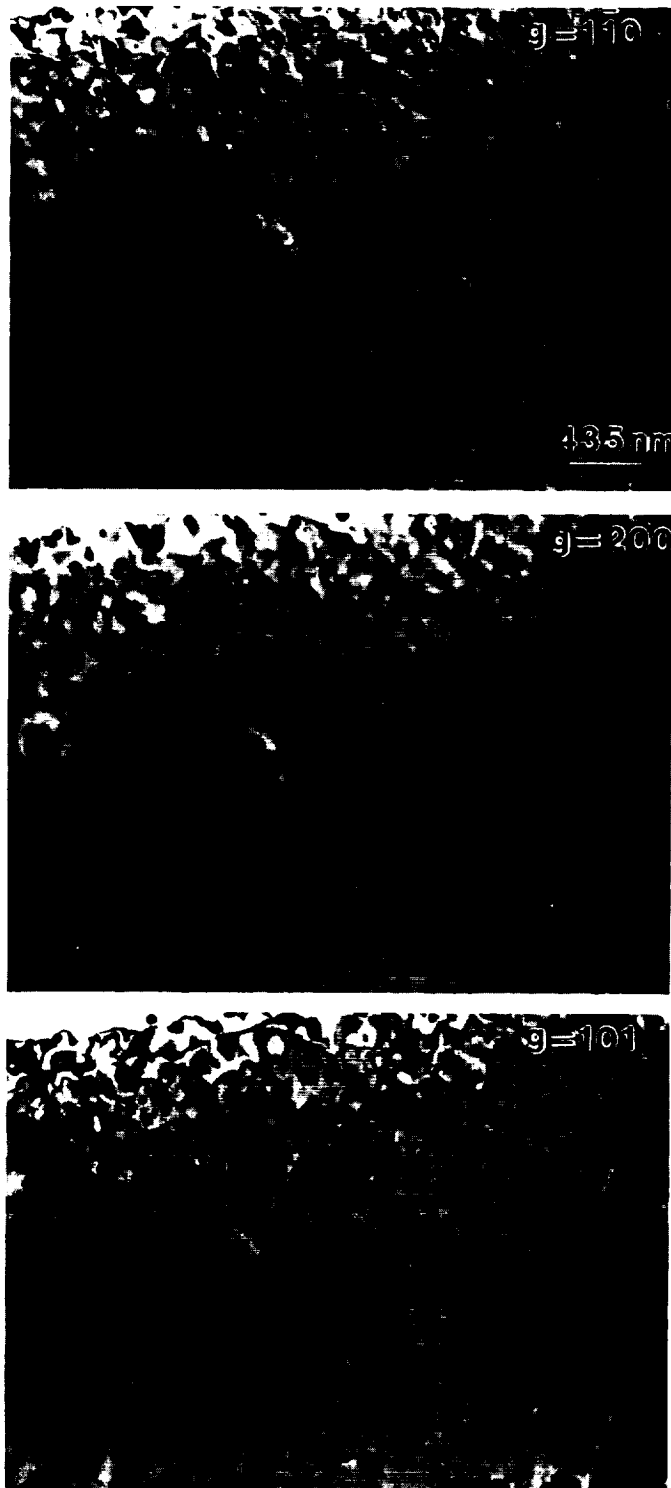
Figure 4-26. TEM Dislocation Analysis Indicating <100> Dislocations in HAM Cast
Ni-48Al-2Cr Deformed 0.6 Percent at 300K

(a)

(b)

Figure 4-27. TEM Microstructure of HAM Cast Ni-49Al-2Cr Deformed 0.6 Percent at 300K (a) Large Precipitates; (b) <100> Dislocations

(a)

(b)

Figure 4-28. Bright Field TEM Micrographs of HAM Cast Ni-50Al-2Cr Deformed 0.2
Percent at 300K
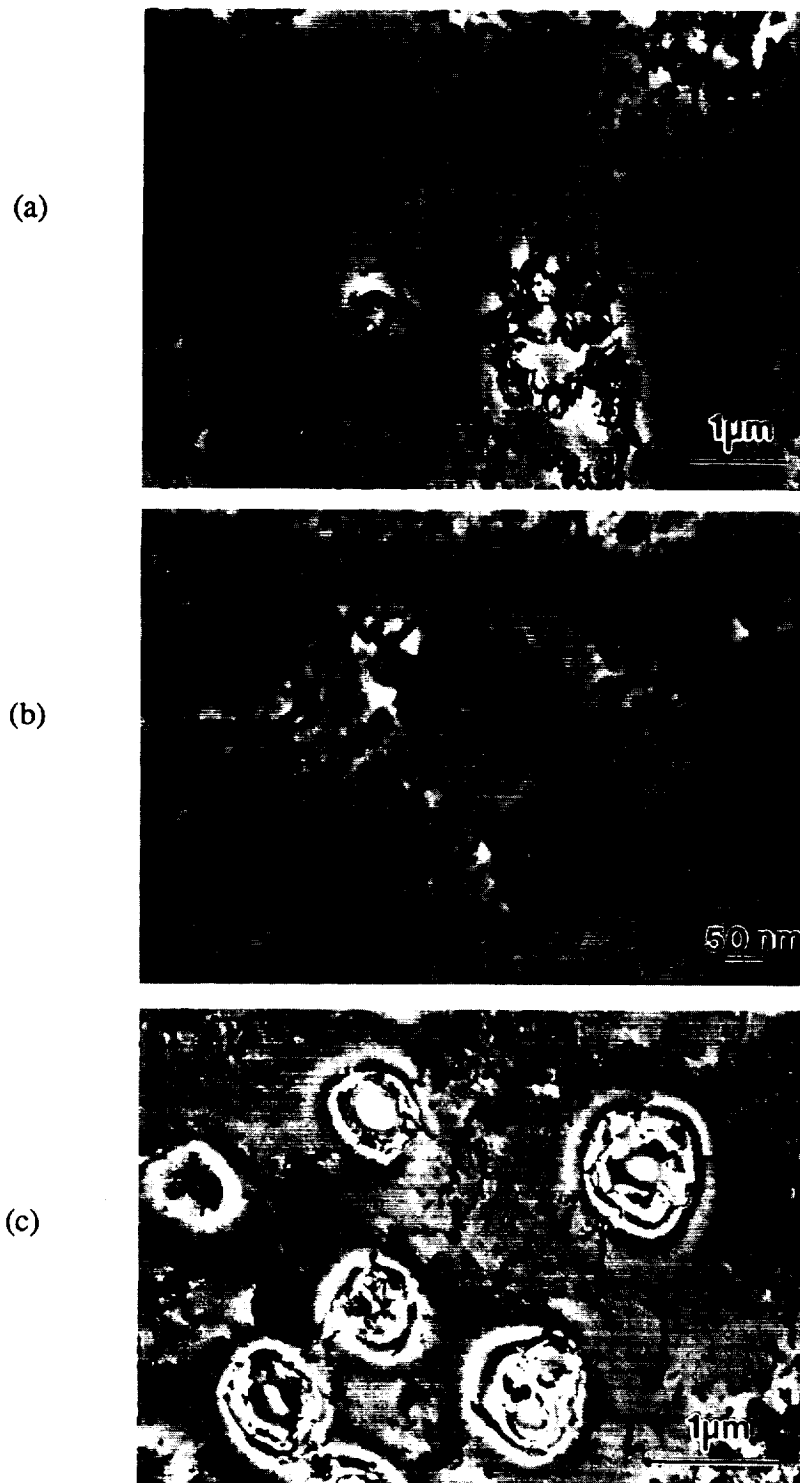
Figure 4-29. TEM Microstructure of HAM Cast Ni-45Al-5 Chromium Deformed 0.3 Percent at 300K (a) Slip Bands; (b) Fine Precipitates and Dislocation Loops; (c) Coarser Precipitates
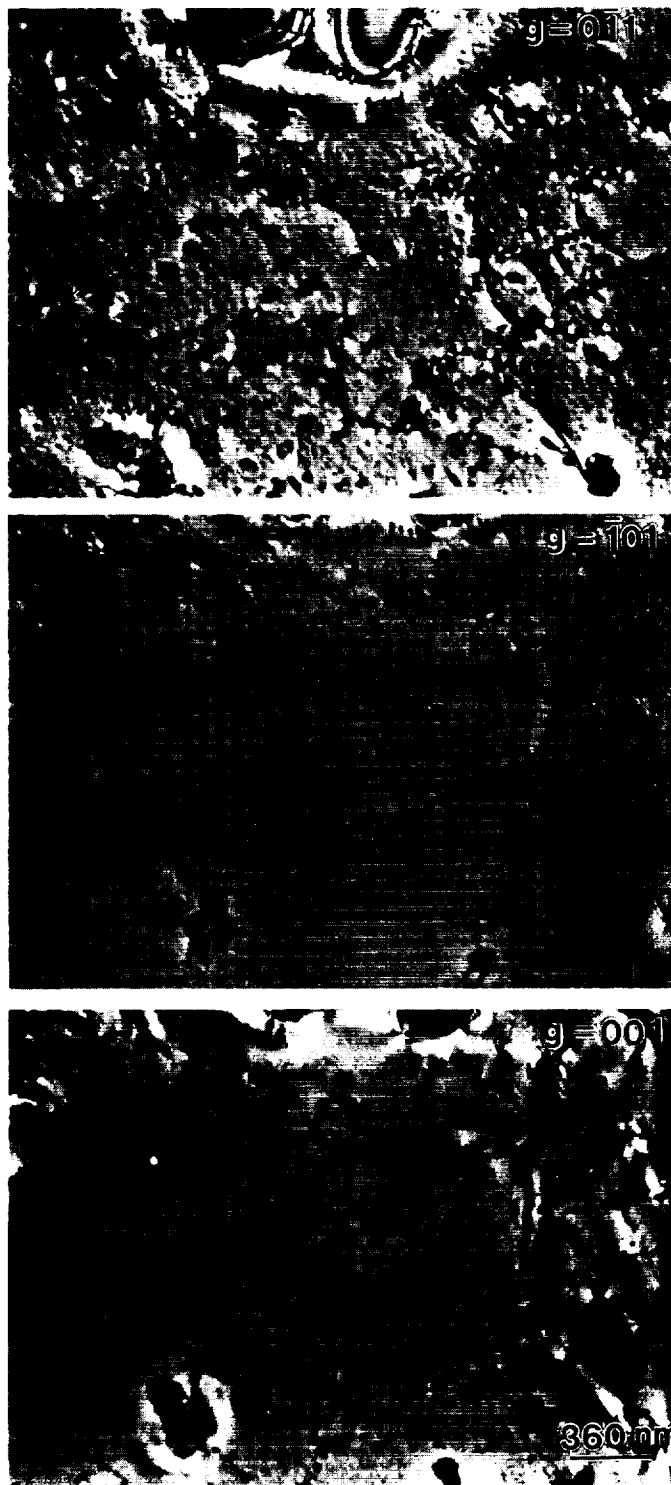
Figure 4-30. TEM Dislocation Analysis Indicating <100> Dislocations in HAM Cast
Ni-47.5Al-5Cr Deformed 0.3 Percent at 300K

84

ORIGINAL PAGE
BLACK AND WHITE PHOTOGRAPH

Figure 4-31. Bright Field TEM Micrographs of Large, Irregular Alpha-Chromium Phase
and Fine Precipitation in HAM Cast Ni-47.5Al-5Cr Deformed 0.3 Percent at 300K

85

360 nm

(a)

0.5 µm

(b)

Figure 4-32. Bright Field TEM Micrographs of HAM Cast Ni-50Al-5Cr Deformed 0.35
Percent at 300K (a) Pinning of <100> Dislocations by Precipitates; (b) Interfacial
Dislocation Nets at Larger Alpha-Chromium Particles
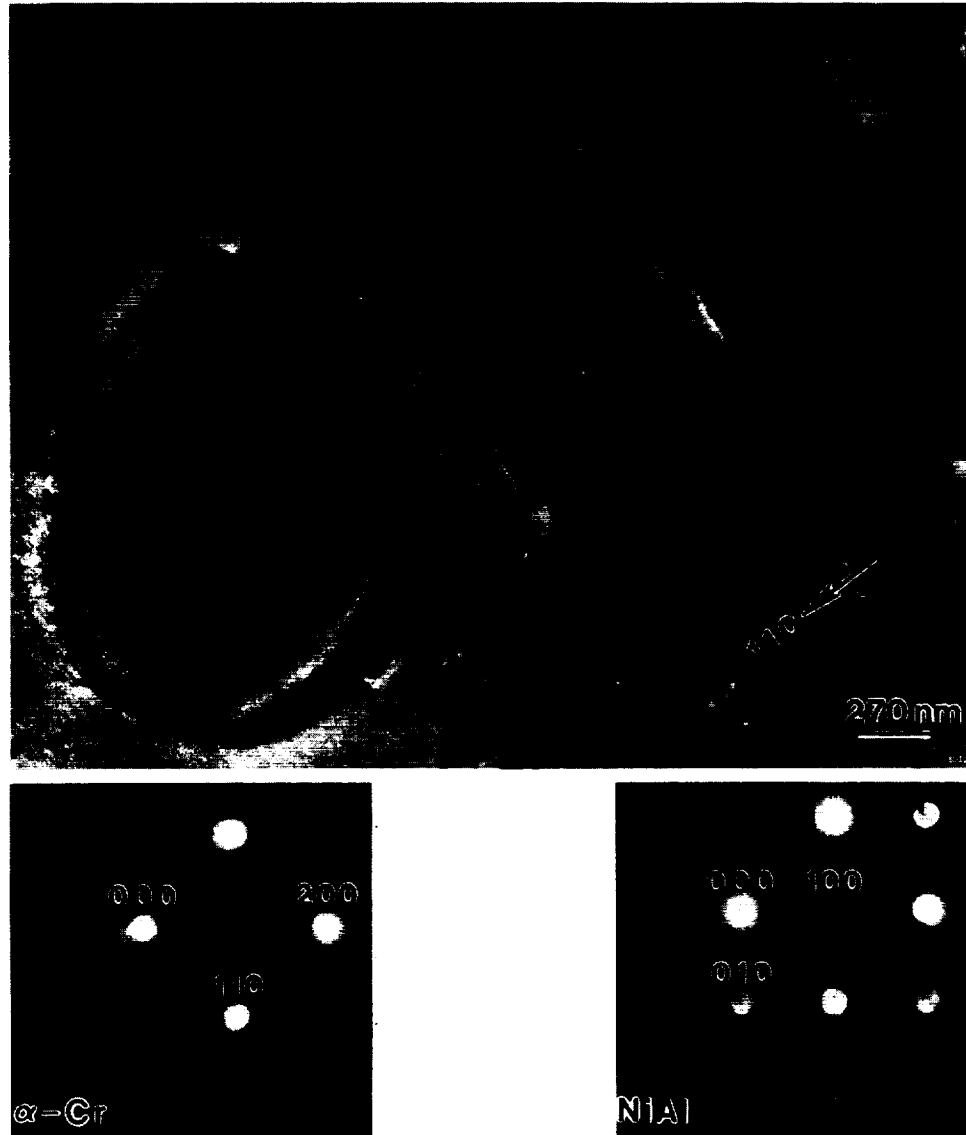
Figure 4-33. Bright Field TEM Micrographs Showing Orientation Relationship Between B2 Matrix and A2 (BCC) Alpha-Chromium Precipitates in HAM Cast Ni-50Al-5Cr Deformed 0.35 Percent at 300K

Figure 4-34. Bright Field TEM Micrographs of AM Cast Ni-48.5Al-5.2Cr Deformed 0.2 Percent at 300K. Note alpha-chromium dendrites and $Cr_{23}C_6$ precipitates.
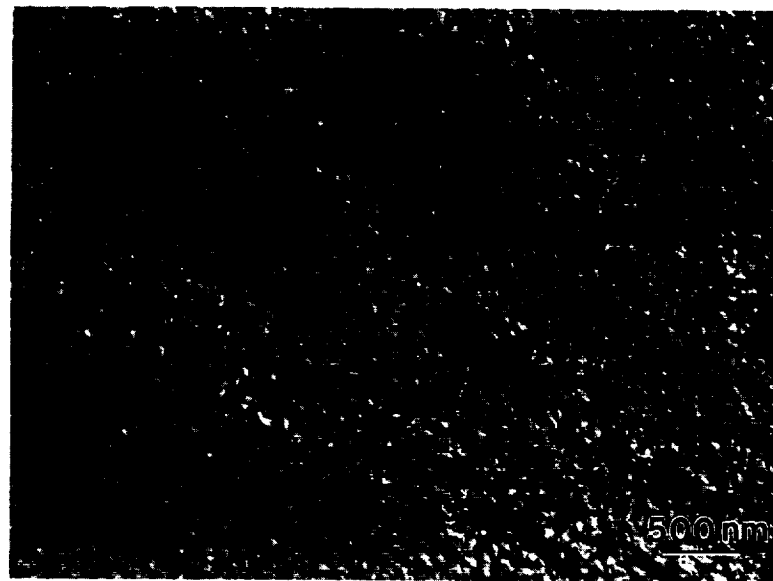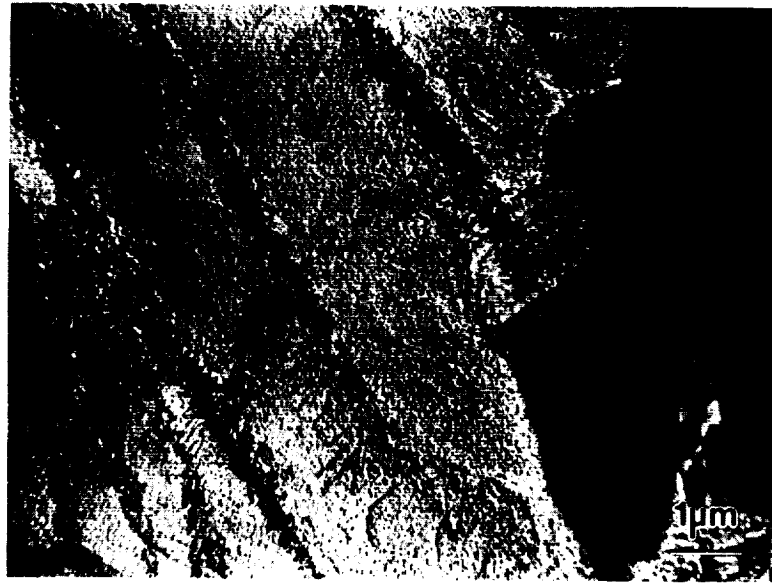
Figure 4-35. Bright Field TEM Micrographs of Slip Bands Containing <100> Dislocations
in AM Cast Ni-48.5Al-5.2 Chromium Deformed 0.2 Percent at 300K
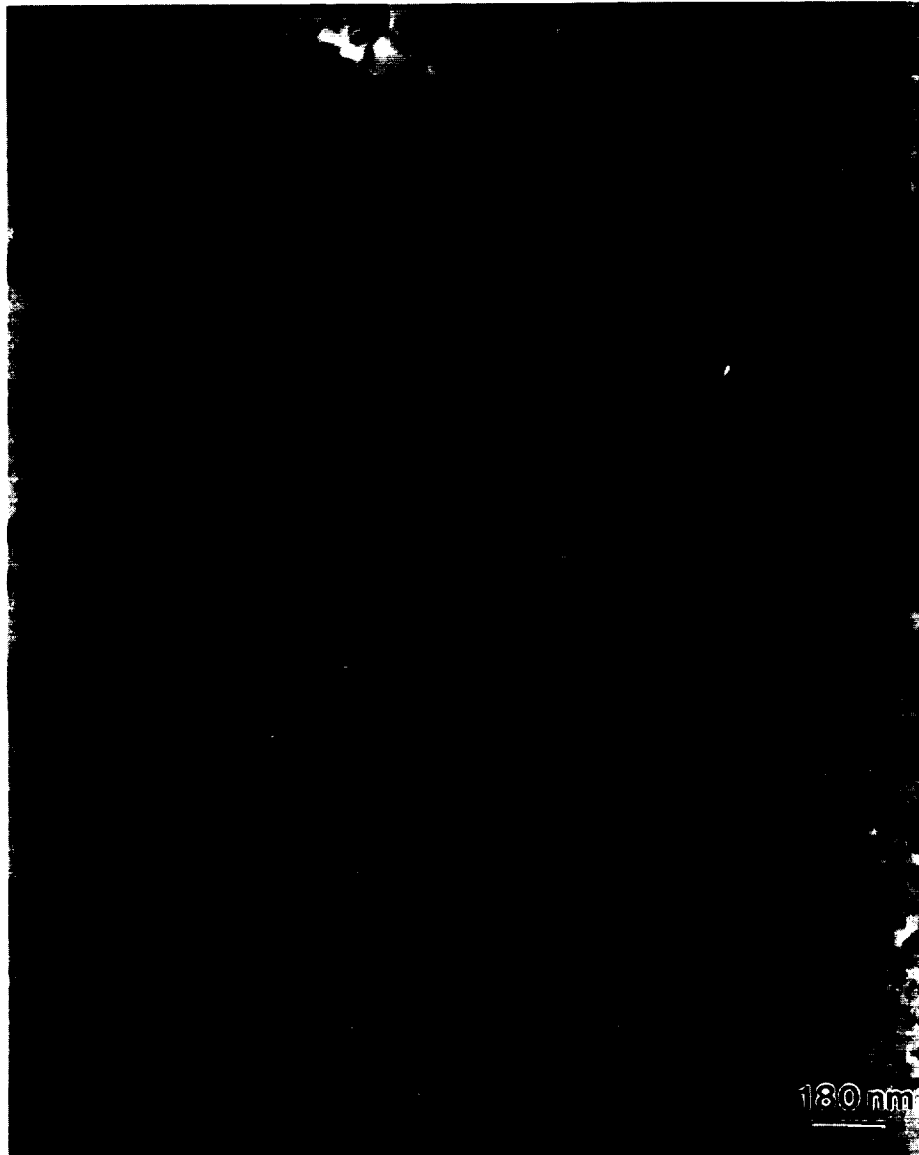
Figure 4-36. Bright Field TEM Micrograph of HAM Cast Ni-48.5Al-5.2Cr Deformed 0.3 Percent at 300K. Note the wide distribution of precipitate diameters.

(a)
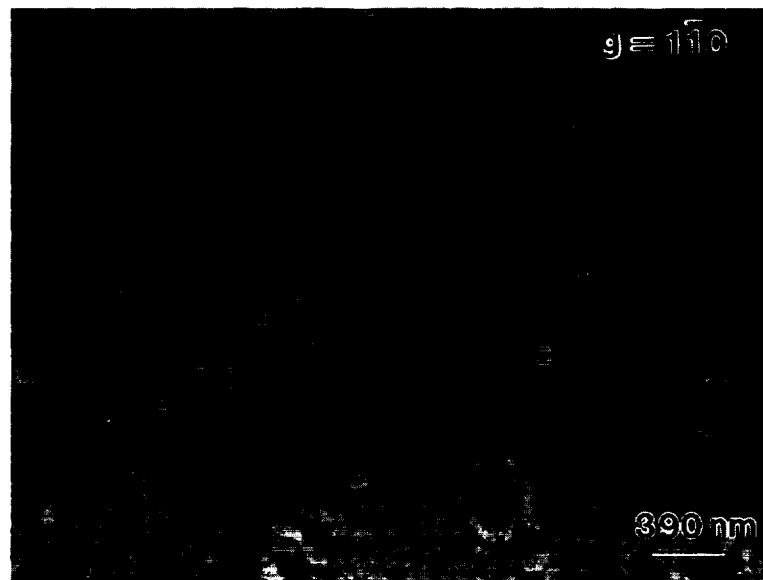
(b)

Figure 4-37. Bright Field TEM Micrographs of HAM Cast Ni-48.5Al-5.2Cr Deformed
0.8 Percent at 300K (a) Homogeneously Distributed <100> Dislocations; (b) Precipitation

91

Figure 4-38. Bright Field TEM Micrograph of As-Extruded XVIM Ni-50Al

Figure 4-39. Bright Field TEM Micrograph of XVIM Ni-50Al Deformed 0.6 Percent at 300K

Figure 4-40. Bright Field TEM Micrograph of XVIM Ni-49.5Al-1Cr Deformed 0.6 Percent at 300K. Slip bands consist of <100> dislocations.
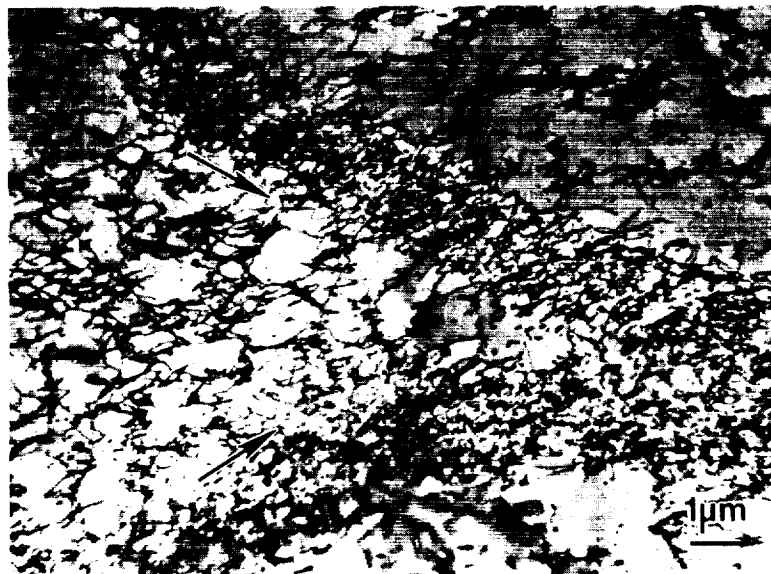
Figure 4-41. Bright Field TEM Micrograph of XVIM Ni-49.5Al-1Cr Deformed 0.6 Percent at 300K. Note curvature of slip band at intersection.

93
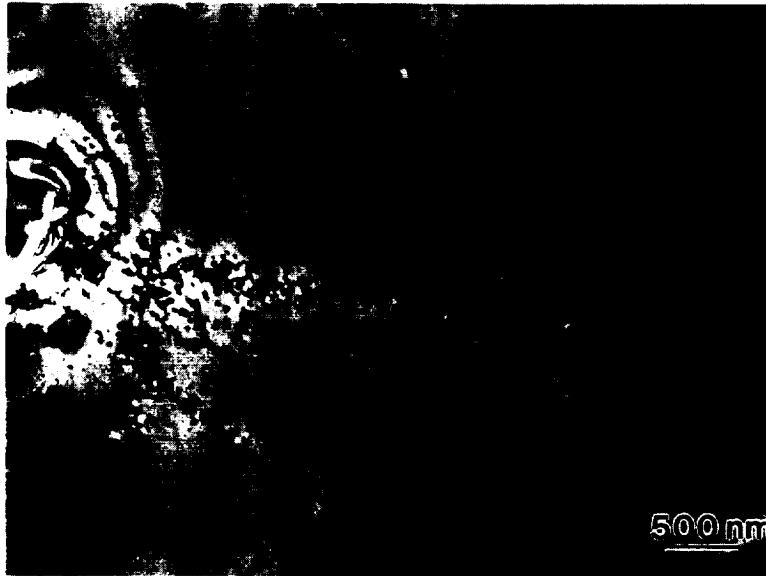
Figure 4-42. Bright Field TEM Micrograph of As-Extruded XVIM Ni-49Al-2Cr

Figure 4-43. Bright Field TEM Micrograph of As-Extruded XVIM Ni-48Al-2Cr.

ORIGINAL PAGE
BLACK AND WHITE PHOTOGRAPH
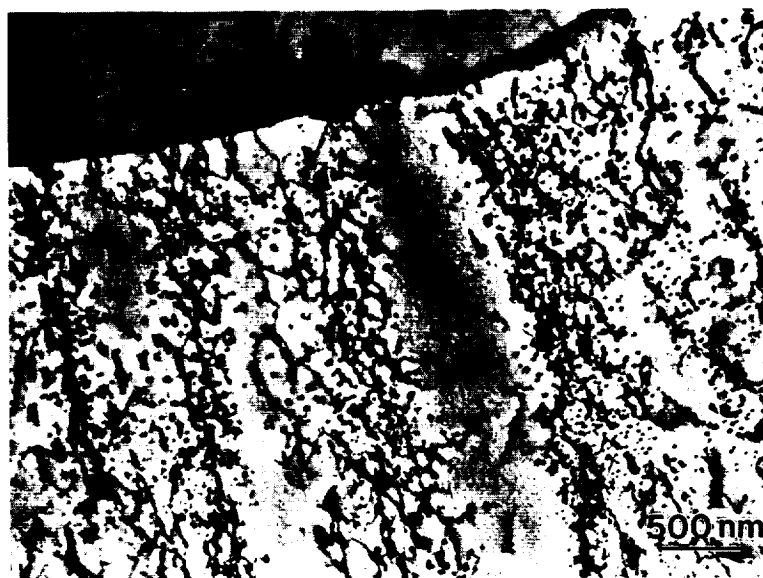
Figure 4-44. Bright Field TEM Micrograph of XVIM Ni-48Al-2Cr Deformed 0.7 Percent
at 300K

Figure 4-45. Bright Field TEM Micrograph of XVIM Ni-49Al-2Cr Deformed 0.1 Percent
at 300K Showing the Intersection of Two Slip Bands of <100> Dislocations
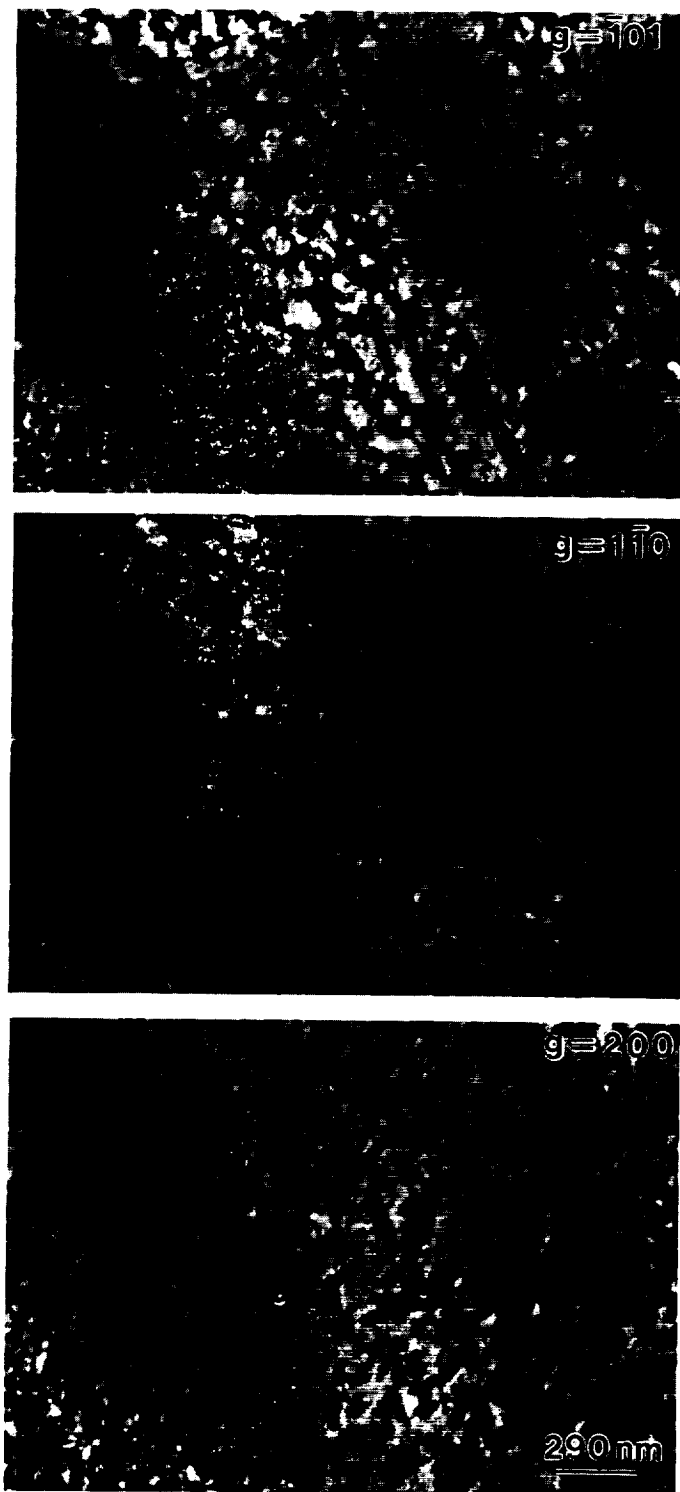
Figure 4-46. TEM Dislocation Analysis of XVIM Ni-48Al-2Cr Deformed 0.7 Percent at
300K. All Burgers vectors were determined to be <100>.

Figure 4-47. Bright Field TEM Micrograph of As-Extruded XAP Ni-45Al-5Cr
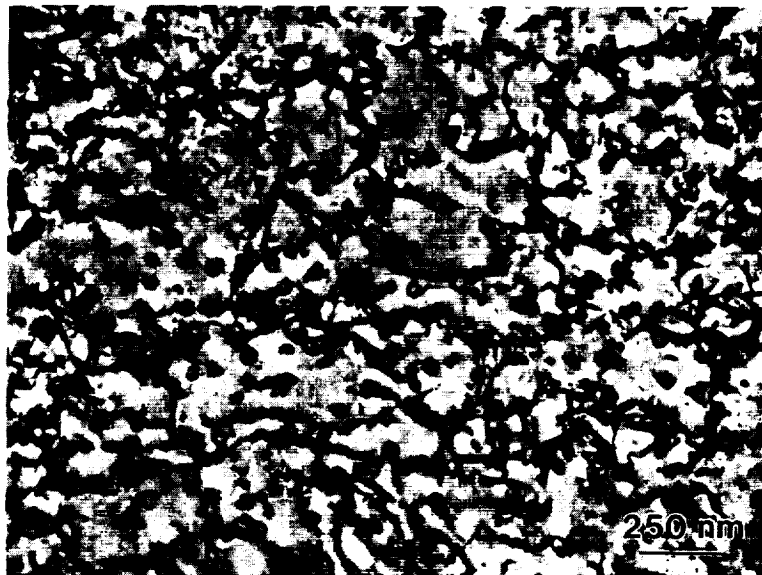
(a)
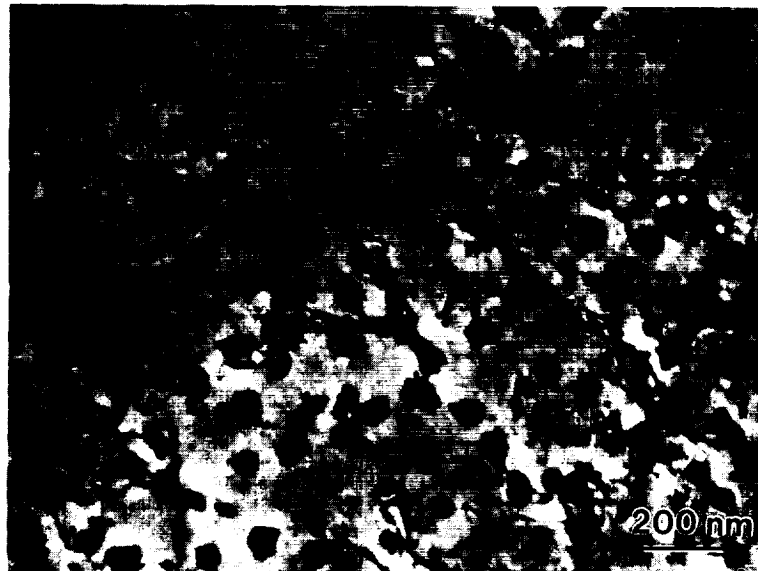
(b)

Figure 4-48. Bright Field TEM Micrographs of XAP Ni-45Al-5Cr Deformed 0.6 Percent at 300K (a) Homogeneously distributed dislocations; (b) Precipitation
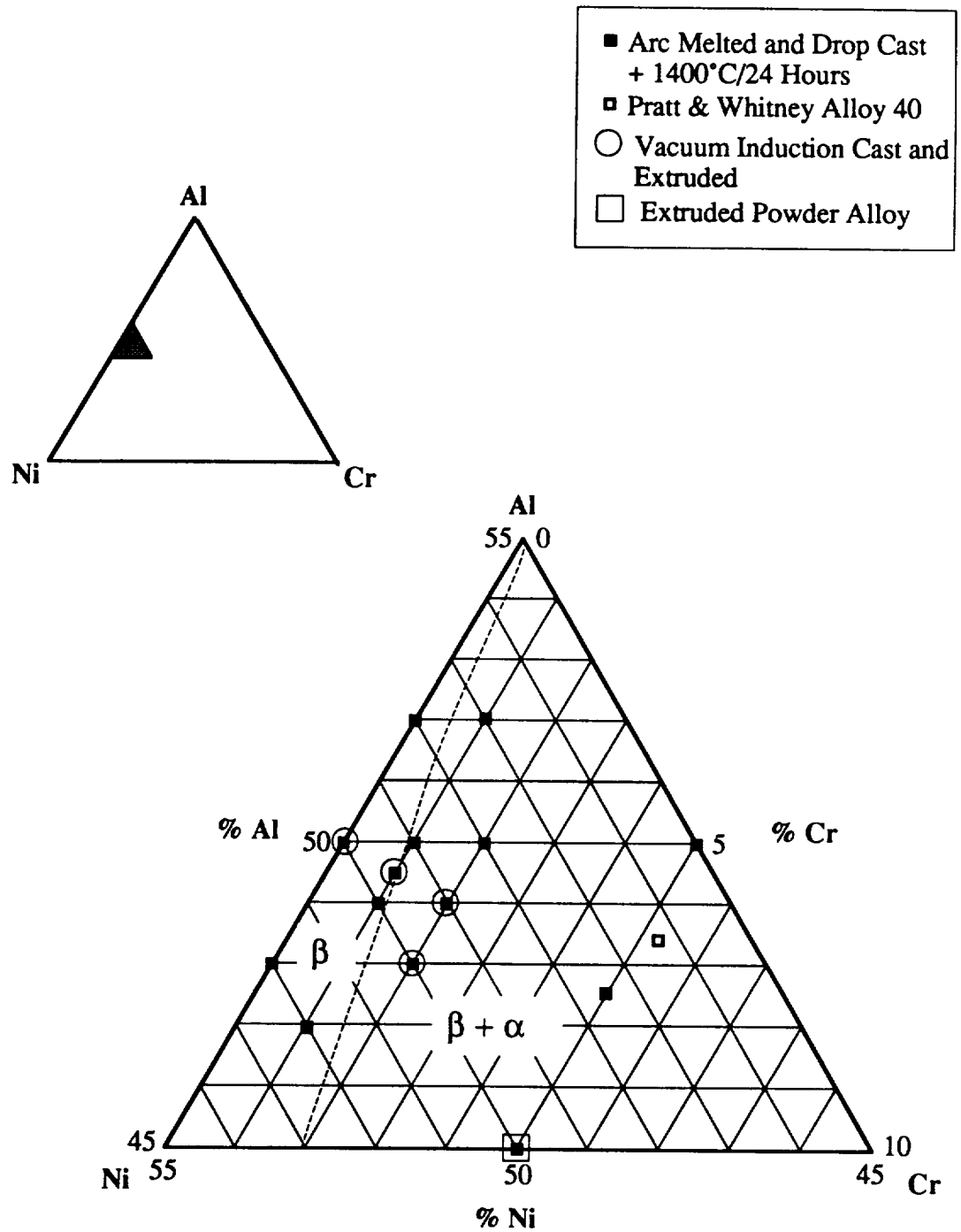
Figure 4-49. Portion of Ternary Ni-Al-Cr Ternary Phase Diagram Derived from Current Study. The dotted line corresponds to the solubility of chromium in NiAl.

Dislocation Analysis

The Burgers vectors of about 2600 dislocations were analyzed. The raw data is given in Appendix B. The results indicate a predominance of <100> Burgers vectors for all alloy compositions and conditions investigated. Very few <111> dislocations were noted (less than one percent overall). Slightly more <110> dislocations (approximately four percent overall) were observed, however, these were primarily in the extrusions. If the extrusions are considered separately, about 10 to 15 percent of the dislocations were <110>s, for either as-extruded or 300K deformed material.

Detailed analyses, summarized in Table 4-7, indicated that the predominant slip plane was {011}, hence, the slip system was usually of the type <100>{011}. An example analysis is shown in Figure 4-51. However, it was not uncommon to find slip on cube planes, i.e. <100>{001}. Analysis of <110> dislocations also indicated a {110} slip plane, Figure 4-52.

Dislocation line directions tended to be near <111> or between <111> and <110> type directions. This produced dislocations of nominally edge or mixed character with typical line-slip vector angles of 40 to 135 degrees. In no case were any pure screw dislocations noted. Although the <110> dislocations were also of edge or near-edge character, their line directions tended to be along <100>.

X-ray Diffractometry

The lattice parameters derived from the X-ray diffractometer traces for B2 NiAl in each alloy are shown in Table 4-8 along with the standard deviation as an estimation of the error. Ni-49Al-2Cr, Ni-50Al-5Cr and Ni-48.5Al-5.2Cr also displayed extra peaks, corresponding to BCC chromium; the lattice parameters of this phase are also given in Table 4-8. A number of the peaks from the other ternary alloys displayed skewed

"shoulders" which probably corresponded to the BCC phase, but the low volume fractions and peak convolution with the B2 NiAl prevented measurement of the lattice parameter. As a result, the lattice parameters of the B2 phase derived from the ternary alloys containing precipitates are probably subject to some error. However, data from the binary alloys, and the ternary alloys containing chromium solely in solid solution, are felt to be reasonably accurate. These values are plotted in Figure 4-53 versus aluminum content.

From this figure is seen that the lattice parameter is maximized at aluminum contents near 50 percent. It is also clear that chromium, as substituted here, has little effect on the lattice parameter of the NiAl phase. In effect, chromium additions below the solubility limit behave as aluminum additions, in agreement with the TEM ALCHEMI results above.
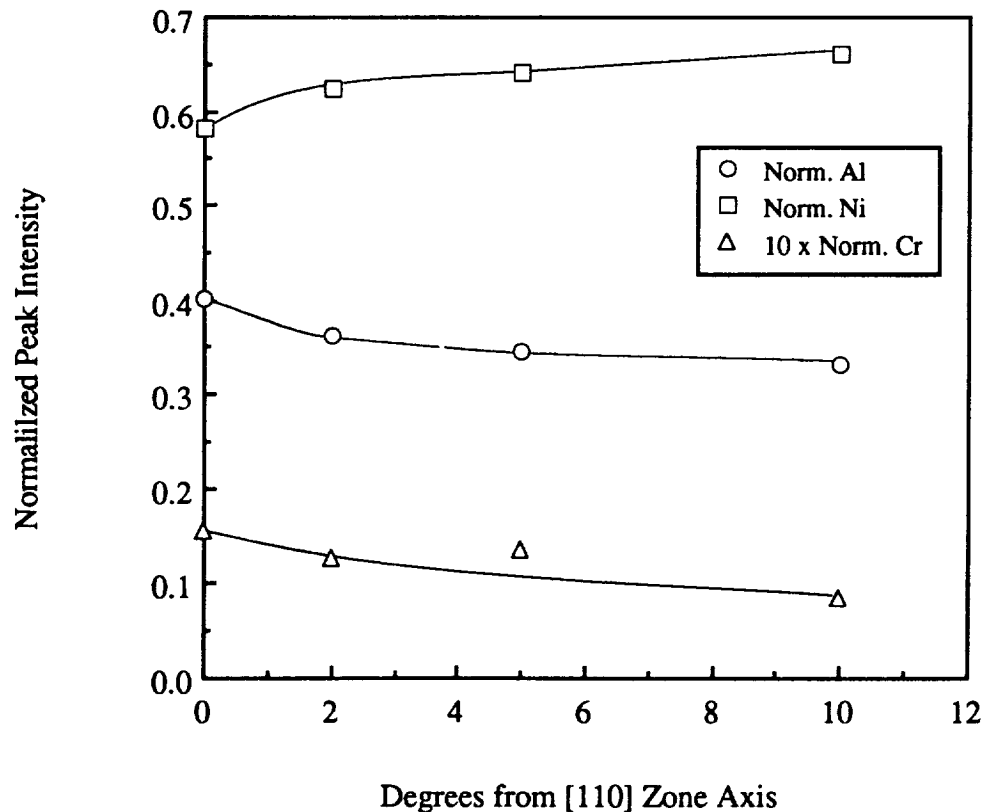
Figure 4-50. Intensity of X-ray Peaks of Nickel, Aluminum and Chromium as a Function of Deviation from the [110] Zone Axis - ALCHEMI Analysis.
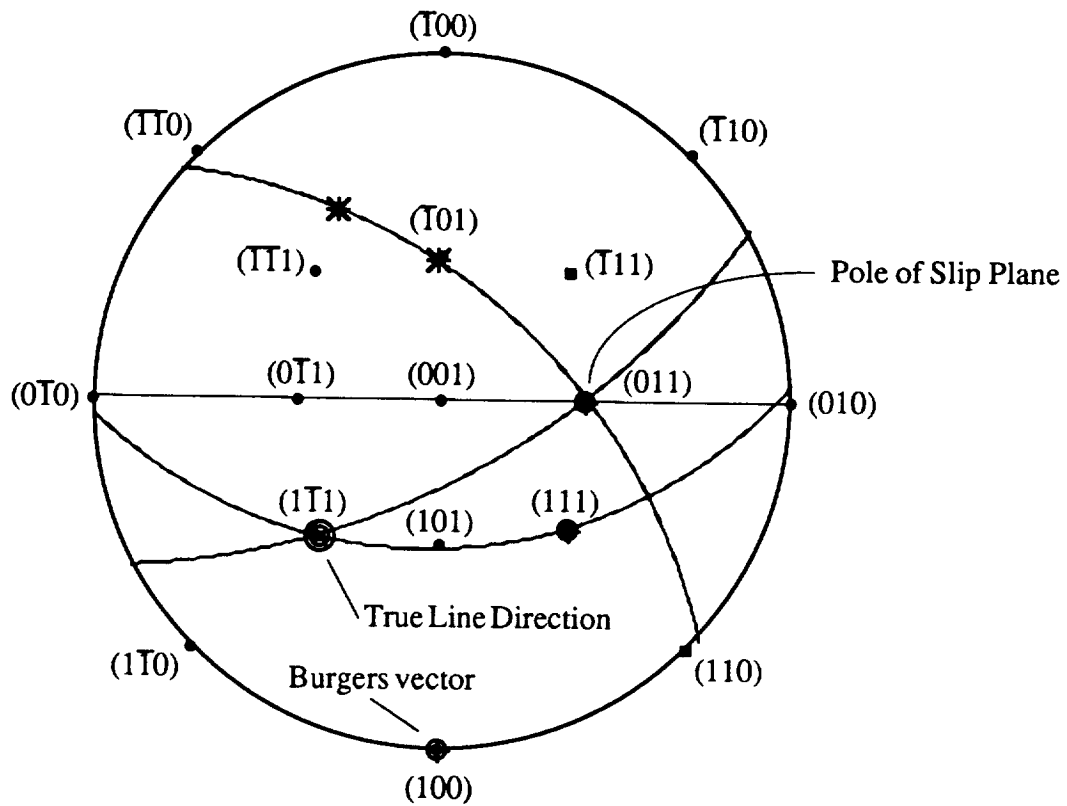
Figure 4-51. Stereographic Projection Showing Slip Plane Analysis of a <100>
Dislocation in Ni-48Al-2Cr Deformed 0.7 Percent at 300K
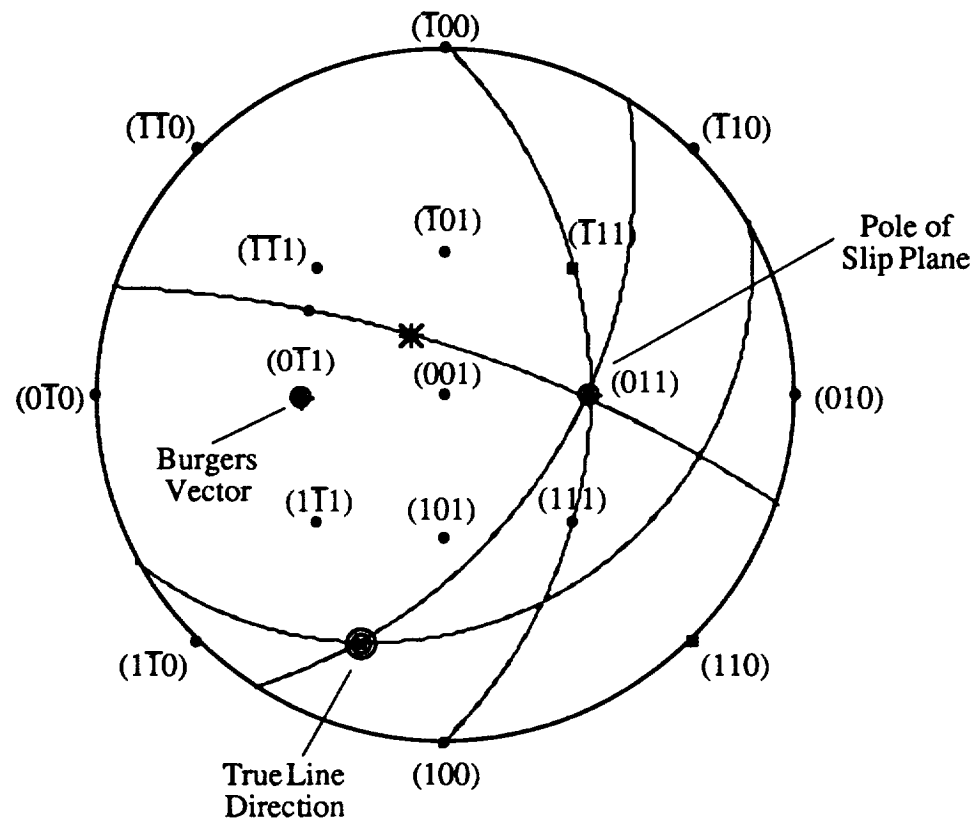
Figure 4-52. Stereographic Projection Showing Slip Plane Analysis of a <110> Dislocation in As-Extruded Ni-49Al-2Cr

Table 4-7. Results of Detailed Analysis of Several Dislocations in Selected NiAl+Cr Alloys

Alloy Composition	Processing Method	Analysis Number	Slip System	Character (degrees)	Line Direction
Ni-50Al	as extruded	3438-3	[010](101)	mixed (50)	near [$\bar{1}\bar{1}$1]
Ni-50Al	as extruded	3438-10	[010](101)	edge (95)	near [$\bar{1}$01]
Ni-50Al	as extruded	3464-4	[010](101)	mixed (42)	near [$\bar{1}\bar{1}$1]
Ni-50Al	as extruded	3464-17	[010](001)	mixed (83)	near [100]
Ni-50Al	extr. + 0.6%	3380-C	[100](011)	mixed (57)	near [1$\bar{1}$1]
Ni-50Al	extr. + 0.6%	3380-I	[100](011)	mixed (68)	near [1$\bar{1}$1]
Ni-50Al	extr. + 0.6%	3380-T	[001](110)	mixed (51)	near [$\bar{1}$11]
Ni-49.5Al-1Cr	extr. + 0.7%	3536-11	[010](001)	mixed (40)	near [111]
Ni-49.5Al-1Cr	extr. + 0.7%	3536-10	[010](101)	mixed (36)	near [110]
Ni-49.5Al-1Cr	extr. + 0.7%	3536-15	[001](100)	mixed (45)	near [011]
Ni-48Al-2Cr	extr. + 0.7%	3550-20	[100](010)	mixed (47)	near [101]
Ni-48Al-2Cr	extr. + 0.7%	3550-6	[100](011)	mixed (52)	near [1$\bar{1}$1]
Ni-48Al-2Cr	extr. + 0.7%	3550-18	[010](101)	mixed (101)	near [$\bar{1}$01]
Ni-49Al-2Cr	as extruded	3494-B	[0$\bar{1}$1](011)	edge (92)	near [100]
Ni-49Al-2Cr	as extruded	3494-F	[0$\bar{1}$1](011)	mixed (114)	near [100]
Ni-49Al-2Cr	as extruded	3494-A	[100](011)	mixed (122)	near [11$\bar{1}$]
Ni-49Al-2Cr	extr. + 0.7%	3506-21	[010](101)	mixed (53)	near [11$\bar{1}$]
Ni-49Al-2Cr	extr. + 0.7%	3506-2	[010](001)	mixed (122)	near [1$\bar{1}$0]
Ni-49Al-2Cr	extr. + 0.7%	3506-11	[001](010)	mixed (135)	near [10$\bar{1}$]
Ni-49Al-2Cr	extr. + 0.7%	3506-11b	[001](110)	edge (93)	near [1$\bar{1}$0]
Ni-45Al-5Cr	as extruded	3473-3	[010]($\bar{1}$01)	mixed (43)	near [111]
Ni-45Al-5Cr	as extruded	3473-9	[100](011)	edge (92)	near [0$\bar{1}$1]
Ni-45Al-5Cr	as extruded	3473-6	[100]($\bar{0}$01)	mixed (82)	near [010]
Ni-45Al-5Cr	as extruded	3473-5	[001]($\bar{1}$10)	mixed (80)	near [110]

Table 4-8. Lattice Parameters of HAM Cast NiAl and NiAl+Cr Alloy Phases

Alloy	NiAl (Å)	α-Cr (Å)
Ni-48Al	2.888 ± 0.001	---
Ni-50Al	2.890 ± 0.001	---
Ni-52Al	2.885 ± 0.004	---
Ni-47Al-1Cr	2.888 ± 0.002	---
Ni-49Al-1Cr	2.890 ± 0.003	---
Ni-49.5Al-1Cr	2.890 ± 0.002	---
Ni-50Al-1Cr	2.885 ± 0.001	---
Ni-52Al-1Cr	2.890 ± 0.002	---
Ni-48Al-2Cr	2.893 ± 0.002	---
Ni-49Al-2Cr	2.889 ± 0.001	2.91 ± 0.01
Ni-50Al-2Cr	2.893 ± 0.001	---
Ni-45Al-5Cr	2.887 ± 0.002	---
Ni-47.5Al-5Cr	2.891 ± 0.001	---
Ni-50Al-5Cr	2.887 ± 0.001	2.934 ± 0.005
Ni-48.5Al-5.2Cr	2.892 ± 0.001	2.92 ± 0.01
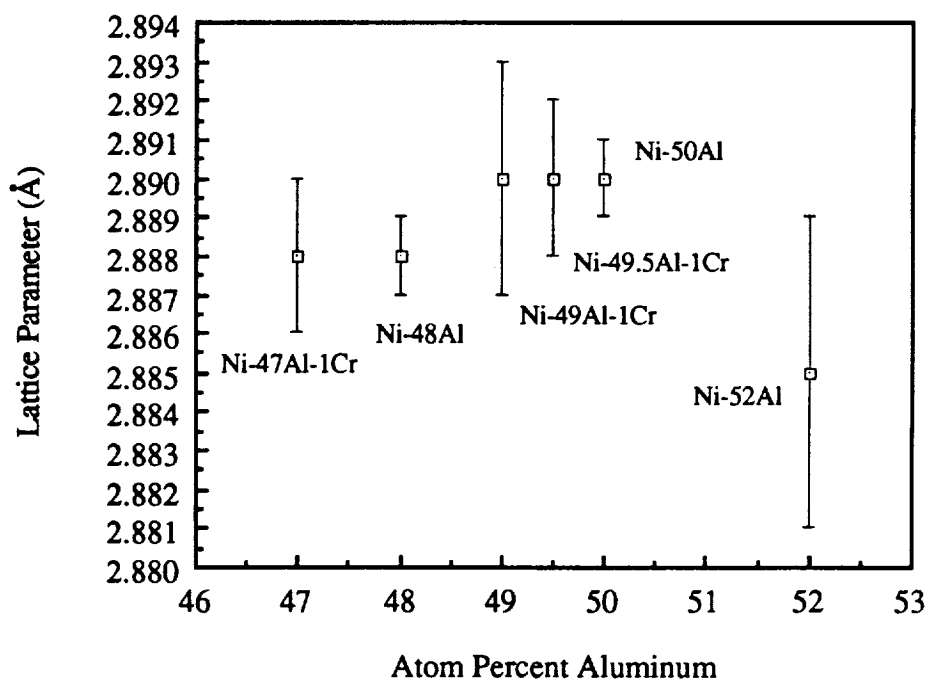
Figure 4-53. Lattice Parameters of Binary NiAl and Ternary NiAl+Cr Single Phase Alloys
as a Function of Aluminum Content

CHAPTER 5
DISCUSSION

The diverse properties exhibited by the alloys in this study merit close evaluation of the interplay between composition, processing, and microstructure. Microstructural evolution of the various alloys is examined first, to describe the environment through which dislocations must travel to produce plastic deformation. The slip systems which have been determined will then be discussed--especially in light of the lack of <111> Burgers vectors, which were expected based on previous research. Finally, the resulting mechanical properties will be rationalized in terms of the various strengthening mechanisms.

Microstructural Evolution

If one takes a vertical slice through the nickel-aluminum-chromium phase diagram, from NiAl to pure chromium, a pseudobinary eutectic diagram is obtained. This diagram is presented in Figure 5-1. By this definition, the nickel-to-aluminum ratio is equal to one for the alloys represented by this figure. However, for the purposes of understanding the solidification sequences, this diagram can be generally applied to all the alloys in this study. Due to the retrograde solvus trace, it can be seen that alloys containing less than about ten atomic percent chromium will precipitate alpha-chromium following solidification. In practice, the fast cooling associated with arc melting prevents equilibrium from being attained, leading to coring and chromium-rich interdendritic liquid. In this manner, the as-cast microstructures are expected to contain interdendritic alpha-chromium, NiAl/Cr eutectic, and NiAl dendrites which contain alpha-chromium precipitates of varying size distribution.
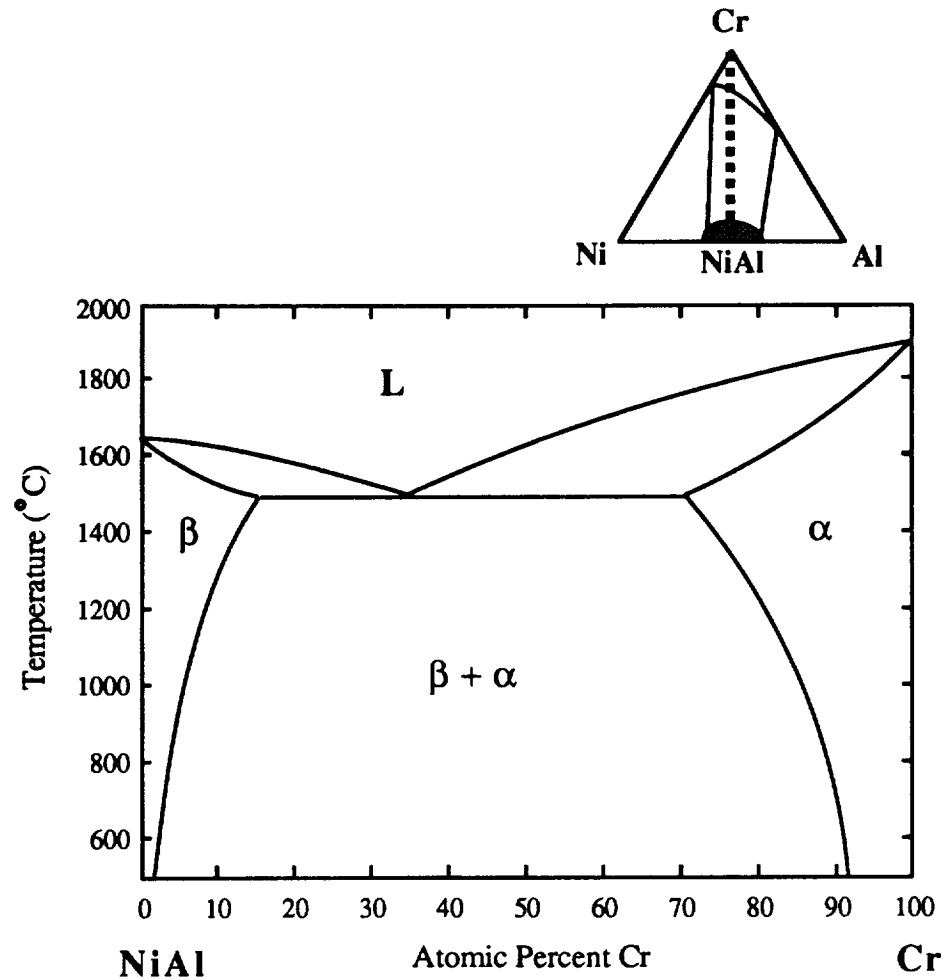
Figure 5-1. NiAl-Cr Pseudobinary Phase Diagram [17]

This interpretation of microstructural evolution is demonstrated by the as-cast microstructure of Ni-48.5Al-5.2Cr shown in Figure 4-34. The gradient in chromium content is indicated by the decreasing volume fraction and scale of precipitation leading away from the interdendritic region.

Upon homogenization at 1400°C, all the compositions in this study should be single phase prior to cooling. The same is true of the extrusions, since extrusion was conducted at about 1100°C. Higher chromium contents are expected to lead to a larger size distribution of alpha-chromium precipitates, since precipitation occurs over a wide

temperature range. Alloys containing less chromium, such as Ni-49Al-2Cr, would not be expected to precipitate until a relatively low temperature, say about 600°C. In this case, the diffusion distances are small and precipitation occurs over a much smaller temperature range than in more chromium-rich alloys; therefore, the precipitate diameter and size distribution are expected to be small. In all alloys, heterogeneous nucleation sites, such as grain boundaries, produce larger precipitates and are surrounded by the expected precipitate-free-zone. Although this description can account, in general, for the microstructures observed, there are some detailed aspects of the microstructures which are worthy of further discussion.

The marked alignment of the precipitates into rows deserves comment. This behavior is most pronounced in aluminum-rich alloys, such as Ni-50Al-5Cr, Figure 4-9. The alignment indicates that, although much of the prior interdendritic alpha-chromium was dissolved during homogenization, the local concentration gradient was not eliminated. On cooling below the specific solvus temperature for each region alpha-chromium reprecipitated as discrete particles. That the aligned rows exhibit orthogonal branching reinforces this explanation, since the growth of NiAl-Cr rod-like eutectic is known to proceed in <100> directions with a cube-on-cube orientation relationship [110]. An alternative explanation for the precipitate alignment is heterogeneous nucleation upon some linear defect, such as a dislocation, or perhaps subgrains. However, the observed row dimensions and the lack of supporting TEM observations make such explanations unlikely.

Another point of discussion is the observation of $Cr_{23}C_6$ carbides embedded within the interdendritic alpha-chromium of the AM Ni-48.5Al-5.2Cr. This particular alloy was produced in an earlier batch of castings using different starting materials from the other 14 HAM alloys. As shown in Table 4-2, the carbon level measured in this alloy was typically four times that of the other alloys. In addition, iron contamination was noted. Although the source of these impurities was not determined, it appears that the chromium had a

strong tendency to "getter" this carbon in the liquid state and cause it to concentrate in the interdendritic regions of the AM casting. On solidification, $Cr_{23}C_6$ may form from the remaining solute-rich liquid, or possibly by solid state precipitation within the interdendritic alpha-chromium.

Dislocation Configurations and Slip

This section addresses the effects that chromium appears to have upon the slip process. The observed Burgers vectors and slip systems are rationalized first, followed by a discussion of the enhanced slip band and loop formation in the chromium-containing alloys. Finally, the interface structure between the precipitates and the matrix is examined.

Observed Slip Systems

The predominance of <100>{011} and <100>{001} slip systems in this study is interesting, since the earlier results of Law and Blackburn [15] reported <111>{112} slip in cast Ni-48.5Al-5.2Cr. The only other references to <111> slip in chromium-modified NiAl alloys dealt with either directionally-solidified material with a <100> orientation [16] or <100> single crystals [18]. In both cases, testing was conducted in the hard orientation, which has been shown to promote <111> slip even in binary NiAl, due to the lack of resolved shear stress upon any of the usual <100>{011} or <100>{001} slip systems. Therefore, the only applicable reference on the effect of chromium in altering the primary slip mode of NiAl is that of Law and Blackburn [15].

There are few explanations to account for the inconsistency of the current results and those of Law and Blackburn's [15]. One is that the particular grain which was analyzed by Law and Blackburn was, by chance, oriented in a hard orientation relative to the primary compressive stress. This would promote <111> slip as described in the single crystal studies. No account was given by Law and Blackburn of the number of grains or

specimens which were analyzed, nor of the grain orientation, so it is difficult to ascribe any degree of statistical significance to their work. Further, since their published reports show only a single bright field image, i.e. no invisibility conditions, their conclusions cannot be verified based on the presented data.

If the results of the present work are considered independently, the sole operation of the <100> Burgers vectors is not unexpected. As shown in Figure 4-49, the solubility of chromium in NiAl is less than two atomic percent. This is considerably less than the amount predicted to reduce the APBE such that <111> slip is promoted, based on theoretical predications [115] and also on the results of iron additions in other work [73].

The observed slip plane on which <100> slip took place in binary Ni-50Al was usually {011}, however, slip on the {001} planes was often observed. Comparison of the Schmid factors for <100>{001} and <100>{011} slip when the compression axis is [111] (the usual fiber texture for the extrusions) indicates the {011} planes are favored by about 40 percent, Table 5-1. However, when the stress axis tends towards <110> the two slip planes become competitive. This may be the reason for the operation either slip plane noted in the results. The low solubility of chromium only allows about two or three aluminum sites in a hundred to be occupied, and roughly competitive processes, such as slip on either {001} or {011} planes, should not be affected.

Table 5-1. Theoretical Schmid Factors for <100> Slip on {011} or {001} in Binary NiAl

Stress Axis	<100>{011}	<100>{001}
[100]	0.471	0.333
[110]	0.354	0.500

The presence of <110> dislocations in some of the specimens indicates that dislocations with these Burgers vectors may play a role in plastic deformation. The fact that the majority of the <110>'s detected were in extruded material suggests that they may be remnants of the elevated temperature deformation. In support, recent work by Miracle

[120] has suggested that the activation of <110> dislocations may be responsible for the BDTT in NiAl. If so, then the percentage of dislocations which have <110> Burgers vectors should be greater in the as-extruded condition than when deformed at room temperature. Simple calculation of these percentages based on the data in Appendix B shows about 1 percent <110>'s in the deformed HAM cast material, about 15 percent for the as-extruded material, and about 11 percent for the extruded and room-temperature deformed material. Since this difference is not extreme, it appears unlikely that the <110> dislocations are retained from elevated temperature deformation and are produced at room temperature.

It is also possible that the <110> dislocations are reaction products between different <100> dislocations gliding in the same grain. A large number of the analyses in this study yielded two, and sometimes three, different <100> Burgers vectors in a single grain. Although <110> and <111> dislocations in NiAl should spontaneously decompose into their associated <100> dislocations according to elastic energy considerations [9], the combination reaction may be possible under stress [120]. In such case, decomposition may not occur at low temperatures due to insufficient thermal activation.

The slip plane determined for the <110> dislocations is {110}. Interestingly, this slip system yields two independent slip systems which are completely independent of the three slip systems produced by the primary <100>{011} system, for a total of five independent systems [74]. Five independent slip systems satisfy the von Mises criterion for arbitrary deformation of a polycrystalline material and should allow some measure of plastic deformation, provided other barriers to slip are absent. Such a conclusion is contingent upon several things, however. First, there must be sufficient numbers of the <110>{1T0} dislocations and they must be able to nucleate easily, i.e., be energetically stable. Second, they must be sufficiently mobile. The results shown in Table 2-6 from Ball and Smallman's calculations show that dislocations with <110> Burgers vectors should be relatively mobile compared to the usual <100>s, regardless of whether they are

of screw or edge character. Presumably, dislocations of mixed character will have a mobility intermediate to either edge or screw. The elastic energy of the <110> dislocations depends largely upon the dislocation character, with those of pure screw character being about 17 percent greater than 100> edge dislocations and about 74 percent greater than <100> screws. Thus, <110> screw dislocations might be somewhat competitive with <100> edge dislocations.

To take advantage of the additional slip systems provided by <110> dislocations, they must not only be mobile within the operative glide plane, but must be able to expand unencumbered by line constraints, such as nodal links with the parent <100> dislocations. This situation is illustrated in Figure 5-2. In this schematic, a [110] dislocation is produced by the combination reaction of two <100> dislocations. For glide of the [110] dislocation to occur, it must form a half-loop extending away from the parent dislocations. Since the energy of the <110> half-loop is inversely proportional to its radius, it will exert a force upon the two nodes in an attempt to lengthen which is ultimately opposed by the external stresses on the crystal. This will produce an equilibrium state in which glide of the <110> dislocation is effectively hindered. To summarize, the mere presence of <110> dislocations is insufficient to make them available for general deformation, if indeed they are only reaction products of <100> dislocations.

Localized Slip and Dislocation Loops

Localized deformation in the form of slip bands is generally a result of cross-slip difficulty. In the case of NiAl, the strong preference for <100>{011} or <100>{001} slip should tend to confine slip to the most highly stressed system with little opportunity for deviation onto alternative systems for a given stress state. The tendency for dislocations to assume an edge-like orientation will also make cross-slip more difficult and so promote localized slip.

One effect of the chromium addition was to increase the propensity for localized deformation, in the form of slip bands, emanating from grain boundaries. Some examples are shown in Figures 4-40 and 4-44. In spite of the expected behavior based on a knowledge of the allowed slip systems, binary NiAl only occasionally displayed this tendency, and then only in a diffuse manner, while Ni-49.5Al-1Cr, Ni-49Al-2Cr and Ni-48Al-2Cr contained well-developed slip bands. The source of the slip bands is obviously the grain boundaries, which may indicate a change in composition or structure at the grain boundaries due to chromium.

Another cause of confined slip is a limited number of dislocation sources. In the case of the HAM castings, the compression tests are essentially those of bicrystals due to the large grain size. Since grain boundaries are common dislocation nucleation sites, such a large grain size might be expected to cause localized slip. However, the extrusions also display localized slip, despite their fine grain size. Therefore, it appears that the increased localized slip is due to chromium in solution. Presumably, chromium in solid solution somehow enhances dislocation nucleation.

Slip bands may also result from the development of a preferred slip "path" through a number of shearable obstacles in the structure, such as precipitates. Since the tendency for slip bands was noted for alloys both with and without precipitation, this cannot be the cause in the present case. Vedula [51] has suggested that substitutional solutes may attract point defects, which are normally dispersed throughout the structure, and create "defect clusters" which function like precipitates. Experimental confirmation of the phenomenon has not been produced, however, if the clusters are assumed to be present and are shearable by precipitates, the tendency for concentrated slip in the ternaries might be explained.

Close scrutiny of the substructure within the concentrated slip bands of the precipitate-containing alloys also reveals a number of small dislocation loops with <100> Burgers vectors surrounding a number of the alpha-chromium precipitates. These appear to be Orowan loops, indicating the precipitates are not sheared by the dislocations.

Composition-Structure-Property Relationships

The mechanical behavior of the alloys in this study is examined below with emphasis upon the room-temperature mechanical properties. The strengthening mechanisms are considered in terms of the various solid solution defects which are possible in this system, as well as precipitation, grain size and orientation contributions. In addition, the direct and indirect effects of tramp interstitial elements are discussed.
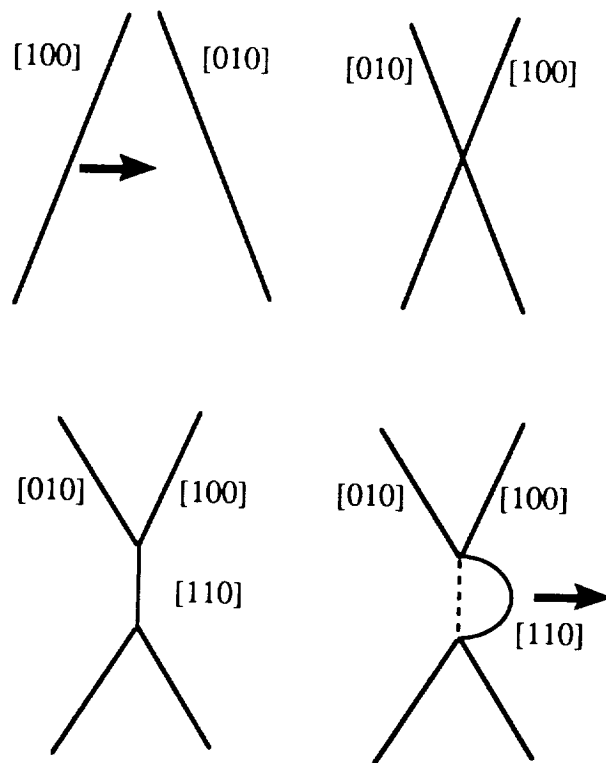
Figure 5-2. Reaction of Two <100> Dislocations to Form a <110> Dislocation

Substitutional Schemes

The majority of the alloys in this study have been alloyed with chromium in one of three systematic ways: substitution solely for aluminum, substitution solely for nickel, and

equal substitution for both nickel and aluminum (See Figure 3-1). In this manner, it was hoped that the effect of site occupation might be understood. However, to isolate the pure solid solution effect of chromium on the mechanical properties, consideration must be given to the indirect effects of the apparent substitutional scheme. For example, the ALCHEMI results indicate that chromium has a preference for the aluminum site in NiAl, when substituted evenly. This behavior may cause chromium to behave like an aluminum atom, effectively creating a surplus of aluminum sites in the structure. It was noted in the literature review that aluminum atoms do not reside on nickel sites. Thus, in Ni-49.5Al-1Cr the chromium atoms increase the number of aluminum sites. It is unclear whether strong site occupation can bring about an equal number of vacancy defects on the nickel sublattice and the associated high hardening observed for aluminum-rich binary alloys. This effect is illustrated in Figure 5-3.

In all likelihood, the addition of a ternary solute such as chromium to NiAl causes equilibrium concentrations of the various constitutional point defects to be established. In simplest form, these defects are: nickel on an aluminum site, chromium on a nickel site, chromium on an aluminum site, and a nickel vacancy. A good example is the substitution of chromium for nickel while the aluminum concentration is 50 percent. Since chromium prefers the aluminum site, it should increase the number aluminum sites and therefore increase the number of nickel site vacancies accordingly. If all the chromium added does not reside on aluminum sites, then some chromium will reside on nickel sites also.

Additions of chromium beyond the solubility limit, in further overall substitution for either aluminum or nickel, will not only cause alpha-chromium precipitation, but will induce other types of defect hardening of the NiAl phase. This defect hardening may be due to nickel substitution on aluminum sites or vacancy hardening, as described in the review. For example, in the Ni-45Al-5Cr alloy, although chromium is substituted completely for aluminum in the overall alloy composition, its limited solubility causes the

composition to lie on a different tie-line in the two-phase region of the ternary isotherm which leads to a nickel-rich B2 phase. This effect is also illustrated in Figure 5-3.

Strengthening Mechanisms

Solid Solution Strengthening. Currently, there are no known theories of solid solution hardening which can be applied to intermetallic compounds, as acknowledged in a recent review by Dimiduk and Rao [121]. However, several general statements can be made: (1) Intermetallic compounds are subject to solid solution hardening, both substitutional and interstitial. (2) The hardening mechanisms are more complex than in metallic solutions. (3) Substitutional elements, in NiAl alloys at least, appear to harden with a linear dependence on atomic concentration [23, 114]. This final point is in agreement with the results of Takeuchi [122] on solute additions to BCC iron.

There are several sources of solid solution hardening in the alloys of the current study, some of which are related as already suggested. First of all, variation of the nickel-to-aluminum ratio within the B2 compound can lead to either antisite or vacancy hardening. Vacancy hardening is considered to be a solid solution hardening mechanism even though it involves the removal of atoms, since the resulting strain field should behave like a small substitutional atom. Nickel-rich compounds may also be considered to be solution hardened, since the excess nickel atoms are accommodated substitutionally on the aluminum sites. A ternary addition, such as chromium, is a third source of solid solution hardening. However, hardening produced by chromium substitution for aluminum may produce a different hardening increment than for nickel. (Although the ALCHEMI results indicated chromium occupies the aluminum site in Ni-49.5Al-1Cr, some site occupancy for the nickel site may be possible when substituted fully for nickel.) A final source of solid solution strengthening is that due to the presence of interstitial elements, in particular carbon and/or oxygen. The chemical analyses shown in Tables 4-1 and 4-2 indicate the

presence of both of these elements at levels varying from 50 to 100 wppm. Since only 300 wppm carbon has been shown to completely embrittle NiAl [35], it is likely that carbon and oxygen both contribute to the flow stress in the present alloys, if they are not sufficiently removed by a gettering reaction.

The hardening effect due to interstitial elements is difficult to establish conclusively. The data in Figure 4-21 suggest that when chromium is added to "high purity" NiAl, a typical linear hardening response is observed. When chromium is added to commercial purity NiAl, the response is flat up to about one percent, suggesting that the chromium is being removed from solution by the formation of carbides or oxides. This marked difference in behavior between the NiAl+Cr alloys produced from two different nickel sources is not easily explained by the chemical analyses shown in Table 4-6. According to the analyses conducted at NASA - LRC, the differences in interstitial content between the two nickel sources are only marginal, and probably within the measurement error. A second analysis, conducted at LECO, also determined only a marginal difference between the oxygen contents of the two materials. In light of the obvious differences in hardness between the two series of alloys, it is logical to assume that the interstitial levels are sufficiently different to account for their behavior, in spite of the difficulty in measuring them.

While an applicable theory of solid solution hardening in intermetallic alloys is not presently available, some of the important factors which have been suggested to occur in metallic alloys may be examined here in a preliminary attempt to explain solution hardening behavior. The most important of these are the "atomic size effect" and the "modulus effect".
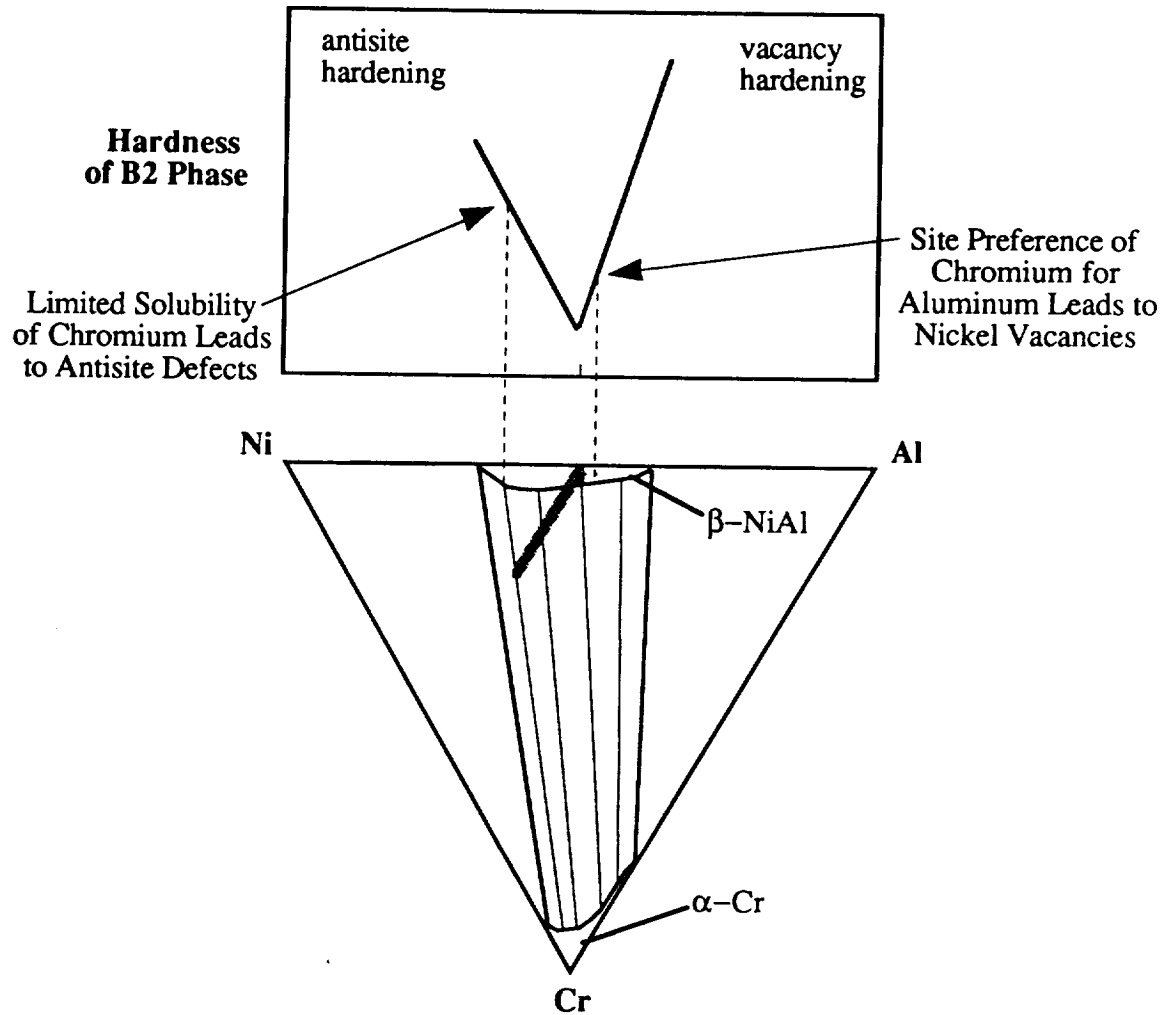
Figure 5-3. Indirect Effects of Chromium on the Hardness of the B2 Phase Due to Site Preference and Limited Solubility for the Case of Chromium Substituted for Aluminum

Mott and Nabarro [123] estimated the misfit strain, ε_a, of a solute atom to be

$$\varepsilon_a = (1/a)(da/dc)$$

where, a is the lattice parameter and c is the concentration of the solute species. Integration of this strain over the spherical volume from one solute atom half-way to another indicated that the stress to induce slip through a random array requires a stress of

$$\sigma = \mu \varepsilon_a^2 c$$

where, μ is the shear modulus of the lattice and c is the atomic concentration of the solute species. Thus, a linear dependence upon concentration is derived. However, there are inadequacies in both theory and application of Mott and Nabarro's equation in considering intermetallics. Primarily, the presence of largely covalent bonding precludes the assumption of a spherical stress state around each solute atom although this is a good assumption for metals. Further, a local change in the character of the bonding cannot be ruled out, although it might be anticipated that this would require rather large solute additions. Another problem concerns the lack of accounting for specific site substitution in the B2 lattice. There is little doubt that solute substituted for nickel will produce different hardening than when substituted for aluminum. This has already been demonstrated in NiAl alloys containing copper in solution in which substitution for aluminum yields a lower hardening rate than substitution for nickel [114]. A further complication is the interactive effects of the addition of a third element to a binary compound. The presence of chromium may induce other kinds of point defects which may have a strong effect on the observed hardening behavior and must be accounted for.

Fleischer [124] pointed out another elastic contribution to the stress state imposed by solute atoms, namely, the modulus effect, ε_G. In this case, the local change of the modulus due to the solute atom is accounted for and assumed to modify the atomic size effect. The modulus effect was estimated by

$$\varepsilon_\mu = (1/\mu)(d\mu/dc)$$

where, μ is the modulus of the alloy. The quantity $d\mu/dc$ was estimated from the macroscopic properties of the pure matrix and bulk pure solute. One difficulty here, in application to intermetallic compounds, is whether to consider the solute species as a metallic atom or as part of an intermetallic species, e.g. a chromium-nickel pair. Based on ideas similar to those of Mott and Nabarro [123] , Fleischer put forth the following expression for the increase in the flow stress due to solid solution hardening.

$$\sigma = \frac{\mu \varepsilon_s^{3/2} c^{1/2}}{350}$$

where, ε_s is a function of both ε_μ and ε_a. Although he found reasonable agreement of this model with experimental results of interstitially hardened alloys, many substitutionally hardened alloys exhibited a linear dependence on concentration. Fleischer also suggested that electrical and chemical interactions between the solute species and the dislocation may be important, although these were not incorporated into his models.

Finally, Suzuki developed a solution hardening model for BCC metals based on thermally-activated kink motion along screw dislocations and their interactions with solute species to create superjogs. Although there has been no evidence that these processes are important in NiAl, he also predicted a near linear dependence of flow strength on solute concentration.

Thus stated, there is a tentative basis for expecting a linear composition dependence in solute strengthened NiAl alloys which is supported by the experimental observations. To represent the various contributions, empirical equations of the the form

$$\sigma_s = K_s \, c$$

may be written, where, σ_s is the contribution of the solute species s to the yield strength, and K_s is the empirically determined hardening rate. Based on the data in Table 4-4 and that of George and Liu [35] (carbon data), the hardening behavior can be summarized.

The atomic radius for nickel is assumed to be that in the NiAl compound, based on Lautenschlager's calculation [62]; for chromium, it is assumed to be intermediate to that of nickel and aluminum in the compound (the mean). The size of the nickel vacancy was determined to be about 1.0 Å by extrapolation of lattice parameter data [125] of the binary compound to 100 percent aluminum. The radii of carbon and oxygen were taken from tabulated values [126].

Table 5-2. Solid Solution Hardening Constants for Several Solutes in NiAl

	Ni (for Al)	Ni Vacancy	Cr (for Al)	Cr (for both)	Carbon	Oxygen
K_s (MPa/at.%)	157	343	302	255	> 3900	?
Atom Radius (Å)	1.324	0.99	1.444	1.444	0.77	0.60

The plot in Figure 5-4 shows the effect of the solute atom size on the solid solution hardening rate. This plot indicates a minimum at about 1.2 Å, which is, coincidentally, the mean atomic radius for binary NiAl based on a lattice parameter of 2.887 Å. The fact that atom sizes larger or smaller than this value indicates solute atom size to be important in solid solution hardening of NiAl, although other factor such as modulus or electronic structure are also important [114].
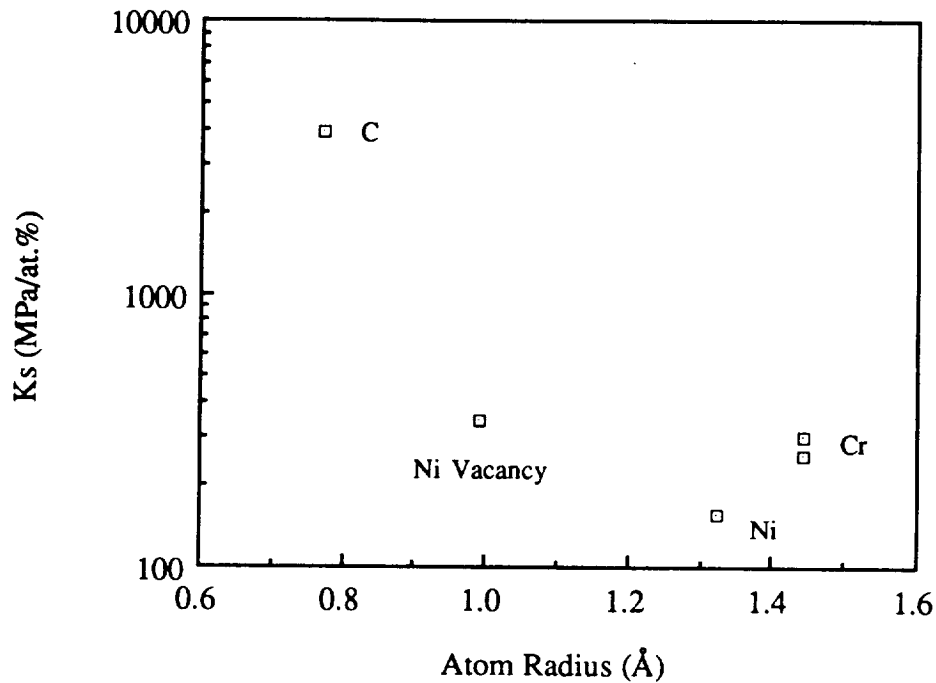
Figure 5-4. Relationship Between Solute Atom Size and Hardening Rate in NiAl Alloys

Precipitation Hardening. Alloys which contain chromium levels beyond the solubility limit are subject to precipitation hardening by alpha-chromium precipitates. Due to the retrograde nature of the solvus surface, much of the precipitation is very fine (about 10 nm in diameter) and either coherent or semicoherent. No sheared particles were observed during TEM characterization, while a number were observed to be surrounded by dislocation loops, usually when lying within a slip band. These loops were taken to be Orowan loops which were produced by the passage of a dislocation. The lack of observation of more than one loop around any given precipitate is probably a result of the small strains imposed. This observation is contrary to the behavior of most precipitation hardened metals, in which coherent particles are usually sheared and not by-passed by loop formation [127]. One reason why the precipitates are not sheared may be that the cube-on-cube orientation relationship with the matrix dictates a change in slip vector within the

precipitate. Coherency misfit strains, interfacial dislocations, and the high Peierls stress of chromium also raise the effective particle strength.

The alloys described here are amenable to current models of precipitation strengthening. The following development is based on that described by Gerold [127].

Consider the interaction of a single dislocation with a linear array of particles. If Orowan looping occurs, then the force exerted by a single particle should at least equal the combined line tension of the dislocation as it loops around the particle. That is,

$$\Delta\tau \, b \, \lambda = 2 \, T$$

where, $\Delta\tau$ is the extra shear stress exerted by the precipitate on the dislocation, b is the Burgers vector, λ is the mean interparticle distance, and T is the line tension of the dislocation. Strictly speaking, the stress only acts on the free distance between the particles, so the particle diameter, d, must be subtracted from λ. Solving for $\Delta\tau$, we now have

$$\Delta\tau = 2 \, T/b(\lambda\text{-}d)$$

The line tension of the dislocation depends on the line energy which in turn is a function of the dislocation orientation or character. Based on the TEM observations, the dislocation character is either edge or mixed. For simplicity, pure edge dislocations are assumed to be the character displayed prior to when a particle is encountered. Upon bending a full 90 degrees around the particle, the character becomes screw, in which case the line tension and line energy are equal and may be defined as

$$T = E_s = (\mu b^2/4\pi) \, \ln \, (r_o/r_i)$$

where, μ is the shear modulus of the matrix, and r_o and r_i are the outer and inner cut-off radii of the elastic strain field of the dislocation, respectively. A reasonable estimate for r_i is b, while r_o may be approximated by d, as shown by Ashby [128]. The particle diameter is an appropriate estimate because the attraction of the oppositely signed screw components around the particle will increase the line tension. Substitution yields the following for the increase in shear strength due to the particle.

$$\Delta\tau = \frac{\mu b}{2\pi(\lambda - d)}\ln\left(\frac{d}{b}\right)$$

By assuming a random array of particles and applying basic stereological principles, λ may be approximated by d/f_p, where f_p is the volume fraction of particles in the microstructure. In turn, f_p may be determined directly from the pseudobinary NiAl-Cr phase diagram (Figure 5-1) based on the concentration of chromium, c, according to the lever rule, i.e.

$$f_p = (c - 0.015)/(0.95 - 0.015)$$

Therefore, the increase in yield strength due to precipitation hardening in the NiAl+Cr system may be represented by

$$\Delta\sigma_p = \frac{\mu b}{\pi d\left(\dfrac{0.935}{c - 0.015} - 1\right)}\ln\left(\frac{d}{b}\right)$$

When appropriate values of μ (55172 MPa) and b (0.2887 nm) [129] are inserted, the strengthening increments for various mean precipitate diameters as a function of chromium concentration may be predicted, as shown in Figure 5-5.

This model indicates that, for 10 nm precipitates, the strengthening due to precipitation should be relatively small, about 70 MPa for 5 percent chromium. Comparison of this estimate to the actual value shown by the yield strength plot in Figure 4-16 indicates very good agreement with the theory. The model may be further increased in accuracy if the full size distribution of precipitates is taken into account, since higher chromium contents should produce a size distribution which is skewed to larger diameters. Of course, concentrations in excess of the maximum solubility limit might be expected to develop different types of microstructures, in which case the model loses validity. However, for the alloys under investigation, it should be an adequate representation.
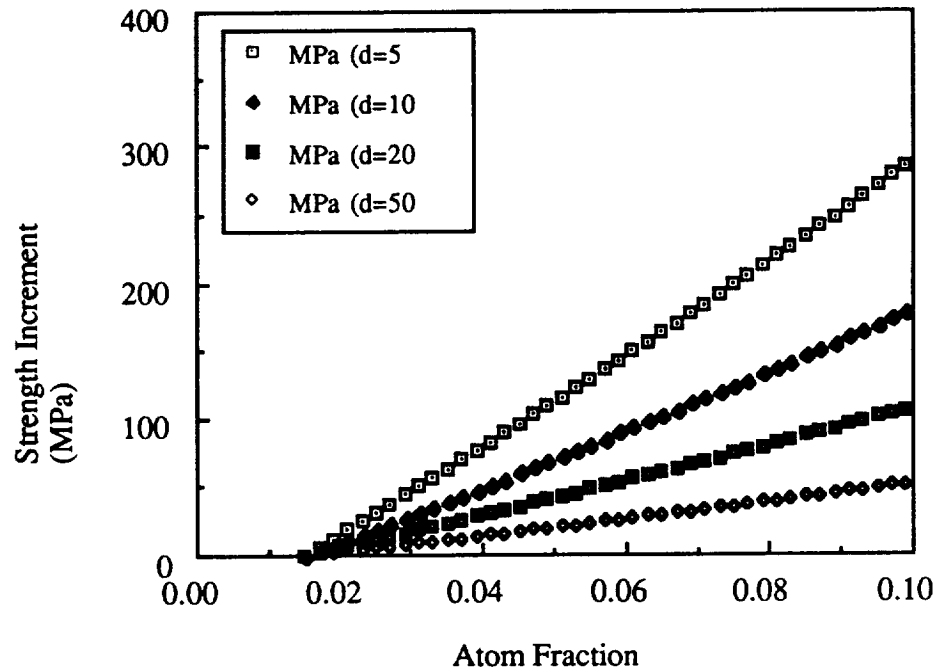
Figure 5-5. Theoretical Strengthening Increment Due to Alpha-Chromium Precipitation in NiAl as a Function of Chromium Content and Mean Precipitate Diameter

Grain Refinement Strengthening. Figure 4-17, which compares the CYS of extrusions and castings of identical composition, indicates a near constant strength differential of the extrusions over the castings of 41 to 65 MPa. Aside from texture

differences (discussed below), the primary microstructural difference between the extrusions and castings is grain size, typically 20 and 5000 μm, respectively. Recent work [36, 37] has shown that the yield strength of Ni-50Al has little dependence on grain size, while off-stoichiometric alloys, such as Ni-48Al, exhibit a stronger dependence. The Hall-Petch equations determined by Baker et al. [37] are

$$
\begin{aligned}
\text{Ni-50Al:} \quad & \sigma_y \text{ (MPa)} = 120 + 155\, d^{-1/2} \\
\text{Ni-49Al:} \quad & \sigma_y \text{ (MPa)} = 195 + 654\, d^{-1/2} \\
\text{Ni-48Al:} \quad & \sigma_y \text{ (MPa)} = 450 + 1231\, d^{-1/2} \\
\text{Ni-45Al:} \quad & \sigma_y \text{ (MPa)} = 548 + 1565\, d^{-1/2}
\end{aligned}
$$

where, d is the grain size in microns. Applying the appropriate equation to the Ni-50Al alloys in the current study, a strength differential of about 33 MPa is predicted, which is reasonably close to that shown in Figure 4-17. However, the other alloys, particularly Ni-48Al-2Cr and Ni-45Al-5Cr, are expected to behave in a fashion similar to off-stoichiometric binary alloys, and therefore exhibit a much greater effect of grain size. For example, Ni-48Al-2Cr contains about one percent chromium in solution residing on the aluminum sites. Therefore, the beta phase consists of about 49 percent aluminum (and chromium) sites and 51 percent nickel sites. Applying the Hall-Petch equation for Ni-49Al predicts a strength differential due to grain size of 137 MPa, whereas the measured differential was only 69 MPa. Similar analysis of Ni-45Al-5Cr predicts a differential in excess of 258 MPa in contrast to the measured difference of 65 MPa.

These departures from the predicted behavior for off-stoichiometric binary NiAl suggest that the presence of chromium in solid solution decreases the Hall-Petch slope. Since the Hall-Petch slope is a measure of the difficulty of slip transmittal across grain boundaries, it may be that chromium enhances this process. Indeed, the TEM observations support this notion, since the nucleation of concentrated slip bands at the grain boundaries appears easier in the ternary alloys. Exactly how this may be accomplished is

open to speculation. Baker et al. [37] suggested that a reduced slope is associated with constitutional disordering at the grain boundaries, based on recent research of Ni_3Al. If so, this would be consistent with theoretical predictions [14, 72] of the effect of chromium on ordering in NiAl, since it is logical that the chromium would have to be concentrated at the boundary to cause such an effect. However, on-going research at the NASA - Lewis Research Center [79] has determined by scanning Auger microscopy that chromium does not segregate to the grain boundaries in NiAl. Another likely explanation is that chromium removes interstitial solute from the NiAl matrix and grain boundaries. It is not unreasonable to assume that interstitial elements would concentrate at the more relaxed environment of a grain boundary and hinder slip accommodation and transmittal during plastic deformation. The addition of chromium can effectively reduce the interstitial concentration, in solid solution by solute clustering, and by the formation of alpha-chromium and $Cr_{23}C_6$ carbide precipitates. A final possibility is that chromium somehow affects the equilibrium point defect population in a manner which promotes slip nucleation and/or transmittal. This notion is currently receiving consideration by researchers at General Electric Aircraft Engines in response to the recent results of very low levels of iron additions to NiAl [3].

Texture Effects. The marked effect of single crystal orientation on mechanical properties in binary NiAl has already been referred to in the review. This anisotropy is also important in polycrystals. The development of a <111> fiber texture in the extrusions places the average crystal in a "soft" orientation; this causes the polycrystalline aggregate to generally be softer than a zero-texture specimen, such as a casting. This effect was of some concern during hardness testing of the polycrystalline specimens, since certain grains displayed unusually low or high hardness values. To establish this occurrence as an orientation effect and not experimental error, the microhardnesses of NiAl single crystals of [100], [111], [123] orientations were measured. The Vickers hardness values were 237 ± 2, 288 ± 6 and 272 ± 6, respectively, demonstrating the effect of orientation. Ultimately,

the effect of the <111> fiber texture is to decrease the strength and increase the ductility in this direction, although the extent would depend upon the degree of texture.

<u>Combination of Strengthening Mechanisms</u>. The yield strength, σ_y, has been shown to consist of contributions from several sources: the intrinsic lattice resistance, σ_r; solid solution strengthening due to nickel on aluminum sites, σ_{Ni}; solid solution strengthening due to vacancies on nickel sites, σ_v; solid solution strengthening due to chromium on nickel sites, $\sigma_{Cr/Ni}$; solid solution strengthening due to chromium on aluminum sites, $\sigma_{Cr/Al}$; solid solution strengthening due to interstitial elements, σ_i; precipitation hardening due to alpha-chromium precipitation, σ_p and grain refinement strengthening, σ_{gs}. The effects of texture are not considered here. That is,

$$\sigma_y = \sigma_r + \sigma_{Ni} + \sigma_v + \sigma_{Cr/Ni} + \sigma_{Cr/Al} + \sigma_i + \sigma_p + \sigma_{gs}$$

The variations in hardness and yield strength as a function of chromium content (Figures 4-16 and 4-20) can be largely accounted for by this model. The plot for each alloy series is schematically represented in Figure 5-6, in which the regions A, B and C are designated to be regions of significantly different types of hardening. Hardening in region A is assumed to be rather flat, due to the gettering effect of chromium for interstitial elements. In fact, chromium will effectively reduce the carbon level to at least 10^{-6} wppm [130], based on binary equilibria data between carbon and chromium. The simultaneous removal of chromium from solid solution will reduce solid solution hardening from chromium in region A; however, if chromium has been purposely substituted for either nickel or aluminum, the associated reduction of these elements will produce their own strength contribution. If the hardening behavior due to interstitial content is considered to be represented by Figure 4-21, it may be assumed that little chromium actually enters solid solution until the level is in excess of 0.75 percent, which marks the boundary between regions A and B. If all the chromium prior to this level is present as $Cr_{23}C_6$, this equates

to an initial matrix carbon level of about 400 appm (1800 wppm), which is somewhat higher than that indicated by the chemical analyses.
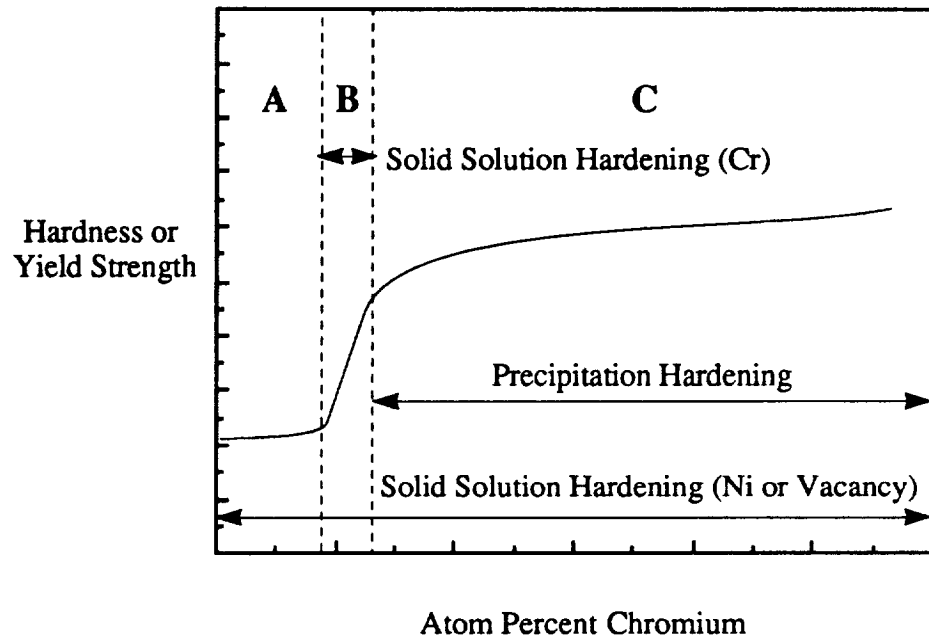
Figure 5-6. Schematic Plot of the Variation of Hardness/Yield Strength with Chromium Content, Based on Figure 4-20

Region B demarcates the range of chromium content in which primarily solid solution strengthening occurs, between about 0.75 and 1.5 percent. Given that chromium exhibits a preference for the aluminum site, solid solution hardening by chromium for aluminum is expected for the Ni/Al=1 and the Cr/Al alloy series. The intentional substitution of chromium for nickel may also result in the presence of some chromium on the nickel sites and induce solid solution hardening (Cr/Ni). It is presently unknown whether the site preference is strong enough to create vacancies on the nickel sublattice and the associated hardening.

Region C is characterized by precipitation hardening for all substitutional schemes, assuming similar volume fractions of precipitate, and also by solid solution hardening by

antisite or vacancy defects. As in the binary compound, aluminum-rich alloys are assumed to harden by vacancies beyond the solubility limit and nickel-rich alloys to harden by antisite defects. By this understanding, the apparent hardening introduced by chromium additions beyond the solubility limit is actually due to solid solution hardening by nickel and vacancy point defects, since precipitation hardening has been shown to have little effect (see Figure 5-3).

For simple comparison, assuming no interactive effects beyond those mentioned, the room-temperature yield strength variation with chromium content may be predicted by this empirical/theoretical model. The predicted variation for each alloy series is shown in Figure 5-7. The points shown for each curve correspond to the known inflections in behavior based on the data in Figures 4-16 and 4-20 and the solubility limit of chromium. The behavior between each plotted point is assumed to be linear.

By comparison with Figures 4-16 and 4-20, it can be seen that there is general agreement with the actual yield strengths of the cast alloys. The alloys for which Ni/Al=1 are the lowest in strength, with the Cr/Al alloys the next highest, and the Cr/Ni alloys the strongest. However, there are some differences between the calculated and experimental behavior. By examining these differences it is endeavored to understand what additional or interactive mechanisms may be important, or what assumptions may be in error.

The most obvious difference is the magnitude of strengthening due to antisite and vacancy defects beyond the solubility limit, in which the predicted strength increments are about twice the actual. This suggests that the solid solution hardening due to antisite defects and, in particular, due to vacancy defects, is substantially less than that in binary alloys. The reason for the reduced hardening may be that chromium in solution alters the point defect configurations in such a way as to allow easier slip -- such as vacancy congregation around solute atoms. The second phase precipitation may also decrease the yield stress by increasing the number of dislocation sources (semicoherent matrix/precipitate interfaces, for instance).
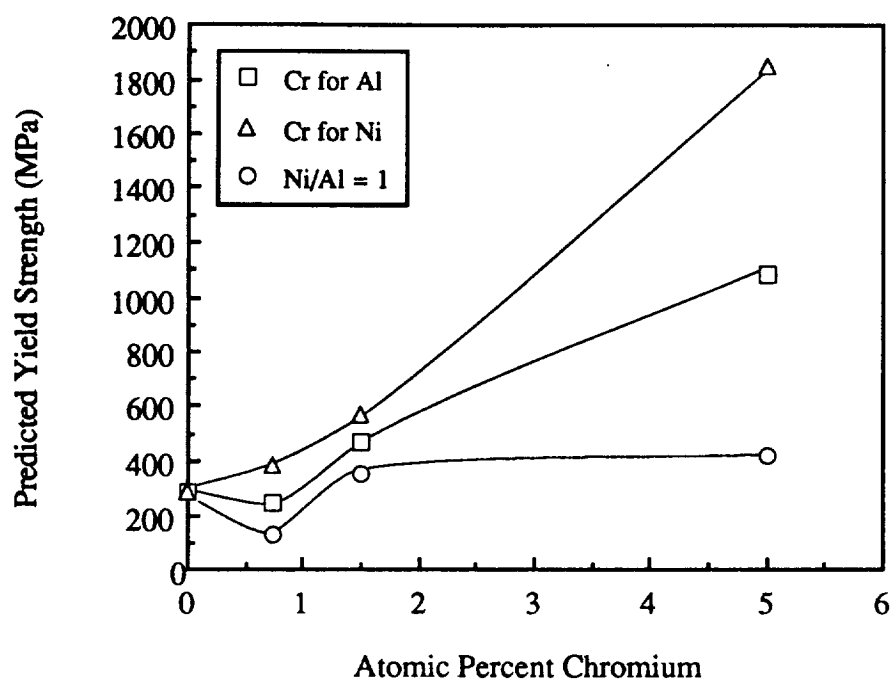
Figure 5-7. Predicted Dependence of Yield Strength of Cast NiAl+Cr Alloys on Chromium Content

The other difference between the predicted and measured yield strengths takes place between 0 and 0.75 percent chromium. The measured strengths (hardnesses) are independent of chromium content, which has been explained as being due to the presence of interstitial elements which remove chromium from solution. If chromium is removed from solution, the Cr/Al and Cr/Ni series of alloys should display a hardening effect in accordance with the reduced aluminum or nickel contents, respectively, as predicted above. The lack of agreement could mean that predicted variations fall within experimental error. It could also indicate that not all the chromium is present as carbides or oxides, but is actually in solution and affects the defect concentrations.

Aside from these differences, the good agreement indicates that the strengthening processes described above are reasonably accurate and representative of the true

relationships between composition, microstructure and properties in these alloys. The primary shortcoming in understanding concerns the role of chromium in affecting the types and concentrations of point defects, which is beyond the scope of the current study. This behavior is consistent with the results of other researchers [3, 131] and is a likely topic for future work.

Elevated Temperature Properties

The elevated temperature yield strengths of the extruded alloys, Figure 4-18a, depended strongly upon test temperature, with increasing slope, $d\sigma/dT$, for higher chromium levels. This may be understood by noting that the room-temperature strength increased in accordance with the arguments already stated for the HAM cast alloys above. That is, solid solution strengthening by chromium, nickel or vacancies is primarily responsible for the strength variations with composition aside from interstitial impurities. Further, the slopes correlate with the nickel-to-aluminum ratio. For example, the curves for Ni-49Al-2Cr and Ni-49.5Al-1Cr are approximately parallel and both of their nickel-to-aluminum ratios are equal to unity. The Ni-48Al-2Cr and Ni-45Al-5Cr slopes scale with deviation of their nickel-to-aluminum ratios from unity. Since the elevated temperature properties are controlled in large part by diffusion-assisted processes, this correspondence is logical, as off-stoichiometric binary NiAl alloys are known to display enhanced diffusivity relative to the stoichiometric compound [61].

The elongations as a function of test temperature, Figure 4-19, indicate that chromium in solid solution elevates the BDTT about 150K relative to binary NiAl. As for the yield strength, comparison of the curves for Ni-49Al-2Cr and Ni-49.5Al-1Cr indicates that the nickel-to-aluminum ratio is the primary factor controlling the BDTT. These alloys exhibit the lowest BDTT of the ternary alloys, while increasing deviation from this ratio

tends to elevate the transition temperature. This is consistent with Vedula's [51] results for binary NiAl alloys.

The 150K elevation of the BDTT due to the presence of chromium in solid solution is rationalized in terms of the difference in the response of the yield and fracture strengths to alloying. As shown above, the yield strength depends strongly upon alloying levels because the nature of plastic deformation by slip dictates a strong interaction between the dislocation and solute atom. In contrast, the fracture strength is more a function of the intrinsic bonding in the compound -- a property which is much more difficult to affect.

Site Preference of Chromium

The preference of chromium for the aluminum site in the NiAl structure is intriguing, since both chromium and nickel are transition metals and may be considered electronically similar. In addition, they are of similar atomic size, both being smaller than aluminum. These factors might lead one to expect that chromium would substitute for nickel rather than aluminum. However, some insight is gained when the most common valences of several transition elements are examined, as summarized in Table 5-3.

The correlation between the substitution behavior of elements of like valence strongly suggests that the alloying behavior is controlled by electronic factors, such as the local charge in the structure, rather than by atomic size. This behavior is analogous to one of the Hume-Rothery rules, which states that good solubility between two elements requires them to be of similar valence, in addition to other requirements. From another viewpoint, the wide separation of nickel and aluminum in the periodic table suggests that some degree of ionicity may exist in their binary compounds. In support, Fu and Yoo [28] have calculated that a significant degree of charge transfer from aluminum to nickel should be present. If so, then the local atomic charge should vary periodically within the structure,

providing sites of greater and lesser negativity which are only appropriate for elements which disturb the resonance the least.

Table 5-3. Common Valence and NiAl Substitution Behavior of Several Transition Metals

Element	Common Valence	Known Substitution
Ni	+2	---
Al	+3	---
V	+3, +5	Al
Cr	+3	Al
Mn	+2	Ni
Fe	+2, +3	Ni or Al
Co	+2	Ni
Cu	+1	Ni or Al
Ga	+3	Al

CHAPTER 6
SUMMARY AND CONCLUSIONS

The effects of chromium additions on the dislocation substructure, microstructure, and mechanical properties of NiAl-base alloys have been characterized. The primary purpose of the investigation was to verify and understand the reported ability of the chromium additions to alter the primary slip system in NiAl during room-temperature deformation. A thorough study of a wide range of compositions and different processing methods has indicated that chromium has no effect on the operative slip system in NiAl. However, a small percentage of chromium in solid solution does appear to affect the nature of plastic deformation by promoting more localized slip relative to stoichiometric, binary NiAl. A definitive cause for this effect was not identified.

The mechanical behavior of the various alloys was considered in terms of solution hardening, precipitation hardening and grain refinement theories. Vacancy and antisite point defects, introduced by deviation of the nickel-to-aluminum ratio from unity, were considered to strengthen the alloy by solid solution hardening and conformed to the observed dependence of hardening rate upon atomic solute size. The role of interstitial elements, in particular carbon, is believed to be very important and was considered in elucidating the effect of chromium in solid solution. Precipitation hardening, due to the presence of alpha-chromium precipitates, and grain refinement produced strengthening increments which could be predicted based on accepted theories for metallic systems. The yield strength variation with chromium content was modeled based on these approaches and found to generally agree with experimental variations. The major discrepancy between predicted and observed behavior suggests that chromium may reduce the degree of antisite

and vacancy hardening usually observed in the binary compound, perhaps by some type of defect "gettering" process.

Based on the results of this investigation, the following conclusions are put forth:

1. The addition of chromium to NiAl does not affect the occurrence of the primary Burgers vector, <001>. However, it does promote more localized slip, perhaps by altering the point defect distribution.

2. Processing to produce a finer grain size marginally increases the number of dislocations with <110> Burgers vectors, apparently due to reactions between different <100> unit dislocations within the same grain. Although the presence of both of these Burgers vectors may satisfy the von Mises criterion, the occurrence and mobility of the dislocations with <110> Burgers vectors are considered restricted by the requirement of a reaction, i.e. they are not independently nucleated.

3. Solid solution hardening by various point defects is a major source of strengthening in NiAl-base alloys. The degree of hardening is a function of the defect size within the compound.

4. The strengthening increment due to precipitation of alpha-chromium is amenable to treatment by classical theory for metallic materials.

5. Site preference of substitutional solute atoms on the NiAl lattice correlates well with the common valence of the solute. That is, elements with a valence of two usually prefer the nickel site, while elements with a valence of three, such as chromium, prefer the aluminum site.

Shown below are compressive true stress-true strain data for Ni-50Al, Ni-49.5Al-1Cr and Ni-49Al-2Cr in both cast and homogenized and cast and extruded conditions. These curves are typical for unalloyed stoichiometric NiAl, single phase ternary NiAl containing chromium, and NiAl containing alpha-chromium precipitation.
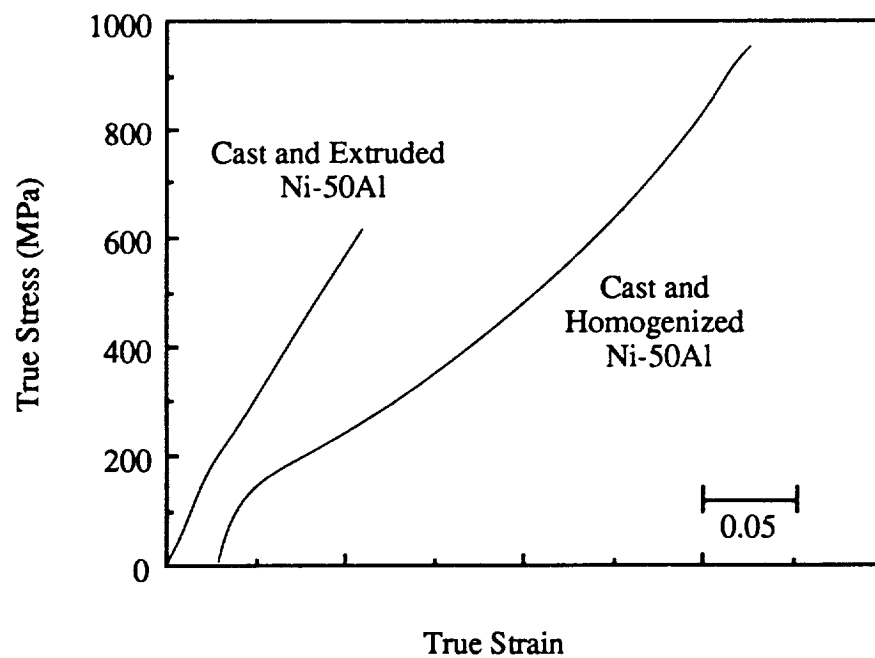
Figure A-1. True Stress-True Strain Curves for Ni-50Al
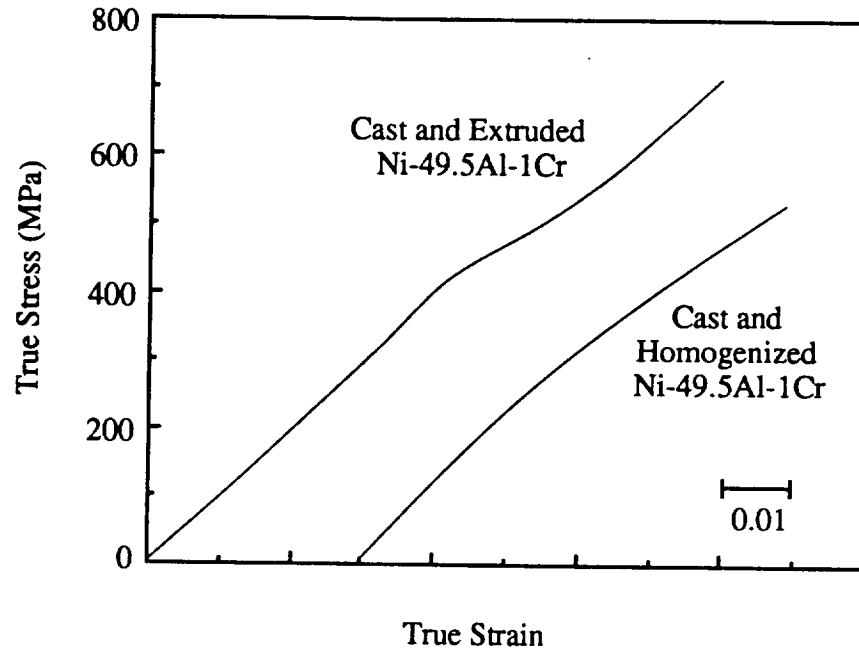
Figure A-2. True Stress-True Strain Curves for Ni-49.5Al-1Cr
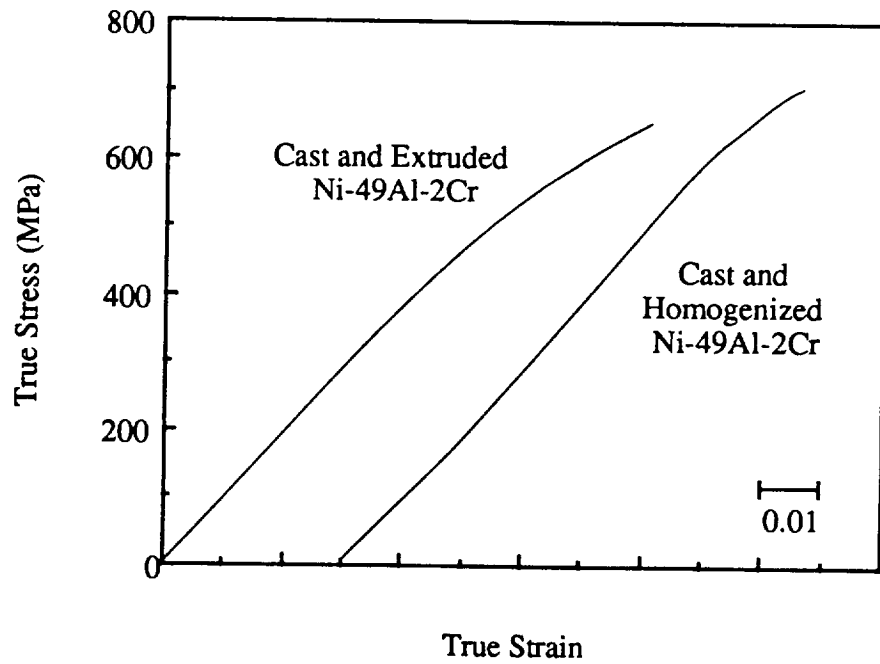
Figure A-3. True Stress-True Strain Curves for Ni-49Al-2Cr

RAW BURGERS VECTOR ANALYSIS DATA

Tabulated below are the raw data derived from the dislocation Burgers vector analyses of the various alloys in this study. Each row corresponds to a single set of TEM plates from which about 10 to 100 dislocations were analyzed. The specific numbers of each Burgers vector type are in the fifth, sixth and seventh columns. In some instances, all dislocations in a single area imaged in an identical fashion (had the same Burgers vector) although the dislocation was too high for an accurate count. These were accounted for by assuming that at least 50 dislocations were visible in the field of view and are recorded below as such.

Alloy	Cond.	% Def.	Film	# <100>	# <110>	# <111>	Distribution
Ni45Al5Cr	HAM	0.30	2948	>50	0	0	dense, <100> bands
Ni45Al5Cr	HAM	0.30	3001	>50	0	0	homog., diffuse all <100>
Ni45Al5Cr	HAM	0.30	3060	89	0	0	mod. density, homog.
Ni45Al5Cr	XAP	0.00	3473	10	0	0	ppts pinning disl.
Ni45Al5Cr	XAP	0.60	2408	10	2	0	homogeneous
Ni45Al5Cr	XAP	0.60	2453	20	1	1	homog. mode. density
Ni45Al5Cr	XAP	0.60	2467	18	2	1	homog., diffuse slip bands
Ni47.5Al5Cr	HAM	0.28	2871	43	1	0	homog.
Ni47.5Al5Cr	HAM	0.28	2992	>50	0	0	homog., all <100>
Ni47.5Al5Cr	HAM	0.28	3064	53	0	0	mod. density, homog.
Ni47Al1Cr	HAM	0.45	2762	3	0	0	homog., sparse
Ni48.5Al5.2Cr	AM	0.20	2964	>50	0	0	<100> slip bands
Ni48.5Al5.2Cr	AM	0.20	2967	>50	0	0	slip bands
Ni48.5Al5.2Cr	AM	0.30	2100	9	1	0	slip bands
Ni48.5Al5.2Cr	AM	0.30	2158	12	0	0	diffuse slip bands
Ni48.5Al5.2Cr	HAM	0.28	2810	35	1	0	homog.
Ni48Al	HAM	0.05	2838	17	0	0	sparse, homog.
Ni48Al2Cr	HAM	0.55	2957	>50	0	0	homog., all <100>
Ni48Al2Cr	HAM	0.55	3056	73	0	0	mod. density, homog
Ni48Al2Cr	XVIM	0.00	2335	0	7	0	homog., sparse
Ni48Al2Cr	XVIM	0.70	2376	11	2	0	diffuse slip bands
Ni48Al2Cr	XVIM	0.70	2582	24	11	0	slip bands, homog.
Ni48Al2Cr	XVIM	0.70	2673	25	4	0	diffuse bands, homog.
Ni48Al2Cr	XVIM	0.70	3550	20	0	0	mod. dense, diffuse bands
Ni49.5Al1Cr	HAM	0.30	2936	31	0	0	homog.
Ni49.5Al1Cr	XVIM	0.59	2920	>50	0	0	<100> slip bands
Ni49.5Al1Cr	XVIM	0.70	2384	6	8	0	diffuse slip bands

APPENDIX B--Continued

Alloy	Cond.	% Def.	Film	# <100>	# <110>	# <111>	Distribution
Ni49.5Al1Cr	XVIM	0.70	2593	60	10	2	slip bands
Ni49.5Al1Cr	XVIM	0.70	2643	28	1	1	slip bands, homog.
Ni49.5Al1Cr	XVIM	0.70	3136	43	2	0	mod. density, slip bands, homog.
Ni49.5Al1Cr	XVIM	0.70	3536	20	0	0	mod. dense, homog.
Ni49Al1Cr	HAM	0.28	2769	32	0	0	slip bands, homog
Ni49Al2Cr	HAM	0.57	2775	24	0	0	diffuse slip bands
Ni49Al2Cr	HAM	0.57	2785	18	2	0	diffuse slip bands
Ni49Al2Cr	HAM	0.57	3044	79	0	0	mod. density, homog.
Ni49Al2Cr	HAM	0.57	3050	110	0	0	mod. density, homog.
Ni49Al2Cr	XVIM	0.00	2553	12	5	2	sparse, homog.
Ni49Al2Cr	XVIM	0.00	2575	36	1	1	sparse, slip bands
Ni49Al2Cr	XVIM	0.10	2821	28	4	0	diffuse slip bands, tensile 1st cut
Ni49Al2Cr	XVIM	0.10	2829	34	5	0	diffuse slip bands, tensile, 2nd cut
Ni49Al2Cr	XVIM	0.10	2896	24	3	0	slip bands
Ni49Al2Cr	XVIM	0.60	2543	22	7	0	mod. dense slip bands
Ni49Al2Cr	XVIM	0.70	3506	18	0	0	dense
Ni49Al2Cr	XVIM	0.70	3521	49	0	0	dense
Ni49Al2Cr	XVIM	0.70	3529	4	0	0	
Ni50Al	HAM	0.30	2697	31	0	0	diffuse bands
Ni50Al	HAM	0.30	2706	31	0	0	diffuse bands
Ni50Al	HAM	0.30	2728	31	2	1	diffuse bands
Ni50Al	XVIM	0.00	3438	19	2	0	homog, sharply bent, low density
Ni50Al	XVIM	0.00	3451	20	5	0	homog, sharply bent, low density
Ni50Al	XVIM	0.00	3464	22	0	0	homog, sharply bent, low density
Ni50Al	XVIM	0.55	2857	44	1	0	homog.
Ni50Al	XVIM	0.55	3288	29	2	0	bands, homog., no loops, bent
Ni50Al	XVIM	0.55	3295	32	3	0	rough bands, homog
Ni50Al	XVIM	0.55	3380	16	3	0	rough bands, homog.
Ni50Al	XVIM	1.10	2845	49	6	0	homog.
Ni50Al1Cr	HAM	0.65	2737	38	0	0	homog.
Ni50Al1Cr	HAM	0.65	2749	61	0	0	homog.
Ni50Al1Cr	HAM	0.65	2756	32	0	0	homog.
Ni50Al2Cr	HAM	0.20	2904	32	1	0	homog.
Ni50Al2Cr	HAM	0.20	3028	79	0	0	mod. density, homog., tangles
Ni50Al5Cr	HAM	0.35	2880	14	1	0	sparse, homog., disl. nets on ppts
Ni50Al5Cr	HAM	0.35	2979	11	5	1	sparse, homog., disl.loops, nets
Ni50Al5Cr	HAM	0.35	3009	16	2	0	sparse, homog., all 3 <100>
P&W alloy 40	AM	0.77	3099	100	0	0	high density, homg, ppt loops

REFERENCES

1.   A.I. Taub and R.L. Fleischer: Intermetallic Compounds for High-Temperature Structural Use, Science, 1989, vol. 243, pp. 616-621.

2.   R.E. Tressler, J.R. Hellmann and H.T. Hahn: Advanced High Temperature Composite Materials for Engine Applications, Report No. CAM-9101, The Center for Advanced Materials, Pennsylvania State University, 410 Walker Building, Dec. 1990.

3.   R. Darolia: NiAl Alloys for High-Temperature Structural Applications, JOM, 1991, vol. 3, pp. 44-49.

4.   K.H. Hahn and K. Vedula: Room Temperature Tensile Ductility in Polycrystalline B2 NiAl, Scripta Metall., 1989, vol. 23, pp. 7-12.

5.   I. Baker and P.R. Munroe: Improving Intermetallic Ductility and Toughness, JOM, 1988, vol. 2, pp. 28-31.

6.   E.M. Grala: Investigation of the NiAl Phase of Nickel-Aluminum Alloys, Report No. TN 3828, National Advisory Committee for Aeronautics, Cleveland, Ohio, Jan. 1957.

7.   R.T. Pascoe and C.W.A. Newey: The Mechanical Behaviour of the Intermediate Phase NiAl, Metal Sci. J., 1968, vol. 2, pp. 138-143.

8.   K. Vedula, K.H. Hahn and B. Boulogne: Room Temperature Tensile Ductility in Polycrystalline B2 NiAl, in High-Temperature Ordered Intermetallic Alloys III, C.T. Liu, A.I. Taub, N.S. Stoloff and C.C. Koch, eds., Materials Research Society, Pittsburgh, Pennsylvania, 1989, pp. 299-304.

9.   A. Ball and R.E. Smallman: The Operative Slip System and General Plasticity of NiAl-II, Acta Metall., 1966, vol. 14, pp. 1517-1526.

10.   M.H. Loretto and R.J. Wasilewski: Transmission Electron Microscopy of Plastically Deformed <100> Single Crystals of NiAl, in The Strength of Metals and Alloys, American Society for Metals, Metals Park, Ohio, 1970, pp. 113-117.

11.   R.T. Pascoe and C.W.A. Newey: Deformation Processes in the Intermediate Phase NiAl, Metal Sci. J., 1971, vol. 5, pp. 50-55.

12.   G.W. Groves and A. Kelly: Independent Slip Systems in Crystals, Phil. Mag., 1963, vol. 81, pp. 877-887.

13.   R. Von Mises: Mechanics of Plastic Form Change of Crystals, Z. Angew. Math. Mech., 1928, vol. 8, pp. 161-185.

14.   R. Darolia, D.F. Lahrman, R.D. Field and A.J. Freeman: Alloy Modeling and Experimental Correlation for Ductility Enhancement in NiAl, in High Temperature Ordered Intermetallic Alloys III, C.T. Liu, A.I. Taub, N.S. Stoloff and C.C. Koch, eds., Materials Research Society, Pittsburgh, Pennsylvania, 1989, pp. 113-118.

15.   C.C. Law and M.J. Blackburn: Rapidly Solidified Lightweight Durable Disk Material, Report No. ED/GPD FR-18674-4, United Technologies Corp., Pratt and Whitney Group, Sep 17, 1985.

16.   D.B. Miracle, S. Russell and C.C. Law: Slip System Modification in NiAl, in High Temperature Ordered Intermetallic Alloys III, C.T. Liu, A.I. Taub, N.S. Stoloff and C.C. Koch, eds., Materials Research Society, Pittsburgh, Pennsylvania, 1989, pp. 225-230.

17.   S.M. Merchant and M.R. Notis: A Review: Constitution of the Al-Cr-Ni System, Mater. Sci. Eng., 1984, vol. 66, pp. 47-60.

18.   R.D. Field, D.F. Lahrman and R. Darolia: The Effect of Alloying on Slip Systems in [001] Oriented NiAl Single Crystals, Acta Metall., to be published.

19.   A.J. Bradley and A. Taylor: An X-Ray Analysis of the Nickel-Aluminium System, Proc. Roy. Soc., London, U.K., 1937, vol. A159, pp. 56-72.

20.   P. Georgopoulos and J.B. Cohen: The Defect Arrangement in (Non-Stoichiometric) β'-NiAl, Acta Metall., 1981, vol. 29, pp. 1535-1551.

21.   H.C. Liu, E. Change and T.E. Mitchell: Investigations of Defective β-NiAl by Transmission Electron Microscopy, in 39th Ann. Proc. Electron Microscopy Soc. Amer., G.W. Bailey, ed., Atlanta, Georgia, 1981, pp. 58-59.

22.   T.B. Massalski: Binary Alloy Phase Diagrams, 1, American Society for Metals, Metals Park, Ohio, 1986, pp. 140-143.

23.   J.H. Westbrook: Temperature Dependence of Hardness of the Equi-Atomic Iron Group Aluminides, J. Electrochem. Soc., 1956, vol. 103, pp. 54-63.

24.   F.J. Bremer, M. Beyss, E. Karthaus, A. Hellwig Schober, T., J.-M. Welter and W. H.: Experimental Analysis of the Ni-Al Phase Diagram, J. Cryst. Growth, 1988, vol. 87, pp. 185-192.

25.   M.S. Petrushevskii, E.S. Levin and P.V. Gel'd: Viscosity and Interatomic Interaction Energy in Nickel-Aluminium Melts, Russ. J. of Phys. Chem., 1971, vol. 45, pp. 1719-1721.

26.   M.J. Cooper: The Electron Distribution in the Phases CoAl and NiAl, Phil. Mag., 1963, vol. 8, pp. 811-821.

27.   A.G. Fox and M.A. Tabbernor: The Bonding Charge Density of β'NiAl, Acta Metall., 1991, vol. 39, pp. 669-678.

28.   C.L. Fu and M.H. Yoo: First-Principles Investigation of Mechanical Behavior of B2 Type Aluminides: FeAl and NiAl, in High-Temperature Ordered Intermetallic Alloys IV, L.A. Johnson, D.P. Pope and J.O. Stiegler, eds., Materials Research Society, Pittsburgh, Pennsylvania, 1991, pp. 667-672.

29.   A.J. Freeman, T. Hong, W. Lin and J. Xu: Phase Stability and Role of Ternary Additions on Electronic and Mechanical Properties of Aluminum Intermetallics, in High-Temperature Ordered Intermetallic Alloys IV, L.A. Johnson, D.P. Pope and J.O. Stiegler, eds., Materials Research Society, Pittsburgh, Pennsylvania, 1991, pp. 3-18.

30.   R.L. Wachtell: An Investigation of Various Properties of NiAl, Report No. WADC 52-291, Wright Air Development Center, Sept. 1952.

31.   W.A. Maxwell and E.M. Grala: Investigation of Nickel-Aluminum Alloys Containing from 14 to 35 Percent Aluminum, Report No. TN 3259, National Advisory Committee for Aeronautics, Aug. 1954.

32.   E.M. Grala: Mechanical Properties of Intermetallic Compounds in 115th meeting of the Electrochemical Society, J.H. Westbrook, eds., John Wiley & Sons, Inc., New York, pp. 358-404.

33.   A.G. Rozner and R.J. Wasilewski: Tensile Properties of NiAl and NiTi, J. Inst. Metals, 1966, vol. 94, 1957, pp. 169-175.

34.   R.D. Noebe, R.R. Bowman, C.L. Cullers and S.V. Raj: Flow and Fracture Behavior of NiAl in Relation to the Brittle-To-Ductile Transition Temperature, in High Temperature Ordered Intermetallic Alloys IV, L. Johnson, D.P. Pope and J.O. Stiegler, eds., Materials Research Society, Pittsburgh, Pennsylvania, 1991, pp. 589-596.

35.   E.P. George and C.T. Liu: Brittle Fracture and Grain Boundary Chemistry of Microalloyed NiAl, J. Mater. Res., 1990, vol. 5, pp. 754-762.

36.   P. Nagpal and I. Baker: The Effect of Grain Size on the Room-Temperature Ductility of NiAl, Scripta Metall. Mater., 1990, vol. 24, pp. 2381-2384.

37.   I. Baker, P. Nagpal, F. Liu and P.R. Munroe: The Effect of Grain Size on the Yield Strength of FeAl and NiAl, Acta Metall. Mater., 1991, vol. 39, pp. 1637-1644.

38.   K. Chan: Theoretical Analysis of Grain Size Effects on Tensile Ductility, Scripta Metall., 1990, vol. 24, pp. 1725-1730.

39.   E.M. Schulson: Comments on the Brittle to Ductile Transition of Long-Range Ordered Alloys, Res. Mechanica Letters, 1981, vol. 1, pp. 111-114.

40.   E.M. Schulson and D.R. Barker: A Brittle to Ductile Transition in NiAl of a Critical Grain Size, Scripta Metall., 1983, vol. 17, pp. 519-522.

41.   E.M. Schulson: The Effects of Grain Size on the Flow and Fracture of Long-Range Ordered Alloys, in High-Temperature Ordered Intermetallic Alloys, C.C. Koch, C.T. Liu and N.S. Stoloff, eds., Materials Research Society, Pittsburgh, Pennsylvania, 1985, pp. 193-204.

42.   I. Baker: The Structure and Properties of Grain Boundaries in B2 Ordered Alloys, Report No. Grant No. DE-FG02-87ER45311, Dartmouth College, Thayer School of Engineering, Hanover, NH 03755, April 21, 1989.

43.   R. Bohn, T. Haubold, R. Birringer and H. Gleiter: Nanocrystalline Intermetallic Compounds - An Approach to Ductility?, Scripta Metall. Mater., 1991, vol. 25, pp. 811-816.

44.   M. Dollar, P. Nash, S. Dymek and S.J. Hwang: Microstructure, Plastic Deformation and Mechanical Properties of Mechanically Alloyed NiAl and NiAl Based Alloys, Report No. 5-54718-1, Illinois Institute of Technology, Metallurgical and Materials Engineering Department, IIT Center, Chicago, IL 60616, April, 1991.

45.   S. Ishiyama, M. Eto, H. Hosoda, T. Mishima and T. Suzuki: Effect of Non-Stoichiometry and Ternary Additions on the Mechanical Properties, in NiAl at Elevated Temperature in Proc. of Inter. Symp. on Intermetallic Compounds - Structure and Mechanical Properties- JIMIS-6, O. Izumi, eds., Japan Institute of Metals, Sendai, Japan, 1991, pp. 609-613.

46.   W.A. Kaysser, R. Laag, J.C. Murray and G.E. Petzow: Improvement of P/M-NiAl by Ti and Nb Additions, Inter. J. Powder Metall., 1991, vol. 27, pp. 43-49.

47.   K. Sasaki, M. Morinaga and N. Yukawa: Alloying Effect on the Solidified Structure of NiAl, in International Symposium on Intermetallic Compounds - Structure and Mechanical Properties - JIMIS-6, O. Izumi, eds., Japan Institute of Metals, Sendai, Japan, 1991, pp. 877-881.

48.   A. Ball and R.E. Smallman: The Deformation Properties and Electron Microscopy Studies of the Intermetallic Compound NiAl, Acta Metall., 1966, vol. 14, pp. 1349-1355.

49.   S.V. Raj, R.D. Noebe and R. Bowman: Observations on the Brittle to Ductile Transition Temperatures of B2 Nickel Aluminides With and Without Zirconium, Scripta. Metall., 1989, vol. 23, pp. 2049-2054.

50.   H. Saka, Y.M. Zhu, M. Kawase, A. Nohara and T. Imura: The Anomalous Strength Peak and the Transition of Slip Direction in β-CuZn, Phil. Mag. A, 1985, vol. 51, pp. 365-371.

51.   K. Vedula and P.S. Khadkikar: Effect of Stoichiometry on Low Temperature Mechanical Properties, in High Temperature Aluminides and Intermetallics, S.H. Whang, C.T. Liu, D.P. Pope and J.O. Stiegler, eds., The Minerals, Metals & Materials Society, Warrendale, Pennsylvania 15086, 1990, pp. 197-217.

52. D.F. Lahrman, R.D. Field and R. Darolia: The Effect of Strain Rate on the Mechanical Properties of Single Crystal NiAl, in High-Temperature Ordered Intermetallic Alloys IV, L.A. Johnson, D.P. Pope and J.O. Stiegler, eds., Materials Research Society, Pittsburgh, Pennsylvania, pp. 603-607.

53. H. Jacobi, B. Vassos and H.-J. Engell: Electrical Properties of β-Phase NiAl, J. Phys. Chem. Solids, 1969, vol. 30, pp. 1261-1271.

54. H. Jacobi and R. Stahl: Optical Properties of Ternary β Electron Phases based on NiAl, J. Phys. Chem. Solids, 1973, vol. 34, pp. 1737-1748.

55. A.H. Cottrell: Theory of Brittle Fracture in Steel and Similar Metals, Trans. Metall. Soc. AIME, 1958, vol. 212, 1958, pp. 192-205.

56. S.J. Hwang, P. Nash, M. Dollar and S. Dymek: Microstructure and Mechanical Properties of Mechanically Alloyed NiAl, in High-Temperature Ordered Intermetallic Alloys IV, L.A. Johson, D.P. Pope and J.O. Stiegler, eds., Materials Research Society, Pittsburgh, Pennsylvania, 1991, pp. 661-666.

57. R.J. Wasilewski, S.R. Butler and J.E. Hanlon: Plastic Deformation of Single-Crystal NiAl, Trans. Metall. Soc. AIME, 1967, vol. 237, 1991, pp. 1357-1364.

58. E.M. Savitskii, G.S. Burkhanov and I.M. Zalivin: Structure and Mechanical Properties of NiAl Compound in Polycrystalline and Monocrystalline States, 1972, vol. 4, pp. 1406-1407.

59. R.D. Field, D.F. Lahrman and R. Darolia: Slip Systems in [001] Oriented NiAl Single Crystals, Acta Metall., to be published.

60. R.D. Field, D.F. Lahrman and R. Darolia: Room Temperature Deformation in "Soft" Orientation NiAl Single Crystals, in High-Temperature Ordered Intermetallic Alloys IV, L.A. Johnson, D.P. Pope and J.O. Stiegler, eds., Materials Research Society, Pittsburgh, Pennsylvania, 1991, pp. 255-260.

61. I. Baker and P.R. Munroe: Properties of B2 Compounds, in High Temperature Aluminides and Intermetallics, S.H. Shang, C.T. Liu, D.P. Pope and J.O. Stiegler, Eds., The Minerals, Metals & Materials Society, 1990, pp. 425-452.

62. E.P. Lautenschlager, T. Hughes and J.O. Brittain: Slip in Hard-Sphere CsCl Models, Acta Metall., 1967, vol. 15, pp. 1347-1357.

63. D.I. Potter: Prediction of the Operative Slip System in CsCl Type Compounds using Anisotropic Elasticity Theory, Mater. Sci. Eng., 1969, vol. 5, pp. 201-209.

64. W.A. Rachinger and A.H. Cottrell: Slip in Crystals of the Caesium Chloride Type, Acta Metall., 1956, vol. 4, pp. 109-113.

65.   R.D. Noebe, R.R. Bowman, J.T. Kim and R. Gibala: The Potential for Ductility Enhancement from Surface and Interface Dislocation Sources, in NiAl in High Temperature Aluminides and Intermetallics, S.H. Whang, C.T. Liu, D.P. Pope and J.O. Stiegler, Eds., The Minerals, Metals & Materials Society, Warrendale, Pennsylvania, 1990, pp. 271-300.

66.   R.T. Pascoe and C.W.A. Newey: Deformation Modes of the Intermediate Phase NiAl, Phys. State. Sol., 1968, vol. 29, pp. 357-366.

67.   M.H. Loretto and R.J. Wasilewski: Slip Systems in NiAl Single Crystals at 300K and 77K, Phil. Mag., 1971, vol. 23, pp. 1311-1328.

68.   G.M. Rowe, J. Ingram and P.R. Strutt: The Operative Glide Systems in β-NiAl during High Temperature Deformations, in Twenty-Ninth Annual Meeting of the Electron Microscopy Society of America, C.J. Arceneaux, eds., Claitor's Publishing Division, Baton Rouge, Louisiana, 1971, pp. 118-119.

69.   R.R. Bowman, R.D. Noebe, S.V. Raj and I.E. Locci: Correlation of Deformation Mechanisms with the Tensile and Compressive Behavior of NiAl and NiAl(Zr) Intemetallic Alloys, Metall. Trans. A, in press.

70.   E.P. Busso, Y.P. Liu, F.A. McClintock and S.M. Allen: Stable Configurations of Dislocations in Homogenized Nickel-aluminide Single Crystals, Phil. Mag. A, to be published.

71.   P. Veyssiere and R. Noebe: Weak-Beam Study of <111> Superlattice Dislocations in NiAl, Phil. Mag. Let. , in press.

72.   T. Hong and A.J. Freeman: Effect of Antiphase Boundaries on the Electronic Structure and Bonding Character of Intermetallic Systems: NiAl, Phys. Rev. B, 1991, vol. 43, pp. 6446-6458.

73.   D.K. Patrick, K.-M. Chang, D.B. Miracle and H.A. Lipsitt: Burgers Vector Transition in Fe-Al-Ni Alloys, in High-Temperature Ordered Intermetallic Alloys IV, L.A. Johnson, D.P. Pope and J.O. Stiegler, eds., Materials Research Society, Pittsburgh, Pennsylvania, pp. 267-272.

74.   J.D. Cotton, M.J. Kaufman and R.D. Noebe: A Simplified Method for Determining the Number of Independent Slip Systems in Crystals, Scripta Metall. Mater., 1991, vol. 25, pp. 2395-2398.

75.   K.-M. Chang, R. Darolia and H.A. Lipsitt: Fracture of B2 Aluminide Single Crystals, in High Temperature Ordered Intermetallic Alloys IV, eds., Materials Research Society, Pittsburgh, Pennsylvania, pp. 597-602.

76.   J.H. Westbrook and D.L. Wood: A Source of Grain-Boundary Embritlement in Intermetallics, J. Inst. Metals, 1962, vol. 91, pp. 174-182.

77.   M.V. Zeller, R.D. Noebe and I.E. Locci: Grain Boundary Segregation Studies of NiAl and NiAl(Zr) Using Auger Electron Spectroscopy in 3rd HITEMP Review 1990, eds., NASA - Lewis Research Center, Cleveland, Ohio, paper 21.

78.   G. Petton and D. Farkas: Grain Boundary Structure Simulations in B2 Ordered NiAl, Scripta Metall., 1991, vol. 25, pp. 55-60.

79.   R.D. Noebe and J.D. Cotton: unpublished research, 1991.

80.   R. Darolia: General Electric Aircraft Engines, Cincinnati, OH 45215, unpublished research, 1991.

81.   R.D. Field, R. Darolia and D.F. Lahrman: Precipitation in NiAl/Ni2AlTi Alloys, Scripta Metall., 1989, vol. 23, pp. 1469-1474.

82.   K. Vedula, V. Pathare, I. Aslanidis and R.H. Titran: Alloys Based On NiAl for High Temperature Applications, in High Temperature Ordered Intermetallic Alloys, eds., Materials Research Society, Pittsburgh, Pennsylvania, 1985, pp. 411-421.

83.   M. Takeyama and C.T. Liu: Microstructures and Mechanical Properties of NiAl-Ni$_2$AlHf Alloys, J. Mater. Res., 1990, vol. 5, pp. 1189-1196.

84.   V.A. Raman and K. Schubert: On the Crystal Structure of Some Alloy Phases Related to TiAl3. III. Investigation in Several T-Ni-Al and T-Cu-Al Alloy Systems (T-Transition Element)., Z. Metallkde., 1965, vol. 56, pp. 99-104.

85.   P.W. Pellegrini and J.J. Hutta: Investigations of Phase Relations and Eutectic Directional Solidification on the NiAl-V Join, J. Crys. Growth, 1977, vol. 42, pp. 536-539.

86.   P. Nash and W.W. Liang: Phase Equilibria in the Ni-Al-Ti System at 1173 K, Metal. Trans. A, 1985, vol. 16A, pp. 319-322.

87.   P.G. Nash, V. Vejins and W.W. Liang: The Al-Ni-Ti (Aluminum-Nickel-Titanium) System, Bulletin of Alloy Phase Diagrams, 1982, vol. 3, pp. 367-374.

88.   P. Villars and L.D. Calvert: Pearson's Handbook of Crystallographic Data for Intermetallic Phases, American Society for Metals, Metals Park, Ohio, 1985.

89.   P.R. Subramanian, M.G. Mendiratta, D.B. Miracle and D.M. Dimiduk: Microstructures and Mechanical Properties of NiAl+Mo In-Situ Eutectic Composites, in Intermetallic Matrix Composites, D.L. Anton, P.L. Martin, D.B. Miracle and R. McMeeking, eds., Materials Research Society, Pittsburgh, Pennsylvania, 1990, pp. 147-154.

90.   E. Stover: Effects of Alloying and Deformation Processing on Mechanical Behavior of NiAl, Part VII, Volume II., Report No. WADC TDR60-184, General Electric Company, September, 1966.

91. D.P. Mason, D.C. Van Aken and J.G. Webber: Microstructural Studies of β-NiAl and α-Re Composites Produced by Eutectic Solidification, in Intermetallic Matrix Composites, D.L. Anton, P.L. Martin, D.B. Miracle and R. McMeeking, eds., Materials Research Society, Pittsburgh, Pennsylvania, 1990, pp. 340-348.

92. I.E. Locci, R.D. Noebe, J.A. Moser, D.S. Lee and M. Nathal: Processing and Microstructure of Melt Spun NiAl Alloys, in High-Temperature Ordered Intermetallic Alloys III, C.T. Liu, A.I. Taub, N.S. Stoloff and C.C. Koch, eds., Materials Research Society, Pittsburgh, Pennsylvania, 1989, pp. 639-647.

93. J.D. Cotton, M.J. Kaufman and R.D. Noebe: Constitution of Pseudobinary Hypoeutectic β-NiAl + α-V Alloys, Scripta Metall. et Mater., 1991, vol. 25, pp. 1827-1832.

94. R.D. Noebe, F.J. Ritzert, A. Misra and R. Gibala: Prospects for Ductility and Toughness Enhancement of NiAl by Ductile Phase Reinforcement, Report No. 103796, NASA - Lewis Research Center, Cleveland, Ohio 44135, July 1991.

95. W.O. Alexander: Copper-Rich Nickel-Aluminium-Copper Alloys. Part II.--The Constitution of the Copper-Nickel-Rich Alloys, J. Inst. of Metals., 1938, vol. 63, pp. 163-183.

96. W.P. Allen, J.C. Foley, R.F. Cooper and J.H. Perepezko: Decomposition Reactions and Toughening in NiAl-Cu Alloys, in Intermetallic Matrix Composites, D.L. Anton, P.L. Martin, D.B. Miracle and R. McMeeking, eds., Materials Research Society, Pittsburgh, Pennsylvania, 1990, pp. 405-412.

97. C.R. Austin and A.J. Murphy: The Ternary System of Copper-Aluminium-Nickel, J. Inst. Metal., 1923, vol. 29, pp. 327-378.

98. I. Jung and G. Sauthoff: Creep Behaviour of the Intermetallic B2 Phase (Ni,Fe)Al with Strengthening Soft Precipitates, Z. Metallkde., 1989, vol. 80, pp. 484-489.

99. G. Sauthoff: Mechanical Properties of Intermetallics at High Temperatures in, High Temperature Aluminides & Intermetallics, S.H. Whang, C.T. Liu, C.T. Pope and J.O. Stiegler, eds., The Minerals, Metals & Materials Society, Warrendale, Pennsylvania, 1990, pp. 329-352.

100. V.G. Rivlin and G.V. Raynor: Phase Equilibria in Iron Ternary Alloys 2: Critical Evaluation of Constitution of Aluminium-Iron-Nickel System, Int. Met. Rev., 1980, vol. 25, pp. 21-38.

101. D.R. Pank, M.V. Nathal and D.A. Koss: Deformation Behavior of NiAl-Based Alloys Containing Iron, Cobalt, and Hafnium, in High-Temperature Ordered Intermetallic Alloys III, C.T. Liu, A.I. Taub, N.S. Stoloff and C.C. Koch, eds., Materials Research Society, Pittsburgh, Pennsylvania, 1989, pp. 561-566.

102. D.J. Chakrabarti: Phase Stability in Ternary Systems of Transition Elements with Aluminum, Metall. Trans. B, 1977, vol. 8B, pp. 121-123.

103. I. Baker, P. Nagpal, S. Guha and J.A. Horton: TEM In-Situ Straining of B2 Compounds, in Proc. Inter. Symp. on Intermetallic Compounds -Structure and Mechanical Properties- JIMIS-6, O. Izumi, eds., Japan Institute of Metals, Sendai, Japan, 1991, pp. 673-677.

104. J. Kostrubanic, D.A. Koss, I.E. Locci and M. Nathal: On Improving the Fracture Toughness of a NiAl-Based Alloy by Mechanical Alloying, in High-Temperature Ordered Intermetallics IV, L.A. Johnson, D.P. Pope and J.O. Stiegler, eds., Materials Research Society, Pittsburgh, Pennsylvania, 1991, pp. 679-684.

105. J.M. Kostrubanic: The Influence of Processing and Thermal History on the Properties of NiAl-Based Alloys Containing Iron, M.S. Thesis, Pennsylvania State University, 1991.

106. S. Guha, P.R. Munroe and I. Baker: Improving the Low Temperature Ductility of NiAl, in High-Temperature Ordered Intermetallic Alloys III, C.T. Liu, A.I. Taub, N.S. Stoloff and C.C. Koch, eds., Materials Research Society, Pittsburgh, Pennsylvania, 1989, pp. 633-638.

107. A. Inoue, T. Masumoto and H. Tomioka: Microstructure and Mechanical Properties of Rapidly Quenched $L2_0$ and $L2_0$ + L12 Alloys in Ni-Al-Fe and Ni-Al-Co Systems, J. Mat. Sci., 1984, vol. 19, pp. 3097-3106.

108. M.A. Crimp and K. Vedula: Room-Temperature Deformation of Single-Crystal B2 Fe-Al Alloys: the Effect of Stoichiometry and Cooling Rate, Phil. Mag. A, 1991, vol. 63, pp. 559-570.

109. J.L. Walter, H.E. Cline and E.F. Koch: Interface Dislocations in Directionally Solidified NiAl-Cr Eutectic, Trans. TMS-AIME, 1969, vol. 245, pp. 2073-2079.

110. H.E. Cline, J.L. Walter, E.F. Koch and L.M. Osika: The Variation of Interface Dislocation Networks with Lattice Mismatch in Eutectic Alloys, Acta Metall., 1971, vol. 19, pp. 405-414.

111. Metals Handbook, 8th, American Society for Metals, Metals Park, Ohio, 1973, pp. 274-350.

112. C. Muller, W. Blau and P. Ziesche: Local Partial DOS and Experimental Al K Spectra of Transition Metal Aluminides, Phys. Stat. Sol. (b), 1983, vol. 116, pp. 561-573.

113. M. Ettenberg, K.L. Komarek and E. Miller: Thermodynamic Properties and Ordering in PdAl, Metall. Trans., 1971, vol. 2, pp. 1173-1181.

114. J.D. Cotton, M.J. Kaufman, R.D. Noebe and M. Behbehani: The Potential for Room Temperature Ductility in Polycrystalline NiAl Through Slip System Modification by Macroalloying, in HITEMP IV, 1991, NASA - Lewis Research Center, Cleveland, Ohio, paper 23.

115.   T. Hong and A.J. Freeman: Electronic Structure and Mechanical Properties of Intermetallics: APB Energies in Ni-Al-Based Systems, in High-Temperature Ordered Intermetallic Alloys III, C.T. Liu, A.I. Taub, N.S. Stoloff and C.C. Koch, eds., Materials Research Society, Pittsburgh, Pennsylvania, 1989, pp. 75-80.

116.   K.H. Hahn and K. Vedula: Ordering Energies of Binary and Ternary Alloys Based on B2 NiAl, Phys. Stat. Solid., to be published.

117.   P.B. Hirsch, A. Howie and M.J. Whelan: A Kinematical Theory of Diffraction Contrast of Electron Transmission Microscope Images of Dislocations and Other Defects, Phil. Trans. Royal. Soc., 1960, vol. 252A, pp. 499-529.

118.   M.T. Otten: A Practical Guide to ALCHEMI, PHILIPS Electron Optics Bulletin, vol. 126, pp. 21-26.

119.   J. Taftø and J.C.H. Spence: Crystal Site Location of Iron and Trace Elements in a Magnesium-Iron Olivine by a New Crystallographic Technique, Science, 1982, vol. 218, pp. 49-51.

120.   D.B. Miracle: Deformation in NiAl Bicrystals, Acta Metall. Mater., 1991, vol. 39, pp. 1457-1468.

121.   D.M. Dimiduk and S. Rao: Deformation Mechanisms and Solid-Solution Strengthening in Ordered Alloys, in High-Temperature Ordered Intermetallic Alloys IV, L.A. Johnson, D.P. Pope and J.O. Stiegler, eds., Materials Research Society, Pittsburgh, Pennsylvania, 1991, pp. 499-513.

122.   S. Takeuchi: Solid-Solution Strengthening in Single Crystals of Iron Alloys, J. Phys. Soc. Japan, 1969, vol. 27, no. 4, pp. 929-940.

123.   N.F. Mott and F.R.N. Nabarro: Dislocation Theory and Transient Creep in Strength of Solids, eds., The Physical Society, 1948, pp. 1-19.

124.   R.L. Fleischer: Solid-Solution Hardening in The Strengthening of Metals, D. Peckner, Eds., Reinhold Publishing Corp., New York, 1964, pp. 93-140.

125.   R.D. Noebe and R.R. Bowman: Review of the Physical and Mechanical Properties of the B2 Compound NiAl, to be published in Int. Met. Rev.

126.   L.H. Van Vlack: Materials Science for Engineers, Addison-Wesley Publishing Co., Reading, Massachusetts, 1970, pp. 506-511.

127.   V. Gerold: Precipitation Hardening in Dislocations in Metallurgy, F.R.N. Nabarro, ed., North-Holland Publishing Company, New York, 1979, pp. 219-260.

128.   M.F. Ashby: The Theory of the Critical Shear Stress and Work Hardening of Dispersion-Hardened Crystals, in Proc. Second Bolton Landing Conf. on Oxide Dispersion Strengthening, Gordon and Breach, 1968.

129. E.P. Lautenschlager, T.C. Tisone and J.O. Brittain: Electron Transmission Microscopy of NiAl, Phys. Stat. Sol., 1967, vol. 20, pp. 443-450.

130. J.J. Poubeau and J. Bigot: Determination de la Solubilite du Carbone Dans le Chrome Par Mesure de la Resistivite Electrique a Basse Temperature, Acta. Metall., 1985, vol. 33, pp. 1137-1141.

131. R. Darolia, D.F. Lahrman, R.D. Field, J.R. Dobbs, K.M. Chang, E.H. Goldman and D.G. Konitzer: Overview of NiAl Alloys for High Temperature Structural Applications, in NATO Advanced Research Workshop on Intermetallic Compounds, C.T. Liu, R.W. Cahn and G. Sauthoff, eds., Kluwer Publishing Co., The Netherlands, 1992 preprint.

REPORT DOCUMENTATION PAGE

Form Approved
OMB No. 0704-0188

1. AGENCY USE ONLY *(Leave blank)*	2. REPORT DATE	3. REPORT TYPE AND DATES COVERED
	March 1992	Final Contractor Report

4. TITLE AND SUBTITLE

The Influence of Chromium on Structure and Mechanical Properties of B2 Nickel Aluminide Alloys

5. FUNDING NUMBERS

WU–505–63–5A
G–NAG3–1079

6. AUTHOR(S)

James Dean Cotton

7. PERFORMING ORGANIZATION NAME(S) AND ADDRESS(ES)

University of Florida
Materials Science and Engineering
Gainesville, Florida 32601

8. PERFORMING ORGANIZATION REPORT NUMBER

None

9. SPONSORING/MONITORING AGENCY NAMES(S) AND ADDRESS(ES)

National Aeronautics and Space Administration
Lewis Research Center
Cleveland, Ohio 44135–3191

10. SPONSORING/MONITORING AGENCY REPORT NUMBER

NASA CR–189124

11. SUPPLEMENTARY NOTES

Project Manager, Michael V. Nathal, Materials Division, NASA Lewis Research Center, (216) 433–3197. Report was submitted as a dissertation in partial fulfillment of the requirements for the degree of Doctor of Philosophy, University of Florida, Gainesville, Florida in 1991.

12a. DISTRIBUTION/AVAILABILITY STATEMENT

Unclassified - Unlimited
Subject Category 26

12b. DISTRIBUTION CODE

13. ABSTRACT *(Maximum 200 words)*

Major obstacles to the use of NiAl-base alloys and composites are low ductility and toughness. These shortcomings result, in part at least, from a lack of sufficient slip systems to accommodate plastic deformation of polycrystalline material (the von Mises Criterion). It has been reported that minor additions of chromium to polycrystalline NiAl cause the predominant slip system to shift from the usual <001>{110} to <111>{112}. If this is true, then a major step toward increasing ductility in this compound may be realized. The purpose of the present study was to verify this phenomenon, characterize it with respect to chromium level and nickel-to-aluminum ratio, and correlate any change in slip system with microstructure and mechanical properties. Compression and tensile specimens were prepared from alloys containing 0 to 5 at. % chromium and 45 to 55 at. % aluminum. Following about one percent strain, TEM foils were produced and the slip systems determined using the $\mathbf{g} \cdot \mathbf{b} = 0$ invisibility criterion. Contrary to the previous results, chromium was found to have no effect on the preferred slip system in of any of the alloys studied. Possible reasons for the inconsistency of the current results with previous work are considered. Composition-structure-property relationships are discerned for the alloys, and good correlations are demonstrated in terms of conventional strengthening models for metallic systems.

14. SUBJECT TERMS

Nickel aluminide; Deformation; Ductility; Strength; Solid solution hardening; Stoichiometry

15. NUMBER OF PAGES

156

16. PRICE CODE

A08

17. SECURITY CLASSIFICATION OF REPORT	18. SECURITY CLASSIFICATION OF THIS PAGE	19. SECURITY CLASSIFICATION OF ABSTRACT	20. LIMITATION OF ABSTRACT
Unclassified	Unclassified	Unclassified	